

Optical Remote Sensing of the Environment (ORS)

24 June - 28 June 2012, Monterey Plaza Hotel, Monterey, California, United States

The scope of the Optical Remote Sensing of the Environment Conference will focus on three general areas: sensors, algorithms and phenomena, and applications. With regard to sensors, the conference will focus especially on hyperspectral and multi-spectral imaging sensors, LiDAR, and multi-sensor imaging (for example, hyperspectral combined with LiDAR or hyperspectral and other non-optical remote sensing modalities such as RADAR).

Under the general area of algorithms and phenomena, papers will focus on topics such as methods to correct data (atmospheric correction), exploitation methods using a variety of methods (for example radiative transfer and image classification, detection, or change detection methodologies). Papers will also address specific topics related to retrievals such as ocean color and land biophysical or geophysical parameters. Other analysis techniques and tools will also be covered, for example, compression, sensor fusion, and data visualization and GIS/information management.

Application topics will address a broad range of topics where optical sensors are used to characterize the environment, such as the coastal ocean, forestry, agriculture, or environmental monitoring and natural resource monitoring and management.

Congress Joint Plenary Speakers

- [Al Bovik](#), *Univ. of Texas at Austin, USA*
Image Quality Assessment: How Blind is Blind?
- [Joseph Goodman](#), *Stanford Univ., USA*
Assessing a New Imaging Modality
- [Bruce Guenther](#), *NOAA-JPSS & University of Maryland of Baltimore County, USA*
Survey of Applications for Ocean Color and Imagery from EOS-MODIS and early results from NPP-VIIRS
- [Henry Helvajian](#), *The Aerospace Corp., USA*
Small Satellites: The Desire for a Mass Producible, Mass Customizable Nanosatellite
- **OSA Corporate Associates:** Executive Speaker Series presents [Michael Silver](#), CEO, *American Elements, USA*

Program Committee

General Chairs

Charles Bachmann, *NRL, USA*
Curt Davis, *Oregon State University, USA*

Program Chair

Chris Parrish, *NOAA, USA*

Sponsor:



Imaging and Applied Optics Congress

24 June 2012 – 28 June 2012, Monterey Plaza Hotel, Monterey, California, USA

The frontiers in imaging and selected areas in applied optics will be examined at the Optics and Photonics Congress (OPC) to be held in Monterey, California. This congress is composed of six complimentary meetings and is designed to present a comprehensive view of the latest developments in imaging and applied optical sciences. Two of the meetings Imaging Systems and Applications (IS) and Computational Optical Imaging and Sensing (COSI) deal with both latest theoretical advances in imaging sciences as well as the application of imaging techniques and processing methodologies in the development of some of the most advanced imaging system designs. Presentations will further describe the employment of these imaging technologies in scientific, commercial, medical, and military applications. In the applied optics arena, papers describing advanced optical sensing technologies and their application to the solution of numerous environmental, industrial, and testing applications will be presented by recognized leaders in these fields. The Applied Industrial Optics (AIO) meeting continues to attract industrial leaders in the application of cutting edge optical sensors in diverse market sectors including defense, oil

& gas, food and beverage and pharmaceuticals to name a few. Advances in optical sensor component technologies and the capabilities demonstrated by these new sensors will be presented in the Optical Sensors (SENSORS) meeting. These advances directly compliments talks presented by speakers in the more applied meeting on Applied Industrial Optics and provide an indication of sensors expected to find use in numerous applied applications. The meeting on Optical Remote Sensing of the Environment (ORS) reports on some of the most advanced sensing techniques used to characterize the environment and the results of studies providing a more complete understanding of the atmosphere. All aspects of optics fabrication and testing ranging from micro-optics to large optical systems will be covered in the meeting on Optical Fabrication and Testing (OF&T). Design concepts and new materials offering novel capabilities as well as fabrication and finishing techniques of aspheric, conformal and freeform optics will be discussed by many of the leaders in this field at this meeting. Together, this Congress represents a form in which the attendees are exposed to the forefront advances in imaging and applied optics and are able to hear discussion of the application of these technologies to important industrial, military and medical problems.

Featured Speakers

Opening General Session, Monday, June 25, 8:00-10:30



[Al Bovik](#), Univ. of Texas at Austin, USA **Image Quality Assessment: How Blind is Blind?**



[Joseph Goodman](#), Stanford Univ., USA **Assessing a New Imaging Modality**



[Bruce Guenther](#), NOAA-JPSS & University of Maryland of Baltimore County, USA
Survey of Applications for Ocean Color and Imagery from EOS-MODIS and early results from NPP-VIIRS



[Henry Helvajian](#), The Aerospace Corp, USA
Small Satellites: The Desire for a Mass Producible, Mass Customizable Nanosatellite

AIO Plenary Session, Monday, June 25, 14:00-16:00



[Scott McEldowney](#), Microsoft, USA **Microsoft Kinect - A Look Inside**

OSA Corporate Associates: Executive Speaker Series, Wednesday, 27 June, 17:30 - 19:30



[Michael Silver](#), American Elements, USA

This event is made possible in part, through generous support from the OSA Fabrication, Design and Instrumentation Division

- [Applied Industrial Optics: Spectroscopy, Imaging, and Metrology \(AIO\)](#)
- [Computational Optical Sensing and Imaging \(COSI\)](#)
- [Imaging Systems and Applications \(IS\)](#)
- [Optical Fabrication and Testing \(OF&T\)](#)
- [Optical Remote Sensing of the Environment \(ORS\)](#)
- [Optical Sensors \(SENSORS\)](#)

Corporate Sponsor:






Sponsor:



Optical Remote Sensing of the Environment (ORS) Program

Conference Program

- [Online Access to Technical Digest Now Available!](#)
 - Full Technical Attendees now have an alternate way to access the digest papers at the meeting. Access the papers through [Optics InfoBase](#) using the same login email address and password provided during the meeting registration process. Access is currently limited to Advanced Photonics Full Technical Attendees only. If you need assistance with your login information, please use the forgot password utility or "Contact Help" link.
- Download Pages from the Program Book!
 - [Abstracts](#)  (pdf)
 - [Agenda of Sessions/Schedule at a Glance](#)  (pdf)
 - [Key to Authors and Presiders](#)  (pdf)
- [Searchable Conference Program Available Online!](#)
 - Browse speakers
 - Browse sessions by type or day.
 - Use Advanced Search to search the program by author, title, OCIS code and more.
 - Plan and print your [personal itinerary](#) before coming to the conference.
 - Add your personal itinerary to your electronic calendar.
 - Email your itinerary to a colleague who might be interested in attending.
- [Invited Speakers](#)

The Optical Remote Sensing of the Environment (ORS) meeting will focus on sensors, algorithms and phenomena, and applications. With regard to sensors, the conference will focus especially on hyperspectral and multi-spectral imaging sensors, LiDAR, and multi-sensor imaging. Under the general area of algorithms and phenomena, topics such as methods to correct data (atmospheric correction), exploitation methods using a variety of methods will be featured. Specific topics related to retrievals such as ocean color and land biophysical or geophysical parameters will be addressed. Application topics will address a broad range of topics where optical sensors are used to characterize the environment, such as the coastal ocean, forestry, agriculture, or environmental monitoring and natural resource monitoring and management.

A number of distinguished invited speakers have been invited to present at the meeting. In addition, the organizers have planned a number of special events to make your meeting experience more enjoyable!

Special Events

General Session

The Congress will start with a joint General Session on Monday 25 June from 8:00 - 10:30. The speakers are Al Bovik from Univ. of Texas at Austin, Joseph Goodman from Stanford Univ., Henry Helvajian from The Aerospace Corp., and Bruce Guenther from Goddard Earth Science and Technology Center. For more information about each speaker visit the [special event page](#).

Conference Reception

The joint conference reception will be on Monday 25 June from 18:30 - 20:00. The reception will feature light fare and is open to all paid registrants.

Poster Sessions

A joint poster sessions will take place on Tuesday 26, June from 17.30 - 19.00. Posters are an integral part of the technical program and offer a unique networking opportunity, where presenters can discuss their results one-to-one with interested parties. Each author is provided with a 4 ft. x 8 ft. (1.22 m x 2.44 m) board on which to display the summary and results of his or her paper.

OSA Corporate Associates: Executive Speaker Series

Michael Silver, CEO of *American Elements*

This special evening event on Wednesday, 27 June begins at 17:30 with a networking reception, followed by a brief student award ceremony and then a one-on-one interview with audience questions.

Sit down for an entertaining and intimate conversation with Michael Silver, Chief Executive Officer, American Elements as he responds to questions from Dr. Stephen Jacobs, from The University of Rochester, about his observations on the current and future demand of Rare Earth, his career path, and personal perspectives. Mr. Silver was one of the first Americans to establish a direct production and distribution supply chain from the rare earth mines in Inner Mongolia, China to North America and Europe and is credited with making American Elements an early participant in many now billion dollar growth industries including solar energy, fuel cells, optical telecommunications and next generation pharmaceuticals. Presented in collaboration with the OSA Fabrication, Design and Instrumentation Division.

Invited Speakers

Expected Synergies Between The Ocean Observatories Initiative and Ocean Color Remote Sensing, Steven Ackleson, *Consortium for Ocean Leadership, USA*

First Results From a High-Resolution Full Waveform Airborne Bathymetric LiDAR System, Craig Glennie, *Natural Resources Canada, Canada*

Combining Lidar Data and Hyperspectral Imagery for Coastal Engineering and Environmental Characterization, J. Heath Harwood, *U.S. Army Corps of Engineers - JALBTCX, USA*

Mapping Applications with Simulated DigitalGlobe WorldView-3 Data, Fred Kruse, *Naval Postgraduate School, USA*

Wide Field of View Hyperspectral Radiometer For Coastal Imaging From Polar Sun Synchronous Orbit, Jeff Puschell, *Raytheon Company, USA*

HICO Observations of Biological and Sediment-Transport Processes in Monterey Bay, California, John Ryan, *Monterey Bay Aquarium Research Institute, USA*

Active-Passive Data Fusion Strategies for Classification of the Shallow-water Seafloor Grady Tuell, *Georgia Tech Research Institute, USA*

Applied Industrial Optics: Spectroscopy, Imaging, & Metrology (AIO)

Computational Optical Sensing and Imaging (COSI)

Imaging Systems and Applications (IS)

Optical Fabrication and Testing (OF&T)

Optical Remote Sensing of the Environment (ORS)

Optical Sensors (SENSORS)

24–28 June 2012

Monterey Plaza Hotel, Monterey, CA, USA

OSA continues the tradition of outstanding conferences and focused meetings with the 2012 Optics and Photonics Congress on Imaging and Applied Optics in beautiful Monterey, CA. The Congress has co-located six topical meetings (listed above) for attendees to benefit from exposure to a diverse collection of optical technologies. The Program includes scientific leaders from around the globe in each topical area which should facilitate networking and the cross-pollination of ideas between attendees. We have planned numerous special congress-wide events; the Opening General Session, a Welcome Reception, a Poster Session and an OSA Corporate Associates event with Michael Silver from American Elements.

The Applied Industrial Optics (AIO) meeting was an unprecedented success last year, and promises to be very exciting this year. Scott MeEldowney from Microsoft will join us as a plenary speaker. The remaining four days of the conference cover a wide range of applied optical technologies and a very diverse set of application areas including medical, food, environmental monitoring, and innovative emerging technology with 29 invited speakers. Invited speakers and contributors include industrial, governmental, and academic scientists at the forefront of applied optics from around the globe. Join us for an exciting meeting and volunteer to join the team to help make next year's meeting even better.

The Computational Optical Sensing and Imaging (COSI) meeting consists of topics that describe theoretical and experimental progress in computational sensing and imaging research. The meeting subject matter spans the areas of fundamental physics, hardware design, and numerical and analytical techniques and has led to significant improvements in the fields of imaging and sensing for medicine, defense, and homeland security, as well as industrial inspection and testing applications. This year, we have prepared an extremely strong program of 12 invited speakers and 34 contributed oral presentations, as well as two joint sessions with the Imaging Systems (IS) topical meeting. We extend a warm welcome to both the longstanding members of the COSI community and those joining us for the first time.

The Imaging Systems and Applications (IS) meeting is an “all-encompassing” conference on imaging that covers topics in imaging system design and components, imaging modalities and systems, and applications of military, industrial, medical and consumer imaging. Its aim is to highlight how different materials, components, and processing combine to determine imaging system performance. Invited speakers from the military, academic, and commercial imaging sectors will address the current status and future of imaging in their organizations. The conference includes 21 invited, 25 contributed oral presentations, and 7 poster presentations that describe recent developments in imaging lens technologies (including gradient index and tunable fluidic lenses), imaging optics (including extended depth of field design and imaging through scattering media), image sensors (including novel SPAD and QD imagers), medical imaging and microscopy (including in vivo brain imaging and compressed sensing microscopy), hyperspectral imaging, military applications, phase space in imaging, computational imaging and digital imaging (including image chain modeling and color imaging for mobile displays).

This year the meeting on Optical Fabrication and Testing (OF&T) consists of 10 sessions organized around topics such as polishing/finishing science, advanced metrology and freeform optics. Twenty-two invited papers from the US and six countries highlight special topics like light scattering from complex optics, engineering of glasses for next generation optics, polishing with a vortex, hybrid glass-polymer optics, aspheres w/o axial symmetry, durable coatings for glass molding tools and x-ray optics for astronomy. Twenty-eight contributed oral presentations and 13 poster papers fill out the three day meeting agenda. During the Opening General Session, Dr. Henry Helvajian will speak about the role of glass-ceramics in micro-satellite construction.

Optical remote sensing of the environment addresses many needs in both civilian and military sectors. The scope of the Optical Remote Sensing of the Environment (ORS) meeting will focus on three general areas: sensors, algorithms and phenomena, and applications. With regard to sensors, the conference will focus especially on hyperspectral and multi-spectral imaging sensors, LiDAR, and multi-sensor imaging (for example, hyperspectral combined with LiDAR or hyperspectral and other non-optical remote sensing modalities such as RADAR). The meeting will include 22 invited and 28 contributed presentations, and 13 poster presentations for you to attend.

The Optical Sensors (SENSORS) meeting consists of six topics which address various sensor types, and include all aspects of optical sensors from the components employed, their configuration through detection schemes and algorithms, and their applications. The conference includes 27 invited, 32 contributed oral presentations, and 8 poster presentations that describe several kinds of micro and nano-engineered sensors, fiber optic and laser-based sensors. Some enabling technologies for advanced sensing are also reported, including the use of pulsed high power lasers, novel materials and imaging methods or new frequency bands, as for example THz radiation. These sensors are used in various applications, namely for quality and process control, chemical and biological applications, metrology, imaging, and remote sensing, to mention a few examples.

AIO

Jess Ford, *Wireline R&D Weatherford Intl., USA*, **General Chair**

Marion O'Farrell, *SINTEF, Norway*, **General Chair**

Sean Christian, *Optrology, Inc., USA*, **Program Chair**

Joe Dallas, *Avo Photonics Inc, USA*, **Program Chair**

Arel Weisberg, *Energy Research Co., USA*, **Program Chair**

COSI

Michael Gehm, *Univ. of Arizona, USA*, **General Chair**

Gerd Haeusler, *Univ. of Erlangen-Nuremberg, Germany*,
General Chair

Andrew Harvey, *Heriot-Watt University, UK*, **Program Chair**

David Gerwe, *Boeing Company, USA*, **Program Chair**

IS

Peter Catrysse, *Stanford Univ., USA*, **General Chair**

John T. Sheridan, *Univ. College Dublin, Ireland*, **General Chair**

Francisco Imai, *Canon USA, Inc., USA*, **Program Chair**

Dale Linne von Berg, *Naval Research Laboratory, USA*,
Program Chair

OF&T

Stephen Jacobs, *Univ. of Rochester, USA*, **General Chair**

James "Ted" Mooney, *ITT Industries, Space System Division, USA*, **General Chair**

Jessica DeGroote Nelson, *Optimax Systems Inc, USA*,
General Chair

Jannick Rolland, *Univ. of Rochester, USA*, **General Chair**

Shai Shafrii, *Corning Incorporated, USA*, **General Chair**

ORS

Charles Bachmann, *Naval Research Laboratory, USA*,
General Chair

Curt Davis, *Oregon State University, USA*, **General Chair**

Chris Parrish, *NOAA, USA*, **Program Chair**

SENSORS

Ishwar Aggarwal, *Univ. of North Carolina at Charlotte, USA*,
General Chair

Mário F.S. Ferreira, *Universidade de Aveiro, Campus de Santiago, Portugal*, **General Chair**

Program Committee

Applied Industrial Optics: Spectroscopy, Imaging, & Metrology (AIO)

General Chairs

Jess Ford, *Wireline R&D Weatherford Intl., USA*
Marion O'Farrell, *SINTEF, Norway*

Program Chairs

Sean Christian, *Optrology, Inc., USA*
Joe Dallas, *Avo Photonics Inc, USA*
Arel Weisberg, *Energy Research Co., USA*

Committee Members

Elfed Lewis, *Univ. of Limerick, Ireland*
Kai Liu, *Sichuan Univ., China*
Sheng Liu, *KLA-Tencor Corp., USA*
Hans-Peter Loock, *Queen's Univ., Canada*
Prasanna Pavani, *Ricoh Innovations, Inc., USA*
Sapna Shroff, *Ricoh Innovations, USA*
Yongchang Wang, *KLA-Tencor Corp., USA*

Computational Optical Sensing and Imaging (COSI)

General Chairs

Michael Gehm, *Univ. of Arizona, USA*
Gerd Haeusler, *Univ. of Erlangen-Nuremberg, Germany*

Program Chairs

Andrew Harvey, *Heriot-Watt University, UK*
David Gerwe, *Boeing Company, USA*

Committee Members

George Barbastathis, *MIT, USA*
Gisele Bennett, *Georgia Tech, USA*
Marc Christensen, *Southern Methodist Univ., USA*
Aristide Dogariu, *UCF-CREOL, USA*
Christy Fernandez-Cull, *MIT Lincoln Labs, USA*
Michael Fiddy, *Univ. of North Carolina-Charlotte, USA*
Jason Fleischer, *Princeton Univ., USA*
Bahram Javidi, *Univ. of Connecticut, USA*
Keith Knox, *Air Force Research Lab., USA*
Kenny Kubala, *Five Focal, USA*
Abhijit Mahalanobis, *Lockheed Martin, USA*
Joe Mait, *Army Research Lab, USA*
Mark Neifeld, *Univ. of Arizona, USA*
Rafael Piestun, *Colorado Univ. at Boulder, USA*
Chrysanthe Preza, *Univ. of Memphis, USA*
Tim Schulz, *Michigan Tech., USA*
Michael Stenner, *MITRE Corp, USA*
Brian Thelen, *Michigan Tech Research Inst., USA*
Sam Thurman, *Lockheed Martin, USA*
David Tyler, *Univ. of Arizona, USA*

Imaging Systems and Applications (IS)

General Chairs

Peter Catrysse, *Stanford Univ., USA*
John T. Sheridan, *Univ. College Dublin, Ireland*

Program Chairs

Francisco Imai, *Canon USA, Inc., USA*
Dale Linne von Berg, *Naval Research Laboratory, USA*

Committee Members

Kenneth Barnard, *Air Force Research Laboratory, USA*
Gisele Bennett, *Georgia Tech, USA*
Kathrin Berkner, *Ricoh Innovations, USA*
David Brady, *Duke University, USA*
Joyce Farrell, *Stanford University, USA*
Jim Fienup, *Univ. of Rochester USA*
Boyd Fowler, *Fairchild Imaging, USA*
Craig Hoffman, *Naval Research Laboratory, USA*
Niel Holt, *Utah State Univ. - Space Dynamic Lab, USA*
Kristina Irsch, *Johns Hopkins University, USA*
Eddie Jacobs, *Univ. of Memphis, USA*
Michael Kriss, *Consultant, USA*
Jun Ke, *University of Hong Kong, USA*
Ofer Levi, *Univ. of Toronto, Canada*
Pierre Magnan, *Institut Supérieur de l'Aéronautique et de l'Espace, France*
Joe Mait, *Army Research Laboratory, USA*
Ricardo Motta, *Nvidia, USA*
Mukul Sarkar, *Indian Institute of Technology Delhi, India*
Guohai Situ, *Princeton Univ., USA*
Torbjorn Skauli, *Norwegian Defense Research Establishment (FFI), Norway*
Albert Theuwissen, *Harvest Imaging, Belgium*
Nobukazu Teranishi, *Panasonic Corporation, Japan*
Edward Watson, *Air Force Research Laboratory, USA*
Laura Waller, *Princeton University, USA*
Changhuei Yang, *California Inst. of Technology, USA*
Zeev Zalevsky, *Bar-Ilan Univ., Israel*

Optical Fabrication and Testing (OF&T)

Chairs

Stephen Jacobs, *Univ. of Rochester, USA*
James "Ted" Mooney, *ITT Industries, Space System Division, USA*
Jessica DeGroot Nelson, *Optimax Systems Inc, USA*
Jannick Rolland, *Univ. of Rochester, USA*
Shai Shafriir, *Corning Incorporated, USA*

Committee Members

Dave Aikens, *Savvy Optics Corp., USA*
Damon Diehl, *Diehl Research Grant Services, USA*
Chris Evans, *Univ. of North Carolina at Charlotte, USA*
Oliver Fanhle, *FISBA OPTIK AG, USA*
Edward Fess, *OptiPro, USA*
John Greivenkamp, *Univ. of Arizona, USA*

Ulf Griesmann, *NIST, USA*
 Joe Howard, *NASA Goddard Space Flight Center, USA*
 Kazuyoshi Itoh, *Osaka University, Japan*
 Matthew Jenkins, *Raytheon Space and Airborne Systems (SAS), USA*
 Dae Wook Kim, *Univ. of Arizona, USA*
 Thomas Milster, *Univ. of Arizona, USA*
 Brigid Mullany, *Univ. of North Carolina at Charlotte, USA*
 Paul Murphy, *QED Technologies Inc, USA*
 Francois Piche, *L-3 Communications IOS Brashear, USA*
 Joseph Randi, *Penn State Univ., USA*
 Kathleen Richardson, *Clemson Univ., USA*
 Joe Robichaud, *L-3 SSG Tinsley, USA*
 Markus Schinhaerl, *Fachhochschule Deggendorf, Germany*
 Katie Schwertz, *Edmund Optics, USA*
 Aric Shorey, *Corning Inc, USA*
 Erika Sohn, *Instituto de Astronomia UNAM, Mexico*
 Tayyab Suratwala, *Lawrence Livermore National Laboratory, USA*
 David Vanderpool, *SCHOTT N America - Adv Optical Materials, USA*
 Daniel Waechter, *Fraunhofer IPT, Germany*
 Ray Williamson, *Ray Williamson Consulting, USA*
 Yongbo Wu, *Akita Prefectural Univ., Japan*
 Weiyao Zou, *ASML Engineering, USA*

Optical Remote Sensing of the Environment (ORS)

General Chairs

Charles Bachmann, *Naval Research Laboratory, USA*
 Curt Davis, *Oregon State University, USA*

Program Chair

Chris Parrish, *NOAA, USA*

Committee Members

Steve Ackleson, *Consortium for Ocean Leadership, USA*
 Francisco Chavez, *MBARI, Mexico*
 Robert Fusina, *Naval Research Lab, USA*
 Roy Hughes, *Defence Science Technology Organization, Australia*
 Fred Kruse, *Naval Postgraduate School, USA*
 Bill Philpot, *Cornell Univ., USA*
 Dar Roberts, *Univ. of California at Santa Barbara, USA*
 Susan Ustin, *Univ. of California at Davis, USA*
 Jan van Aardt, *Rochester Ins. of Technology, USA*

Optical Sensors (SENSORS)

General Chairs

Ishwar Aggarwal, *Univ. of North Carolina at Charlotte, USA*
 Mário F.S. Ferreira, *Universidade de Aveiro, Campus de Santiago, Portugal*

Sensors 1: Micro and Nano-Engineered Sensors

Limin Tong, *Zhejiang Univ., China, Chair*
 Bai-Ou Guan, *Jinan Univ., China*
 Misha Sumetsky, *OFS Laboratories, USA*
 Dong Ning Wang, *Hong Kong Polytechnic Univ., Hong Kong*

Sensors 2: THz Sensing

Jason Deibel, *Wright State Univ., USA, Chair*
 Enrique Castro Camus, *Centro de Investigaciones en Optica AC, Mexico*
 David Hilton, *Univ. of Alabama at Birmingham, USA*
 Mona Jarrahi, *Univ. of Michigan, USA*
 Sushil Kumar, *Lehigh Univ., USA*

Sensors 3: Imaging Sensors

Sebastian Schluecker, *Univ. Osnabrück, Germany, Chair*
 Rohit Bhargava, *Univ. of Illinois at Urbana-Champaign, USA*
 Marcus Cicerone, *NIST, USA*
 Benjamin Dietzek, *Friedrich-Schiller-Universität Jena, Germany*
 Costel Flueraru, *NRC Inst. for Microstructural Sciences, Canada*
 Robert Huber, *Ludwig-Maximilians-Universität München, Germany*
 Alex Vitkin, *McMaster Univ., Canada*
 Costel Flueraru, *Inst. for Microstructural Sciences, Canada*

Sensors 4: Fiber Optical Sensors

Gilberto Brambilla, *Univ. of Southampton, USA, Chair*
 Jaques Albert, *Carleton Univ., Canada*
 John Canning, *Sydney Univ., Australia*
 Alexandre Francois, *Univ. of Adelaide, Australia*
 Wei Jin, *Hong Kong Polytechnic Univ., Hong Kong*
 Jose Miguel Lopez Higuera, *Universidad de Cantabria, Spain*
 Tanya Monro, *Univ. of Adelaide, Australia*

Sensors 5: Laser Based Sensors

Byoung-ho Lee, *Seoul Natl. Univ., Korea, Chair*
 Pietro Ferraro, *National Inst. for Applied Optics, Italy*
 Yoshio Hayasaki, *Utsunomiya Univ., Japan*
 Myung K. Kim, *Univ. of South Florida, USA*
 Wolfgang Osten, *Institut für Technische Optik, Germany*
 Gang-Ding Peng, *Univ. of New South Wales, Australia*

Sensors 6: Optical Chemical and Biological Sensors

Ken Ewing, *Naval Research Labs, USA, Chair*
 Vince Rotello, *Program in Molecular and Cell Biology, Univ. of Massachusetts, USA*
 Robert J. Levis, *Temple University, Center for Advanced Photonics Research, USA*
 George Coyle, *DRS Inc., USA*
 Brandon Shaw, *Naval Research Laboratory, USA*

Special Events

Opening General Session

Monday, 25 June, 8:00–10:30

The Dolphins, Upper Plaza



Joseph Goodman, Stanford Univ., USA

Joseph W. Goodman received an A.B. Degree from Harvard, an M.S degree and a Ph.D. degree, both from Stanford University. He joined the faculty of the Department of Electrical Engineering at Stanford in 1967, chaired the department from 1989 to 1996, and served as Senior Associate Dean of Engineering until 1999. He retired from Stanford in January of 2001. Dr. Goodman

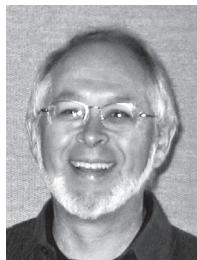
is the author of the books *Introduction to Fourier Optics* (now in its 3rd edition), *Statistical Optics*, and *Speckle Phenomena in Optics*. He has received numerous awards from the IEEE, ASAE, OSA and SPIE, including the highest awards given by the latter two societies.



Al Bovik, Univ. of Texas at Austin, USA

Al Bovik holds the Curry/Cullen Trust Endowed Chair Professorship at The University of Texas at Austin. His recent interests are in the areas of perceptual image and video processing and computational vision. He is the author of *The Handbook of Image and Video Processing*, *Modern Image Quality Assessment*, and two recent books, *The Essential Guides to Image and*

Video Processing. Al was named “Imaging Scientist of the Year” by IS&T/SPIE for 2011. He is a Fellow of the IEEE, OSA, and SPIE. Al served on the Board of Governors of the IEEE Signal Processing Society, co-founded and served as Editor-in-Chief of the IEEE journal *Transactions on Image Processing*, and created and served as the first General Chairman of the IEEE International Conference on Image Processing.



Bruce Guenther, NOAA-JPSS & University of Maryland of Baltimore County, USA

Dr. Bruce Guenther is the NOAA SDR Calibration lead for NPOESS and JPSS Programs since 2007. He was the Chief VIIRS Scientist for the final calibrations and characterizations testing of the NPP VIIRS, and was responsible for the first calibration products published for the EOS Terra MODIS sensor. Guenther’s current research

interests are exploiting VIIRS advances in calibration design and accuracy for uses in optical oceanography studies. Guenther received a Ph.D. degree from the University of Pittsburgh in Aeronomy in 1974. He is a University of Maryland, Baltimore County employee serving in a mobility assignment to NOAA.



Henry Helvajian, The Aerospace Corp., USA

Dr. Henry Helvajian is a senior scientist at The Aerospace Corporation. Aerospace is a private, nonprofit corporation created in 1960 by Congressional decree with the goal to provide research, development, and advisory services to the US Government in the area of space systems development.

Henry Helvajian joined The Aerospace Corporation in 1984. He has worked on gas phase photochemistry and kinetics of activated radical species for chemical laser development and on the photophysical processes of low fluence laser/material interaction phenomenon. In 1992 he began investigations on the applications of microsystems (MEMS) to space systems and in the miniaturization of satellites and satellite subsystems. He has been involved in the design of the first 1 kg mass nanosatellite and in the development of various space microthrusters. Recently, he has been developing a laser processing technique for the fabrication of MEMS in glass/ceramic materials and in the development of the world’s first all glass/ceramic satellite.

AIO Plenary Session

Monday, 25 June 14:00–15:00

Cypress 4



Scott McEldowney, Microsoft, USA

Scott McEldowney is a principal engineer at Microsoft Corporation. He has spent his 3 years at Microsoft working on the development of Natural User Interface technologies based on gesture recognition. Prior to Microsoft, Scott worked for 18 years in the Advanced Optical Technology division of JDSU developing optical components sub-

systems for consumer electronics, medical instrumentation, and aerospace. Scott holds a MS degree in Mechanical Engineering and PhD in Optical Sciences.

Joint Conference Reception

Monday, 25 June, 18:30–20:00

The Dolphins on the Upper Plaza

The reception will feature light fare and is open to all registrants.

Joint Poster Session

Tuesday, 26 June, 17:30–19:00

The Dolphins on the Upper Plaza

Poster presentations offer an effective way to communicate new research findings and provide an opportunity for lively and detailed discussion between presenters and interested viewers.

Postdeadline Paper Presentations

The program committees of AIO, COSI, ORS, OF&T, and SENSORS accepted postdeadline papers for presentation. The purpose of postdeadline sessions is to give participants the opportunity to hear new and significant materials in rapidly advancing areas. Only those papers judged to be truly excellent and compelling were accepted.

For more information, including a complete schedule of talks, abstracts and papers, see the separate Postdeadline papers booklet.

OSA Corporate Associates: Executive Speaker Series with Michael Silver, American Elements, USA

Wednesday, 27 June, 17:30–19:30
The Dolphins on the Upper Plaza

Sit down for an entertaining and intimate conversation with Michael Silver, Chief Executive Officer, American Elements as he responds to questions from Dr. Stephen Jacobs, from The University of Rochester, about his observations on the current and future demand of Rare Earth, his career path, and personal perspectives. Mr. Silver was one of the first Americans to establish a direct production and distribution supply chain from the rare earth mines in Inner Mongolia, China to North America and Europe and is credited with making American Elements an early participant in many now billion dollar growth industries including solar energy, fuel cells, optical telecommunications and next generation pharmaceuticals.

The program begins with a networking reception, followed by a brief student award ceremony and then a one-on-one interview with audience questions at the end.

Presented in collaboration with the OSA Fabrication, Design and Instrumentation Division.

IS Best Student Paper Award

This year the OSA Imaging Systems and Applications (IS) topical meeting established an award for the best student paper. The decision of the best student paper is made by an award committee that will judge the technical merit of qualifying student submissions that were accepted in the program. The best paper will be recognized during the meeting. This award is sponsored by Canon U.S.A. Inc.

OF&T Best Student Paper Award & Presentation

The OF&T Best Student Paper Award has been established to encourage excellence in research and scientific presentation skills in the student optics community. Awards include a cash prize and a certificate. There will be first- and second-place winners for both oral and poster presentations.

Students participating in the competition are noted within the abstracts section of this program. Please support the next generation of optical engineers and scientists by attending the student presentations and the awards presentation.

Robert S. Hilbert Memorial Student Travel Grant

Established in 2009 in memory of Robert S. Hilbert, President and Chief Executive Officer of Optical Research Associates (ORA), this program recognizes the research excellence of students in the areas of optical engineering, lens design and/or illumination design. Grant has been awarded to two students presenting their work at the Imaging and Applied Optics: OSA Optics and Photonics Congress. The grant is sponsored by ORA, and administered by OSA Foundation.

Anthony Visconti, *School of Engineering and Applied Sciences, Univ. of Rochester, USA*

IM2C.2, Large Diameter Radial Gradient-Index Lenses Fabricated by Ion Exchange

Matthew Barnum, *College of Optical Sciences, Univ. of Arizona, USA*

CM2B.5, Experimental Comparison of Computational Approaches to Focus Invariant Optical Systems

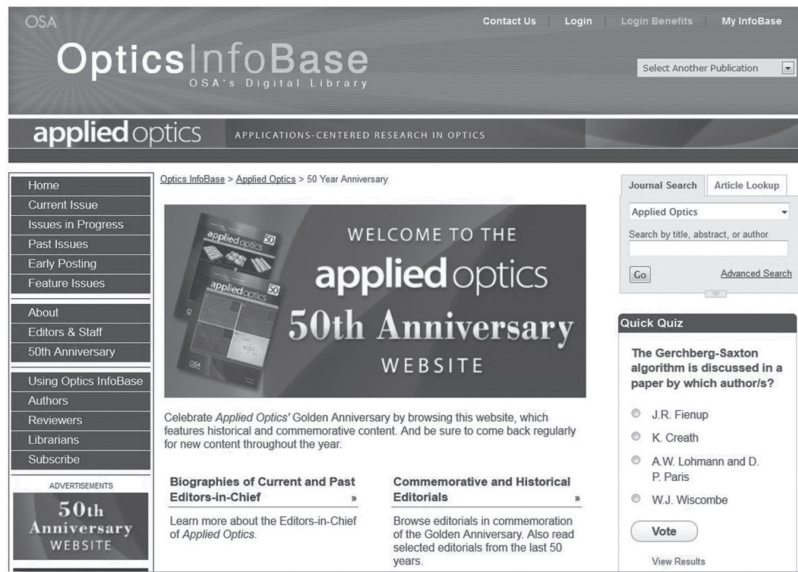
Exhibit Hall

The Dolphins on the Upper Plaza

Monday, 25 June	18:30–20:00	Welcome Reception
Tuesday, 26 June	10:00–10:30	Exhibit Hall & Coffee Break
	15:00–15:30	Exhibit Hall & Coffee Break
	17:30–19:00	Joint Poster Session
Wednesday, 27 June	10:00–10:30	Exhibit Hall & Coffee Break
	15:30–16:00	Exhibit Hall & Coffee Break

IMAGING AND APPLIED OPTICS CONGRESS ATTENDEES:

Celebrate *Applied Optics'* 50th Anniversary with us!

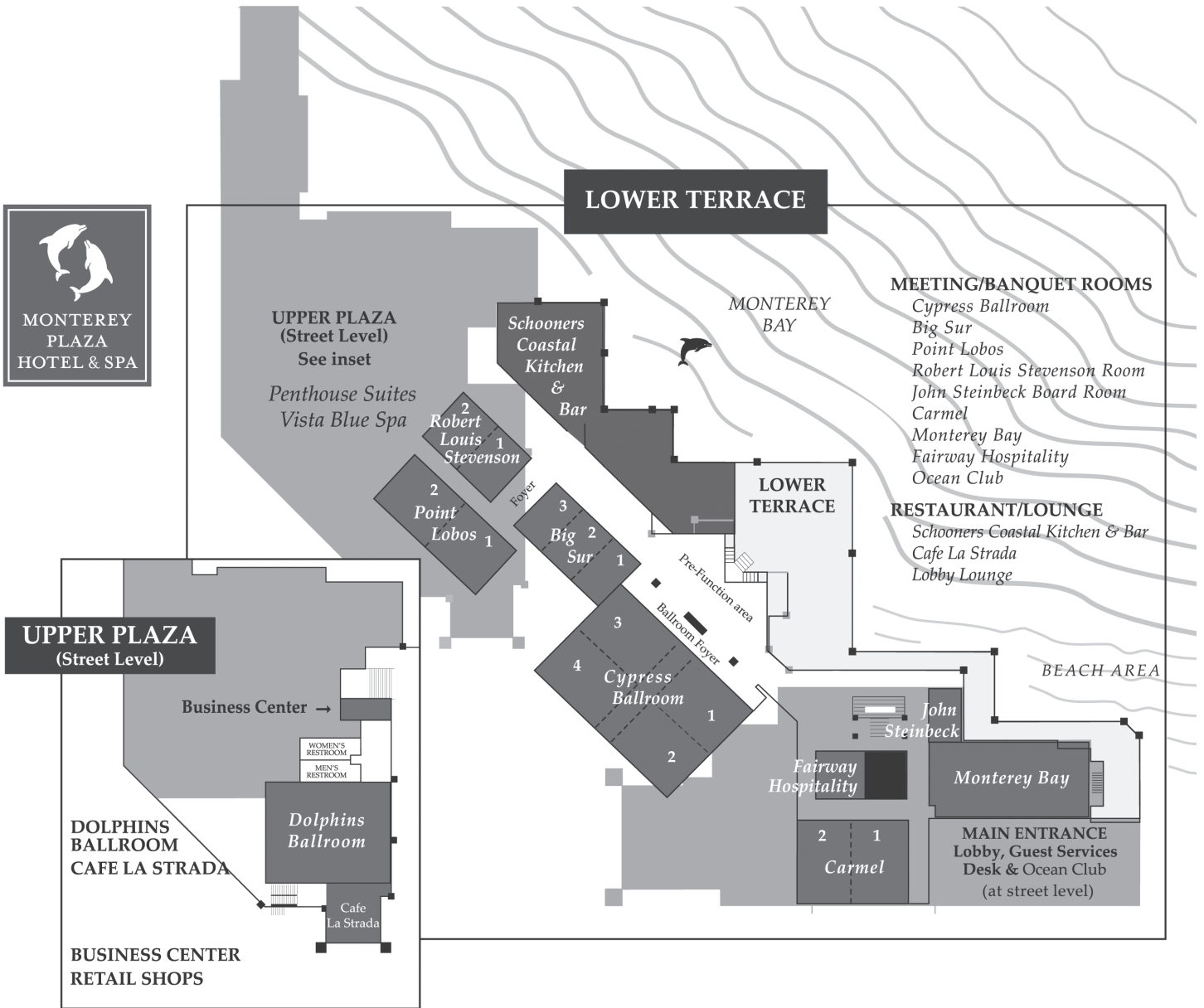


OSA is continuing its yearlong celebration of the 50th anniversary of *Applied Optics* with you!

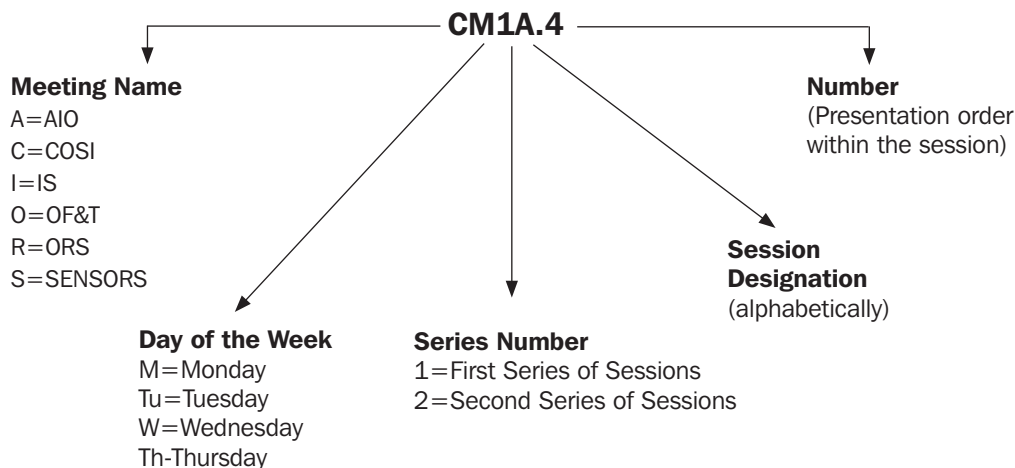
As a conference attendee, you'll receive an *Applied Optics* anniversary booklet, which features the 50 most cited articles from the journal's history as well as biographies of the journal's current and former Editors-in-Chief. You'll also receive a commemorative gift as a token of our appreciation for your support.

To stay up-to-date with *Applied Optics'* anniversary,
visit <http://ao.osa.org/anniversary>.


Monterey Plaza Hotel



Explanation of Session Codes



The first letter of the code designates the meeting (For instance, A=AIO, C=COSI, I=IS, O=OF&T, R=ORS, S=SENSORS, J=Joint Session). The second element denotes the day of the week (Monday=M, Tuesday=Tu, Wednesday=W, Thursday=Th). The third element indicates the session series in that day (for instance, 1 would denote the first parallel sessions in that day). Each day begins with the letter A in the fourth element and continues alphabetically through a series of parallel sessions. The lettering then restarts with each new series. The number on the end of the code (separated from the session code with a period) signals the position of the talk within the session (first, second, third, etc.). For example, a presentation coded CTu1A.4 indicates that this paper is part of COSI (C) and is being presented on Tuesday (Tu) in the first series of sessions (1), and is the first parallel session (A) in that series and the fourth paper (4) presented in that session.

Invited papers are noted with 

Plenaries are noted with 

Captured Content Sessions are noted with 

New Features for OSA Topical Meetings

Online Access to Technical Digest Now Available!

Full Technical Attendees now have an alternate way to access the digest papers at the meeting. Access the papers through Optics InfoBase (<http://www.opticsinfobase.org/conferences.cfm>) using the same login email address and password provided during the meeting registration process. Access is limited to Imaging and Applied Optics Congress Full Technical Attendees only.

Recorded Technical Sessions on Demand

We are delighted to announce that your 2012 Imaging and Applied Optics Congress technical registration includes a valuable new enhancement! A portion of the sessions at this year's congress are being digitally captured for on-demand viewing. All captured content from listed sessions will be live for viewing within twenty-four hours of being recorded. Just look for the symbol in the Agenda of Sessions and abstracts to easily identify the presentations being captured. Content will be available for 60 days following the Congress. To access it visit OSA's Media Library (http://www.osa.org/video_library/Technical_Sessions_Symposia.aspx) and selecting Imaging Congress from the list on the left hand side.

Agenda of Sessions — Sunday, 24 June

15:00–18:00	Registration , <i>Fairway Foyer on Lower Terrace</i>
-------------	---

— Monday, 25 June

	Cypress 4	Cypress 1 & 2	Cypress 3	Point Lobos	Big Sur	Carmel
	AIO	COSI	IS	OF&T	ORS	SENSORS
07:00–18:00	Registration , <i>Fairway Foyer on Lower Terrace</i>					
08:00–10:30	JM1A • Opening General Session , <i>The Dolphins on the Upper Plaza</i> ▶					
10:30–11:00	Coffee Break , <i>Cypress Foyer on Lower Terrace</i>					
11:00–12:30	AM2A • Emerging Technology (ends at 13:00)	CM2B • Computational High Depth-of-Field Imaging	IM2C • Imaging Lens Technologies	OM2D • Optical Materials	RM2E • New Uses of Optical Remote Sensing	SM2F • Devices and Systems for Laser-based Sensors
12:30–14:00	Lunch , <i>on your own</i>					
14:00–16:00	AM3A • Wow, You Can Do All This With Optical Systems ▶	CM3B • Optical Coding and Microscopy	IM3C • Imaging Optics	OM3D • Polishing	RM3E • Current and Future Imaging Systems	SM3F • Digital Holography and Raman Scattering
16:00–16:30	Coffee Break , <i>Cypress Foyer on Lower Terrace</i>					
16:30–18:30	AM4A • LIBS ▶	CM4B • Compressive & Spectral Imaging	IM4C • Medical Imaging and Microscopy	OM4D • Figuring and Finishing Science		SM4F • Fiber Gratings and Displacement Sensors
18:30–20:00	Joint Conference Reception & Exhibit Hall Opening , <i>The Dolphins on the Upper Plaza</i>					

Key to Conference Abbreviations

AIO	Applied Industrial Optics: Spectroscopy, Imaging, & Metrology
COSI	Computational Optical Sensing and Imaging
IS	Imaging Systems and Applications
OF&T	Optical Fabrication and Testing
ORS	Optical Remote Sensing of the Environment
SENSORS	Optical Sensors

Agenda of Sessions — Tuesday, 26 June

	Cypress 4	Cypress 1 & 2	Cypress 3	Point Lobos	Big Sur	Carmel
	AIO	COSI	IS	OF&T	ORS	SENSORS
07:00–18:00	Registration, Fairway Foyer on Lower Terrace					
08:00–10:00	ATu1A • Industrial Spectroscopy	ITu1C • Military Applications	CTu1B • Aperture Synthesis, Fourier Optics, Coherence ▶	OTu1D • Optical Testing I	RTu1E • Sensor Fusion and Lidar I	STu1F • Temperature and Photonic Crystal Fiber Sensing
10:00–10:30	Exhibit Hall & Coffee Break, The Dolphins on the Upper Plaza					
10:30–12:00	ATu2A • Micro-Optical Systems (ends at 12:30)	ITu2C • Hyperspectral Imaging	CTu2B • Image Restoration ▶	OTu2D • Optical Testing II	RTu2E • Sensor Fusion and Lidar II	STu2F • Gas and Voltage Sensing
12:00–13:30	Lunch, on your own					
13:30–15:00	ATu3A • Optical Systems for the Food Industry (13:20 – 15:10)	CTu3B • Compressive Imaging	ITu3C • Phase Space in Imaging ▶	OTu3D • Assembly, Alignment and Control		STu3F • Distributed and Acoustic Sensors
15:00–15:30	Exhibit Hall & Coffee Break, The Dolphins on the Upper Plaza					
15:30–17:30	ATu4A • Optical Design and Packaging	CTu4B • Computational Imaging	ITu4C • Image Sensors ▶	OTu4D • Nanostructures and Films		STu4F • Micro and Nano-Engineered Sensors
17:30–19:00	JTu5A • Joint Poster Session, The Dolphins on the Upper Plaza					

Key to Conference Abbreviations

AIO	Applied Industrial Optics: Spectroscopy, Imaging, & Metrology
COSI	Computational Optical Sensing and Imaging
IS	Imaging Systems and Applications
OF&T	Optical Fabrication and Testing
ORS	Optical Remote Sensing of the Environment
SENSORS	Optical Sensors

Agenda of Sessions — Wednesday, 27 June

	Cypress 1 & 2	Cypress 3	Cypress 4	Point Lobos
	Joint Sessions	AIO & IS	COSI & SENSORS	OF&T
07:00–18:00	Registration , <i>Fairway Foyer on Lower Terrace</i>			
08:00–10:00	JW1A • Resolution Limits & Spectral Imaging (IS & COSI) ▶	AW1B • Energy and Applied Optics	SW1C • THz Sensors I	OW1D • Process Engineering
10:00–10:30	Exhibit Hall & Coffee Break , <i>The Dolphins on the Upper Plaza</i>			
10:30–12:00	JW2A • Sensing with Optical Fiber (AIO & SENSORS) ▶ (ends at 12:15)	IW2B • Digital Imaging	CW2C – COSI Postdeadline Paper Session	OW2D • Freeform Optics
12:00–13:30	Lunch , <i>on your own</i>			
13:30–15:30	JW3A • Computational Imaging Sensors (COSI & IS) ▶	AW3B • What's next in Applied Imaging	SW3C • THz Sensors II	OW3D • Large Optics
15:30–16:00	Exhibit Hall & Coffee Break , <i>The Dolphins on the Upper Plaza</i>			
16:00–17:30	JW4A • Applied Imaging (AIO & IS) ▶ (ends at 18:05)		SW4C • SENSORS Postdeadline Paper Session	OW4D • OF&T Postdeadline Paper Session
17:30–19:30	OSA Corporate Associates: Executive Speaker Series Michael Silver, CEO of American Elements <i>The Dolphins on the Upper Plaza</i>			

— Thursday, 28 June

	Cypress 3	Cypress 1 & 2
	AIO	SENSORS
07:00–15:00	Registration , <i>Fairway Foyer on Lower Terrace</i>	
8:00–10:00	ATH1A • Spectroscopy, Lasers, and Imaging, Oh My! ▶	STh1B • Optical Chemical and Biological Sensors: I
10:00–10:30	Coffee Break , <i>Cypress Foyer on Lower Terrace</i>	
10:30–12:00	ATH2A • Pharmaceutically and Medically Applied Optics ▶ (ends at 12:30)	STh2B • Optical Chemical and Biological Sensors: II
12:00–13:30	Lunch , <i>on your own</i>	
13:30–15:00		STh3B - Imaging

Key to Conference Abbreviations

AIO	Applied Industrial Optics: Spectroscopy, Imaging, & Metrology
COSI	Computational Optical Sensing and Imaging
IS	Imaging Systems and Applications
OF&T	Optical Fabrication and Testing
ORS	Optical Remote Sensing of the Environment
SENSORS	Optical Sensors

The Dolphins on the Upper Plaza

07:00–18:00 **Registration**, *Fairway Foyer on Lower Terrace*

08:00–10:30

JM1A • Opening General Session ▶

JM1A.1 • 08:15

Assessing a New Imaging Modality, Joseph Goodman, *Stanford Univ., USA*. I will consider some of the factors to be considered when assessing the capability and limitations of a new imaging modality, using holography in the 60's and 70's as an example.

JM1A.2 • 08:45

Image Quality Assessment: How Blind is Blind?, Al Bovik, *Univ. of Texas at Austin, USA*. Blind Image Quality Assessment (Blind IQA) is usually synonymous with “no-reference” IQA, viz., without a pristine image available for quality comparison. However, other sources of information are used to design IQA models: human opinion scores, mathematical models of distortion, perceptual models; statistical models of distorted images, and statistical models of images that are not distorted.

JM1A.3 • 09:15

Survey of Applications for Ocean Color and Imagery from EOS-MODIS and Early Results from NPP-VIIRS, Bruce Guenther, *NOAA-JPSS & University of Maryland of Baltimore County, USA*. Interesting and useful images come from orbiting MODIS and VIIRS instruments, including the ~375-m resolution VIIRS imaging bands and nighttime images from the Day/Night Band. There are five VIIRS imaging bands out to 11450 nm.

JM1A.4 • 09:45

Small Satellites: The Desire for a Mass Producible, Mass Customizable Nanosatellite, Henry Helvajian, *The Aerospace Corp., USA*. This talk describes the role of small satellites, and work at The Aerospace Corporation to develop an integrated cold gas propulsion system for a 1 kg class nanosatellite vehicle made largely from photostructurable glass ceramics.

10:30–11:00 **Coffee Break**, *Cypress Foyer on the Lower Terrace*

NOTES

Cypress 4

Applied Industrial Optics: Spectroscopy,
Imaging, & Metrology

Cypress 1 & 2

Computational Optical Sensing and Imaging

Cypress 3

Imaging Systems and Applications

These concurrent sessions are grouped across two pages. Please review both pages for complete session information.

11:00–13:00**AM2A • Emerging Technology**Joseph Dallas; Avo Photonics Inc, USA,
President**AM2A.1 • 11:00** **Invited**

Monolithic Waveguide Spectrometer for Mid-Infrared Applications, Eric J. Olson¹; ¹Spectro Inc., USA. Spectro Inc. has commercialized a ruggedized mid-IR spectrometer platform based on a unique wedge waveguide design that integrates input optics, diffraction grating, and array detector into a monolithic system operating in the 2.5 to 12 micron wavelength range.

AM2A.2 • 11:40

Simultaneous High-Resolution and High-Throughput Spectrometer Design Based on Virtual Slit Technology, Bradley Schmidt¹, Jeffrey Meade¹, Bradford B. Behr³, Arsen R. Hajian²; ¹Arjae Spectral, Canada; ²Tornado Medical Systems, Canada; ³Arjae Spectral, USA. The classic trade-off between resolution and throughput in a dispersive spectrometer is eliminated using virtual slit technology. An optimized spectrometer incorporating a virtual slit designed from the ground up is experimentally demonstrated.

AM2A.3 • 12:00

Study of the two-dimensional Spectrum-folded Spectrometer, Liang-Yao Chen¹, Jian-Ke Chen¹, Song-You Wang¹, Rong-Jun Zhang¹, We-Jie Lu¹, Yue-Mei Yang¹, Hai-Bing Zhao¹, Jing Li¹, Rong-Er Zheng², Ji-Dong Lu³, Shun-Chun Yao³; ¹Fudan Univ., China; ²Ocean Univ. of China, China; ³South China Univ. of Technology, China. The spectrum-folded spectrometer with a two-dimensional CCD array detector combined with 10 gratings working in the full 200–1000nm wavelength region is designed, and has the advantage applied in the rapid spectral extraction and analysis fields.

11:00–12:30**CM2B • Computational High Depth-of-Field Imaging**Michael Gehm; Univ. of Arizona, USA,
President**CM2B.1 • 11:00** **Invited**

Focus in Multiscale Imaging Systems, David J. Brady¹; ¹Duke Univ., USA. We consider first order lens design for micro-camera-based focus in multiscale cameras, we compare focal and spectral tomography and we compare dynamic focal scanning with alternative EDoF and focal stacking strategies.

CM2B.2 • 11:30

High Resolution Image Reconstruction for Plenoptic Imaging Systems using System Response, Sapna Shroff¹, Kathrin Berkner¹; ¹Ricoh Innovations, Inc., USA. Plenoptic imaging systems with a microlens array imaging the pupil at the sensor typically produce low resolution images. We introduce an inverse problem solver using the system response to obtain high resolution image reconstructions.

CM2B.3 • 11:45

Improved Extended Depth-of-Field Microscopy through PSF Engineering and Robust Processing, Shuai Yuan¹, Chrysanthe Preza¹; ¹Univ. of Memphis, USA. Performance investigation of improved extended depth-of-field microscopy achieved with point-spread function engineering to reduce image artifacts due to depth-induced aberrations and processing that is robust to system noise.

CM2B.4 • 12:00

Experimental Verification of Computational Superposition Imaging for Compensating Defocus and Off-axis Aberrated Images, Tomoya Nakamura¹, Ryoichi Horisaki¹, Jun Tanida¹; ¹Osaka Univ., Japan. An aberration compensation method with computational superposition imaging is demonstrated. In this method, aberrated images are superposed to equalize the point spread function three-dimensionally and the superposed image is deconvolved with a filter.

11:00–12:30**IM2C • Imaging Lens Technologies**

Peter Catrysse; Stanford Univ., USA, President

IM2C.1 • 11:00 **Invited**

New Gradient-index Materials and Designs with Polymers, Glass and ALON, Duncan T. Moore¹; ¹Univ. of Rochester, USA. The Univ. of Rochester is researching new gradient-index (GRIN) materials and designs with polymers, glass and ALON. GRIN materials open up additional degrees of freedom in optical system design.

IM2C.2 • 11:30

Large Diameter Radial Gradient-Index Lenses Fabricated by Ion Exchange, Anthony Visconti¹, Duncan T. Moore¹, Julie L. Bentley¹; ¹The Institute of Optics, Univ. of Rochester, USA. Large diameter radial gradient-index (GRIN) lenses were fabricated using ion exchange in titania silicate glasses. Simple doublet designs are used to illustrate the potential for new GRIN elements to correct color in complex imaging systems.

IM2C.3 • 11:45

Polymer GRIN lens design, Erin F. Fleet¹, Guy Beadie¹, James Shirk¹; ¹US Naval Research Laboratory, USA. Lenses with spherically contoured layered polymer gradient index (GRIN) distributions can be tailored to mitigate multiple types of aberrations, including spherical and chromatic. We will present modeling, designs and testing of GRIN lens systems.

IM2C.4 • 12:00 **Invited**

Large-Format Tunable Fluidic Lenses for High-Resolution Rapid Focusing, Robert G. Batchko¹, Sam Robinson¹, Jei-Yin Yiu¹, Andrei Szilagyi¹, Justin Mansell¹; ¹Holochip Corporation, USA; ²Active Optical Systems, LLC, USA. We present optical analysis of electrically-actuated adaptive fluidic lenses having apertures of 10 mm and 40 mm. Zernike decomposition and resolution testing is presented for the 10-mm aperture lens. Focal power and imaging resolution characteristics of the 40-mm aperture lens are provided. The data for the lenses show both formats are suitable for numerous adaptive lens applications demanding high optical quality.

These concurrent sessions are grouped across two pages. Please review both pages for complete session information.

11:00–12:30

OM2D • Optical Materials

Oliver Faehnle; FISBA OPTIK AG, Switzerland, President

OM2D.1 • 11:00 **Invited**

The Role of Ce³⁺ vs. Ce⁴⁺ during the Polishing of Silicon Dioxide and Silicon Nitride Films using Ceria Abrasives, S. V. Babu¹, Veera P. Dandu^{2,1}; ¹Center for Advanced Materials Processing, Clarkson Univ., USA; ²Intel, USA. The role played by the different cerium oxidation states of cerium (Ce³⁺ vs. Ce⁴⁺) during the chemical mechanical planarization of silica and related substrate materials, including Si₃N₄ films will be discussed.

OM2D.2 • 11:30 **Invited**

Synthetic Fused Silica: Unique Material Properties and Some New Applications, Ralf Takke¹; ¹Division Optics, Heraeus Quarzglas GmbH, Germany. Synthetic fused silica, one of the purest man made materials, shows unique optical properties like ultralow absorption, birefringence and high power laser durability in the UV and IR. Some new applications will be discussed.

OM2D.3 • 12:00 **Invited**

Withdrawn

11:00–12:30

RM2E • New Uses of Optical Remote Sensing

Charles Bachmann; US Naval Research Laboratory, USA, President

RM2E.1 • 11:00

Use of Imaging Spectrometer Data and Multispectral Imagery for Improved Earthquake Response, Fred A. Kruse^{1,2}, Chris C. Clasen², Angela M. Kim^{1,2}, Sarah C. Carlisle²; ¹Physics Department, Naval Postgraduate School, USA; ²Remote Sensing Center, Naval Postgraduate School, USA. Multispectral imagery and imaging spectrometer data are used to develop prototype map products for improved earthquake response. A tiered approach keyed to post-event communications infrastructure is directed at providing critical information to emergency services personnel.

RM2E.2 • 11:15

Determining Bathymetry Near Oahu, Hawaii Using WorldView-2 Imagery Acquired at Multiple Angles, Krista Lee^{1,2}, Richard C. Olsen^{1,2}, Fred A. Kruse^{1,2}; ¹Physics Department, Naval Postgraduate School, USA; ²Remote Sensing Center, Naval Postgraduate School, USA. This research uses multispectral imagery data to investigate whether acquisition angle plays a role in depth determination in shallow coastal areas. WorldView-2 (WV-2) data acquired on 30 July 2011 over Oahu are used.

RM2E.3 • 11:30

A Dark Channel Approach to Quantify Aerosol Properties Using a Commercial Digital Camera, David Stoker¹, Erik Matlin¹; ¹SRI International, USA. We show how a digital image restoration algorithm used for haze removal and a consumer camera can be used to measure aerosol optical thickness and aerosol particle size parameters.

RM2E.4 • 11:45 **Invited**

HICO Observations of Biological and Sediment-Transport Processes in Monterey Bay, California, John Ryan¹, Nicholas Tufillaro², Curtiss Davis²; ¹Monterey Bay Aquarium Research Institute, USA; ²Oregon State Univ., USA. Coastal marine biological and sediment-transport processes are examined with HICO (Hyperspectral Imager for the Coastal Ocean) data and other remote sensing and in situ observations. The value of HICO spatial and spectral resolution is illustrated.

11:00–12:30

SM2F • Devices and Systems for Laser-based Sensors

Yoshio Hayasaki; Utsunomiya Univ. Japan, President

SM2F.1 • 11:00 **Invited**

SLM-based Multipoint Vibrometry, Tobias Haist¹, Christian Lingel¹, Wolfgang Osten¹, Christian Rembe², Marcus Winter², Moritz Giesen²; ¹Institute fuer Technische Optik, Univ. of Stuttgart, Germany; ²Polytec, Germany. We present a spatial light modulator-based multipoint vibrometer realizing 14 independent fast heterodyne interferometry channels for measuring vibrations. The positions of the measurement spots on the object are controlled using dynamic holography.

SM2F.2 • 11:30 **Invited**

Thermal Characteristics of Rare-earth-doped Optical Fibers and their Applications to Temperature Sensing, Yoonchan Jeong¹, Luis A. Vazquez-Zuniga¹, Seung Jong Lee¹, Geunchang Choi¹, Hyuntai Kim¹; ¹Seoul National Univ., Republic of Korea. We investigate thermal characteristics of rare-earth-doped optical fibers with particular attention to ytterbium- and erbium/ytterbium-based optical fibers when they are highly pumped, and discuss their prospects for applications to temperature sensing.

SM2F.3 • 12:00

Improved Interaction Geometries for Efficient Acousto-Optic Beam Deflection Sensing in Air, Barmak Heshmat¹, Thomas E. Darcie¹, Hamid Pahlevaninezhad¹, Keith Taylor¹; ¹Univ. of Victoria, Canada. We demonstrate two different approaches for intensification of acousto-optic beam deflection in air. Both approaches do not require increasing acoustic amplitude or frequency. Measured results show up to eight fold improvement.

Cypress 4

Applied Industrial Optics: Spectroscopy,
Imaging, & Metrology

Cypress 1 & 2

Computational Optical Sensing and Imaging

Cypress 3

Imaging Systems and Applications

These concurrent sessions are grouped across two pages. Please review both pages for complete session information.

AM2A • Emerging Technology—Continued

AM2A.4 • 12:20 **Invited**

Dielectric Optical Resonators for Mechanical and Chemical Sensing Using Frequency Combs, Gianluca Gagliardi¹; ¹CNR-Istituto Nazionale di Ottica, Italy. Strain sensing at the 10-13 level is performed using a fiber Bragg-grating resonator interrogated by an optical-comb stabilized laser. The comb is also used as a coherent radiation source for fiber cavity-enhanced spectroscopy of liquids.

CM2B • Computational High Depth-of-Field Imaging—Continued

CM2B.5 • 12:15

Experimental Comparison of Computational Approaches to Focus Invariant Optical Systems, Joshua I. Brent¹, Matt Barnum¹, Saul Corrales², Nan Ding¹, Kate Green², Lena Wolfe¹; ¹College of Optical Sciences, Univ. of Arizona, USA; ²System & Industrial engineering Department, Univ. of Arizona, USA. Many aerospace sensor platforms have a fixed opto-mechanical layout due to harsh environmental conditions. This design decision results in tight opto-mechanical tolerances. An experimental test bed of computational approaches to alleviate this constraint is presented.

IM2C • Imaging Lens Technologies—Continued

12:30–14:00 Lunch, on your own

14:00–16:00

AM3A • Wow, You Can Do All This With Optical Systems 

Marion O'Farrell; SINTEF, Norway, *Presider*

14:00–16:00

CM3B • Optical Coding and Microscopy

Andrew Harvey; Univ. of Glasgow, UK, *Presider*

14:00–16:00

IM3C • Imaging Optics

Zeev Zalevsky; Bar-Ilan Univ., Israel, *Presider*

AM3A.1 • 14:00 **Plenary**

The Kinect Story, Scott McEldowney¹; ¹Microsoft, USA. Kinect is a state-of-the-art depth, video, and audio sensor that allows individuals to naturally interact with devices. This presentation summarizes Kinect development focusing on challenges involved in transition from technology to product.

CM3B.1 • 14:00 **Invited**

Tunable Complex Amplitude Masks for Computer Imaging, Jorge Ojeda-Castaneda¹; ¹Universidad de Guanajuato, Mexico. We present a method that uses tunable complex amplitude masks, for acquiring and pre-processing pictures, which are suitably post-processed and average into a final image. We visualize the method in terms of the ambiguity function.

IM3C.1 • 14:00 **Invited**

Design and Performance of Tailored EDof Digital Cameras, Nicholas George¹; ¹Univ. of Rochester, USA. Extended depth of field cameras have been designed and evaluated with $f/\#$ 2.2 to 2.5 and superior image quality with diffraction-limited performance is obtained from 125 mm to infinity as verified by slanted edge and Strehl ratio tests.

CM3B.2 • 14:30

Design of Double-helix Point Spread Functions for 3D Super-resolution Imaging, Ginni Grover¹, Keith DeLuca², Sean Quirin¹, Jennifer DeLuca², Rafael Piestun¹; ¹Department of Electrical, Computer and Energy Engineering, Univ. of Colorado at Boulder, USA; ²Department of Biochemistry and Molecular Biology, Colorado State Univ., USA. The application specific design of double-helix point spread functions enables control of parameters such as the efficiency and depth of field. We demonstrate a design and implementation in single molecule super-resolution microscopy.

IM3C.2 • 14:30

Tricks in Analyzing non-Conventional Optical Systems, Gisele Bennett¹; ¹GTRI, Georgia Institute of Technology, USA. Fresnel propagation that may be used to simplify the analysis of non-conventional imaging in particular Lukosz-type optical systems.

CM3B.3 • 14:45

Chromatic depth from defocus : a theoretical and experimental performance study, Pauline Trounev¹, Frédéric Champagnat¹, Guy Le Besnerais¹, Guillaume Druart¹, Jérôme Idier²; ¹ONERA-The French Aerospace Lab, France; ²LUNAM Université, IRCCyN, France. We present a new computational imaging system which combines a chromatic lens and a dedicated processing in order to extract depth. A theoretical performance model of this system is then compared to experimental results.

IM3C.3 • 14:45 **Invited**

Optical Freeform Surfaces in Integrated Optical Microsystems, Stefan Sinzinger¹; ¹Technische Optik, Technische Universität Ilmenau, Germany. Freeform surfaces provide degrees of freedom which are essential specifically for the optimization and integration of optical microsystems. We discuss design, optimization as well as fabrication concepts and applications of (micro-)systems involving such non-conventional surfaces.

These concurrent sessions are grouped across two pages. Please review both pages for complete session information.

OM2D • Optical Materials—Continued**RM2E • New Uses of Optical Remote Sensing—Continued****SM2F • Devices and Systems for Laser-based Sensors—Continued****RM2E.5 • 12:15**

The Portable Remote Imaging Spectrometer (PRISM) Coastal Ocean Sensor, Pantazis Mouroulis¹, Byron E. Van Gorp¹, Robert O. Green¹, Michael Eastwood¹, Daniel W. Wilson¹, Brandon Richardson¹, Heidi Dierssen²; ¹Jet Propulsion Laboratory, USA; ²Marine Sciences, Univ. of Connecticut, USA. We present characterization measurements of PRISM, an airborne pushbroom imaging spectrometer for the coastal ocean with high uniformity, high signal to noise ratio and low polarization sensitivity.

SM2F.4 • 12:15

Plasmonic Effects of Ag Nanocube with Silica Shell on Fluorescence Enhancement, Hansik Yun¹, Dawoon Choi¹, Taerin Chung¹, Byoungho Lee²; ¹Electrical Engineering, Seoul National Univ., Republic of Korea. Silver nanocubes with silica shell could highly enhance the fluorescence intensity between the nanoparticles and metal layer because of their plasmonic coupling. They have potential applications in chemical and biological sensing.

12:30–14:00 Lunch, on your own

14:00–16:00

OM3D • Polishing

Dave Aikens; Savvy Optics Corp., USA, President

14:00–16:00

RM3E • Current and Future Imaging Systems

Curtiss Davis; Oregon State Univ., USA, President

14:00–16:00

SM3F • Digital Holography and Raman Scattering

Yoonchan Jeong; Seoul National Univ., Republic of Korea, President

OM3D.1 • 14:00 Invited

A Tribute to Norm Brown's Technical Contributions to the Field of Optical Fabrication and Testing, Jessica D. Nelson¹, Robert Wiederhold²; ¹Optimax Systems Inc, USA. We will pay tribute to Norman J. Brown as we review his technical contributions to the field of optical fabrication and testing during this presentation.

RM3E.1 • 14:00

Ten Years of Data Products and Science Findings from the Atmospheric Infrared Sounder (AIRS) on Aqua, Thomas Pagano¹; ¹NASA/JPL, USA. The Atmospheric Infrared Sounder enables retrievals of temperature and water vapor profiles and a wide range of geophysical variables. We discuss the accuracy and stability of the AIRS data and major findings over the last decade.

SM3F.1 • 14:00 Invited

Adaptive Optics by Digital Holography, Myung K. Kim¹; ¹Physics, Univ. of South Florida, USA. We present new techniques of adaptive optics by digital holography, with potential applications from ophthalmic to astronomical imaging systems. Wavefront sensors and modulators are replaced with digital holographic sensing and compensation processes.

RM3E.2 • 14:15

HICO On-Orbit Performance and Future Directions, Curtiss Davis¹, Nicholas Tufillaro¹, Jeffery Bowles², Bo-Cai Gao², Mike Corson², Bob Lucke²; ¹CEOAS, Oregon State Univ., USA; ²Remote Sensing Division, Naval Research Laboratory, USA. The Hyperspectral Imager for the Coastal Ocean (HICO) is flying on the International Space Station. Here we give a brief overview of HICO on-orbit performance and suggest future directions for imaging the coastal ocean.

SM3F.2 • 14:30 Invited

Parallel Phase-shifting Digital Holography for Recording 3-D Motion Pictures of Dynamic Phenomena, Yasuhiro Awatsuji¹, Takashi Kakue¹, Tatsuki Tahara¹, Peng Xia¹, Kenzo Nishio¹, Shogo Ura¹, Toshihiro Kubota², Osamu Matoba²; ¹Kyoto Institute of Technology, Japan; ²Kubota Holography Laboratory Corporation, Japan; ³Kobe Univ., Japan. Using parallel phase-shifting digital holography with a high-speed camera, the authors succeeded in phase-shifting interferometry at the rate of 180,000 frames/s. Motion pictures of three-dimensional image of dynamically moving objects were demonstrated.

OM3D.2 • 14:30 Invited

Polishing with a Vortex: A Decade in Hydrodynamic Radial Polishing, Erika Sohn^{1,2}; ¹Instituto de Astronomia UNAM, Mexico; ²Universidad Nacional Autonoma de Mexico, Mexico. We present a review of ten years of polishing with HyDRa, a deterministic polishing tool based on radial expulsion hydrodynamics. This system has reached maturity and has proven its ability to polish complex free-form surfaces.

RM3E.3 • 14:30

Validation of VIIRS Calibrations for Oceans, Bruce W. Guenther^{1,2}; ¹JPSS, NOAA-NESDIS, USA; ²JCET, Univ. of Maryland, Baltimore County, USA. New methods to create VIIRS ocean-color products are reviewed, with recommendations for handling an on-orbit NIR anomaly, exploiting hyperspectral characterization, and correcting for polarization in an operational data-processing environment.

RM3E.4 • 14:45 Invited

Mineral Mapping using Simulated Short-Wave-Infrared bands planned for DigitalGlobe WorldView-3 Data, Fred A. Kruse¹, Sandra Perry²; ¹Naval Postgraduate School, USA; ²Perry Remote Sensing LLC, USA. Airborne hyperspectral data were used to simulate imagery from DigitalGlobe's proposed WorldView-3 (WV-3) satellite. A proposed new band configuration, including eight additional short-wave-infrared channels, demonstrates improved capability for geologic mapping and other applications.

Cypress 4

Applied Industrial Optics: Spectroscopy,
Imaging, & Metrology

Cypress 1 & 2

Computational Optical Sensing and Imaging

Cypress 3

Imaging Systems and Applications

These concurrent sessions are grouped across two pages. Please review both pages for complete session information.

AM3A • Wow, You Can Do All This With Optical Systems—Continued

AM3A.2 • 15:00 **Invited**

Exploiting High Efficiencies in a Deep LED Water Treatment Device, *Oliver Lawal*¹, *Aquionics Inc, USA*. Water disinfection employing UV-C LEDs in lieu of mercury based technology has been heralded as a breakthrough poised on the brink of commercialization. Presented are results of an innovative UV LED reactor proving commercial readiness.

AM3A.3 • 15:40

Optical Fibre Based Scintillation Probe for Radiotherapy Dosimetry, *Sinead O'Keefe*¹, *Denis McCarthy*¹, *Peter Woulfe*², *John Cronin*², *Elfed Lewis*¹; ¹*Optical Fibre Sensors Research Centre, Univ. of Limerick, Ireland*; ²*Dept. of Radiotherapy Physics, Galway Clinic, Ireland*. A PMMA based plastic optical fibre coated with radiation sensitive inorganic scintillators, which fluoresce when exposed to ionising radiation, is presented for use in applications for monitoring radiation doses a patient receives during radiotherapy.

CM3B • Optical Coding and Microscopy—Continued

CM3B.4 • 15:00

Turbid Stochastic Optical Reconstruction Microscopy (TSTORM), *Jacob Lapenna*¹, *Jason W. Fleischer*¹; ¹*Electrical Engineering, Princeton Univ., USA*. Stochastic optical reconstruction microscopy (STORM) relies on time resolving overlapping point-spread functions (PSFs) to increase image resolution. Here, we extend STORM from diffraction-limited PSFs to those dominated by scattering.

CM3B.5 • 15:15

DEEP-dome: Towards Long-Working-Distance Aberration-Free Synthetic Aperture Microscopy, *Daniel Feldkhun*¹, *Kelvin H. Wagner*¹; ¹*ECEE, Univ. of Colorado at Boulder, USA*. A DEEP microscope synthesizes images from dynamic structured-illumination Fourier measurements using a single-element detector, enabling high-resolution imaging with aberrated optics. We describe wide-field 20cm-working-distance DEEP microscopy using a large 0.4 NA diamond-turned reflector.

CM3B.6 • 15:30

3D deconvolution Microscopy using a Microfluidic Tilted Channel, *Nicolas C. Pegard*¹, *Jason W. Fleischer*¹; ¹*Princeton Univ., USA*. We present a 3D microfluidic microscope. Focal stacks are recorded by observing samples flowing through a tilted microfluidic channel and then digitally deconvolved. Experimental results are shown on flowing yeast cells.

CM3B.7 • 15:45

Microfluidic Structured Illumination Microscope, *Chien-Hung Lu*¹, *Nicolas C. Pegard*¹, *Jason W. Fleischer*¹; ¹*Princeton Univ., USA*. We apply the principle of structured illumination to microfluidic microscopy. Sample flow across the illumination pattern automatically gives the necessary phase shifts. We experimentally demonstrate the technique by reconstructing a superresolution image of yeast cells.

IM3C • Imaging Optics—Continued

IM3C.4 • 15:15

Wave-Plate-Enhanced Retinal Birefringence Scanning for True Foveal Fixation Detection, *Kristina Irsch*¹, *Boris Gramatikov*¹, *Yi-Kai Wu*¹, *David Guyton*¹; ¹*School of Medicine, Johns Hopkins Univ., USA*. We use spinning and fixed wave plates, optimized using an algorithm and related computer program, based on Müller-Stokes matrix calculus, to enhance foveal fixation detection while minimizing interference from corneal birefringence in retinal birefringence scanning.

IM3C.5 • 15:30 **Invited**

Recent Advances in Imaging Through Scattering Media, *Demetri Psaltis*¹, *Ye Pu*¹, *Xin Yang*¹; ¹*Ecole Polytechnique Federale de Lausanne, Switzerland*. We will describe recent progress in using digital holography and second harmonic nanoparticles to focus light into scattering media. The nanoparticles act as beacons on which light is phase conjugated.

16:00–16:30 Coffee Break, Cypress Foyer on the Lower Terrace

These concurrent sessions are grouped across two pages. Please review both pages for complete session information.

OM3D • Polishing—Continued

OM3D.3 • 15:00 **Invited**

New Approaches to MRF®, Andrew W. Kulawiec¹, William Kordonski², Sergei Gorodkin¹; ¹QED Technologies Inc., USA. The discussed advancements in MRF technology offer greater flexibility and productivity in fabrication of modern optics. This is achieved with new efficient structural components, novel system configuration, high performance polishing fluids and improved control algorithms.

OM3D.4 • 15:30 **Invited**

Abrasive Jet Polishing Approaches to the Manufacture of Micro-optics with Complex Shapes, Oliver W. Faehnle¹; ¹FISBA OPTIK AG, Switzerland. Requirements for polishing of micro-aspheres are discussed identifying abrasive slurry jet techniques as possible solution featuring submillimeter footprints. Their application to the removal of submillimeter structures and the generation of micro-aspheres are presented.

RM3E • Current and Future Imaging Systems—Continued

RM3E.5 • 15:15

Multi-Slit Optimized Spectrometer: An Innovative Design for Geostationary Hyperspectral Imaging, Tim Valle¹, Chuck Hardesty¹, Curtiss Davis², Nicholas Tuffillaro², Michelle Stephens¹, William Good¹, Peter Spuhler¹; ¹Ball Aerospace & Technologies Corp., USA; ²Oceanic and Atmospheric Sciences, Oregon State Univ., USA. Multi-Slit Optimized Spectrometer is a spatial multiplexing hyperspectral imager designed to reduce mission cost and risk for hyperspectral sensing from geostationary orbit. The multi-slit prism design resulting in 50% telescope aperture reduction will be presented.

RM3E.6 • 15:30 **Invited**

Wide Field of View Hyperspectral Radiometer for Coastal Imaging from Polar Sun Synchronous Orbit, John Silny¹, Jeff Puschell¹; ¹Raytheon Company, USA. High spatial resolution wide FOV hyperspectral imaging spectroradiometry offers capability for isolating spectral radiance components in complex coastal waters. This paper reports on designs for hyperspectral coastal imagers that measure key data products from sun synchronous orbit.

SM3F • Digital Holography and Raman Scattering—Continued

SM3F.3 • 15:00 **Invited**

In vivo Molecular Labeling of Halogenated Volatile Anesthetics using Adaptively Phase-modulated Femtosecond Pulses, Kazuhiko Misawa^{1,2}; ¹Department of Applied Physics, Tokyo Univ. of Agriculture and Technology, Japan; ²Interdisciplinary Research Unit in Photon-Nano Science, Tokyo Univ. of Agriculture and Technology, Japan. We determined the low-frequency vibrational modes of one of the most representative volatile anesthetics molecules, sevoflurane, in a live squid giant axon by anti-Stokes Raman scattering microscopy using adaptively phase-modulated femtosecond pulses.

SM3F.4 • 15:30

Holographic three-dimensional Position Tracking of an Optically Trapped Gold Nanoparticle, Sato Akira¹, Yui Ohmura¹, Satoshi Hasegawa², Yoshio Hayasaki²; ¹Utsunomiya Univ., Japan. We demonstrate the three-dimensional position tracking of a 100nm-gold nanoparticle held in optical tweezers in solution using an in-line low-coherence digital holographic microscope with a spatial resolution of single nanometer.

SM3F.5 • 15:45

Filament-Based Impulsive Remote Raman Spectroscopy for Chemical Detection, Robert J. Levis¹; ¹Temple Univ., USA. The remote detection of gas phase molecules remains a challenge. Laser filamentation can be used to enhance the cross section for Raman scattering of gas phase molecules and the method will be presented along with applications to signature molecules.

16:00–16:30 Coffee Break, Cypress Foyer on the Lower Terrace

Cypress 4

Applied Industrial Optics: Spectroscopy,
Imaging, & Metrology

Cypress 1 & 2

Computational Optical Sensing and Imaging

Cypress 3


Imaging Systems and Applications

These concurrent sessions are grouped across two pages. Please review both pages for complete session information.

16:30–18:30

AM4A • LIBS Arel Weisberg; Energy Research Co, USA,
PresidentAM4A.1 • 16:30 

Measuring Thermal Properties of Coal with a Commercial Bench Top LIBS System, Joseph Craparo¹, Robert De Saro¹, Carlos Romero², Zheng Yao², Andrew Whitehouse³, Arel Weisberg¹; ¹Energy Research Co, USA; ²Energy Research Center, Lehigh Univ., USA; ³Applied Photonics Ltd., UK. Measurements with a bench top commercial LIBS system demonstrate that thermal properties of coal can be measured using LIBS. Knowledge of these properties is crucial for efficient operation of coal fired boilers in power plants and other industries.

AM4A.2 • 17:10 

Laser Induced Breakdown Spectroscopy (LIBS) for Real Time Analysis of Materials: Challenges and Future, Mohamad Sabsabi¹; ¹National Research Council Canada, Canada. We will give an overview about LIBS applications for on-line measurements such as molten materials, metal ore processing, effluents, slurries, liquids, nuclear industry etc., and we will present some approaches to improve the LIBS sensitivity.

AM4A.3 • 17:50 

Laser-Induced Breakdown Spectroscopy for the Standoff Detection of Explosive Residues, Jennifer Gottfried¹, Frank C. De Lucia¹; ¹US Army Research Laboratory, USA. Recent advances in laser-induced breakdown spectroscopy (LIBS) such as double pulse LIBS and advanced chemometric analysis have enabled discrimination between explosive and non-explosive residues on various surfaces at standoff distances.

16:30–18:30

CM4B • Compressive & Spectral Imaging

David Gerwe; Boeing Company, USA,
PresidentCM4B.1 • 16:30 

Spectroscopy for Intact Particles, Thomas van Dijk¹, Rohit Bhargava^{1,2}, P. Scott Carney^{1,3}; ¹Beckman Institute for Advanced Science and Technology, Univ. of Illinois at Urbana-Champaign, USA; ²Department of Bioengineering, Univ. of Illinois at Urbana-Champaign, USA; ³Department of Electrical and Computer Engineering, Univ. of Illinois at Urbana-Champaign, USA. In infrared microscopy, the structure and the chemistry of a sample are commingled, distorting the recorded spectra and confounding chemical identification. We provide a physics-based method to recover the material response from spheres.

CM4B.2 • 17:00 

Chip-Scale Low Power Analog Hardware Implemented Compressed Sensing and Target Detection Algorithms for Hyperspectral Imaging Applications, Peter Petre¹; ¹HRL Labs, USA. Low cost, low power hyperspectral imaging sensors and real-time, low power processing of hyperspectral data are needed for mobile platforms for agricultural, mineralogical, surveillance and physics applications. In this presentation we will show how two novel technologies - Compressed Sensing (CS) and analog Asynchronous Pulse Processing (APP) - are successfully applied to real time HSI sensing and processing.

CM4B.3 • 17:30

Dynamically Programmable, Dual-Band Computational Imaging System, Brant M. Kaylor¹, Amit Ashok², Eric M. Seger¹, Charlie J. Keith¹, Randy R. Reibel¹; ¹Bridger Photonics, Inc, USA; ²College of Optics, Univ. of Arizona, USA. A dynamically programmable computational imaging system has been demonstrated. The system operates in the visible and near infrared bands. Principal components and random binary measurements were used with the imaging hardware to demonstrate compressive imaging.

CM4B.4 • 17:45

AFSSI-C: the Adaptive Feature-Specific Spectral Imaging Classifier, Matthew Dunlop¹, Peter Jansen¹, Dathon R. Golish¹, Michael E. Gehm^{1,2}; ¹Electrical and Computer Engineering, the Univ. of Arizona, USA; ²College of Optical Sciences, the Univ. of Arizona, USA. We have developed an architecture for spectral classification in spectral imaging. Adaptive kernels are designed using probabilistically-weighted principal component analysis. Simulation predicts orders-of-magnitude reduction in error rates, and a prototype system is currently under construction.

16:30–18:30

IM4C • Medical Imaging and Microscopy


Joyce Farrell; Stanford Univ., USA, President

IM4C.1 • 16:30 

In vivo Brain Imaging with Miniaturized Optical Systems, Mark Schnitzer¹; ¹CNC Program, Stanford Univ., USA. A longstanding challenge in neuroscience is to understand how populations of individual neurons contribute to animal behavior and brain disease. Addressing this challenge has been difficult partly due to lack of brain imaging technology for use in awake behaving animals. I will describe two approaches to studying the brains of awake behaving mice, one of which also allows time-lapse studies of cells in deep brain areas. Using these methodologies we have studied the dynamics of cerebellar Purkinje cells and hippocampal pyramidal neurons and relationships to rodent behavior.

IM4C.2 • 17:00

Optical Imaging System Designed for Biosensing using a Photonic Crystal Membrane to Detect Nanoparticles, Jon Olav Grepstad^{1,5}, Peter Kaspar³, Olav Solgaard⁵, Ib-Rune Johansen⁴, Aasmund S. Sudbo^{2,5}; ¹NTNU, Norway; ²UiO, Norway; ³ETH, Switzerland; ⁴SINTEF, Norway; ⁵Univ. Graduate Center, Norway; ⁶E.L. Ginzton Lab, Stanford Univ., USA. We have built an optical microscope for a new biosensor application, incorporating a 2D photonic crystal membrane enabling detection of particles with a radius less than 50 nm. The microscope has been characterized experimentally.

IM4C.3 • 17:15 

Comparison of CMOS and MCMCCD Cameras for Computational Imaging with Application to Super-resolution Localization Microscopy, Tadashi Maruno¹, Eiji Toda¹, Keith Bennett²; ¹System Division, Hamamatsu Photonics, Japan; ²Hamamatsu Corporation, USA. Gen II scientific CMOS (sCMOS) cameras provide higher signal to noise ratios than EM-CCD cameras for most fluorescence microscopy applications, including single molecule imaging. We discuss implications for computational imaging.

IM4C.4 • 17:45

Speckle based Sensing Device for Fast Detection of Malaria, Dan Cojoc², Sara Finaurini², Pavel Livshits¹, Eran Gur³, Alon Shapira⁴, Vicente Mico⁵, Zeev Zalevsky¹; ¹Bar-Ilan Univ., Israel; ²Area Science Park - Basovizza, Istituto Officina dei Materiali IOM-CNR, Italy; ³Jerusalem College of Engineering, Israel; ⁴Departamento de Óptica, Universitat de València, Spain. We propose a new technique for malaria detection. It is based upon extraction of correlation based statistics of speckle patterns generated while illuminating red blood cells with a laser and inspecting them under a microscope.

These concurrent sessions are grouped across two pages. Please review both pages for complete session information.

16:30–18:30

OM4D • Figuring and Finishing Science

Erika Sohn; Instituto de Astronomia UNAM, Mexico, Presider

OM4D.1 • 16:30 **Invited**

Control of Mid-spatial-frequency Errors for Large Steep Aspheric Surfaces, Dae Wook Kim¹, Hubert Martin², James H. Burge^{1,2}; ¹College of Optical Sciences, Univ. of Arizona, USA; ²Steward Observatory, Univ. of Arizona, USA. Control of mid-spatial-frequency errors on precision optical surfaces is very important for next-generation optical systems. We present results of smoothing experiments and of polishing runs utilizing figuring and smoothing for the 8.4m GMT off-axis segment.

OM4D.2 • 17:00

Minimize Mid-Spatial Frequencies on Aspherical Surfaces, Joseph Ellison¹, Steven VanKerkhove¹; ¹Corning, USA. Removal of Mid-Spatial Frequency features on aspherical surfaces is challenging. This paper presents results obtained from novel fabrication and measurement techniques used to reduce MSF errors achieving less than 2nm rms residual error while preserving the aspheric form to better than 30nm PV.

OM4D.3 • 17:15 **OF&T Student Paper Contest Participant**

Laser Polishing of Lenses of Fused Silica and BK7, Annika Richmann¹, Edgar Willenborg², Konrad Wissenbach²; ¹Lehrstuhl für Technologie optischer Systeme TOS, Germany; ²Fraunhofer-Institut für Lasertechnik, Germany. A novel process for polishing lenses made of fused silica and BK7 with CO₂-laser radiation is presented. First results on polishing spherical and aspherical lenses of both materials with an adapted processing strategy are presented.

OM4D.4 • 17:30

The Role of the Zetapotential in the Polishing Process of Optical Glasses, Elisabeth Becker¹, Marcel Achtsnick¹; ¹Berliner Glas KGaA, Germany. This paper shows the significant role of the colloidal chemistry of the polishing suspension in the polishing process. The main properties are the stability of the suspension and the agglomeration state of the polishing grains, which both influence the surface quality of the polished glass.

OM4D.5 • 17:45 **OF&T Student Paper Contest Participant**

Evaluating the Effect of Single Frequency Vibrations on Pitch Polishing Outcomes, Mohammad Maimuddin¹, Brigid A. Mullany¹; ¹Univ. of North Carolina at Charlotte, USA. To isolate the roles vibration frequency content and amplitude on polishing metrics (material removal, surface finish), polishing tests were undertaken on a specifically designed platform with pitch tooling. Higher frequency vibrations appear more pivotal.

16:30–18:30

SM4F • Fiber Gratings and Displacement Sensors

John Canning, Univ. of Sydney, Australia, Presider

SM4F.1 • 16:30 **Invited**

Implementation and Characterization of Polarimetric Heterodyning Fiber Grating Laser Sensors, Bai-Ou Guan¹, Long Jin¹, Hwa-Yaw Tam²; ¹Jinan Univ., China; ²The Hong Kong Polytechnic Univ., China. In this paper, we briefly review our recent work on polarimetric heterodyning fiber grating laser sensors, including the characterization, implementation, and multiplexing of the polarimetric sensors.

SM4F.2 • 17:00 **Invited**

Remote Sensing Networks for Fiber Optic Sensors, Manuel Lopez-Amo¹, Montserrat Fernandez-Vallejo¹; ¹Ingenieria Electrica y Electronica, Universidad Publica de Navarra, Spain. This paper presents an overview of optical fiber sensor networks for remote sensing including lasing and non-lasing configurations. The main factors to take into consideration in the design of a fiber optic remote sensor system are gathered.

SM4F.3 • 17:30

Study of the Linearity Performances of a Polarization-Based Vibration Sensor, Nicolas Linze¹, Pierre Tihon², Olivier Verlinden², Patrice Mégret¹, Marc Wuilpart¹; ¹Electromagnetism and Telecommunication Department, Univ. of Mons, Belgium; ²Department of Theoretical Mechanics, Dynamics and Vibrations, Univ. of Mons, Belgium. In this paper the performances of a polarimetric vibration sensor are theoretically and experimentally analyzed. We show that this sensor can recover the vibration spectrum without distortions up to an acceleration of 300 m/s².

SM4F.4 • 17:45

Dynamic monitoring of an elevated water reservoir with a biaxial optical accelerometer, Paulo Antunes^{1,2}, Hugo Rodrigues², José Melo², Humberto Varum², Paulo S. Andre^{1,2}; ¹Instituto de Telecomunicacoes, Portugal; ²Univ. of Aveiro, Portugal. The dynamic monitoring of an elevated water reservoir, employing a biaxial optical accelerometer, is described. The structure natural frequencies were measured with an error of 0.06 %, when compared with the values attained from seismograph.

Cypress 4

Cypress 1 & 2

Cypress 3

Applied Industrial Optics: Spectroscopy, Imaging, & Metrology

Computational Optical Sensing and Imaging

Imaging Systems and Applications

These concurrent sessions are grouped across two pages. Please review both pages for complete session information.

AM4A • LIBS—Continued

CM4B • Compressive & Spectral Imaging—Continued

IM4C • Medical Imaging and Microscopy—Continued

CM4B.5 • 18:00

Spectrally Selective Compressive Imaging by Matrix System Analysis, Henry Arguello^{1,2}, Gonzalo Arce¹; ¹Univ. of Delaware, USA; ²Computer Science, Universidad Industrial de Santander, Colombia. A new CASSI formulation is presented which allows the design of spectrally selective measurements. Given a desired spectral sensing profile, the model permits the calculation of the required structure of the code apertures.

IM4C.5 • 18:00 **Invited**

Compressive Fluorescence Microscopy for Biological and Hyperspectral Imaging, Maxime Dahan¹; ¹Ecole Normale Supérieure, France. We present a novel approach to fluorescence bioimaging based on the theory of compressed sensing and demonstrate its potential on sparse fluorescent samples as well as hyperspectral images.

CM4B.6 • 18:15

Coded-Aperture Compressive Spectral Image Classification, Ana Ramirez¹, Gonzalo Arce¹, Brian Sadler²; ¹Depart. of Electrical and Computer Engineering, Univ. of Delaware, USA; ²Army Research Laboratory, USA. A classification method of compressed hyperspectral images acquired by using a Coded Aperture Snapshot Spectral Imaging (CASSI) system is proposed. A sparse vector that represents the HSI image in a multidimensional representation of the scene is used to determine the class label of the test pixel.

18:30–20:00 **Joint Conference Reception & Exhibit Hall Opening**, *The Dolphins on the Upper Plaza*

NOTES

These concurrent sessions are grouped across two pages. Please review both pages for complete session information.

OM4D • Figuring and Finishing Science—Continued

OM4D.6 • 18:00 **Invited**

Aspheric Finishing of Glass and SiC Optics, Flemming Tinker¹, Kai Xin¹; ¹Aperture Optical Sciences, Inc, USA. Aperture Optical Sciences Inc. was founded in 2010 to develop and produce advanced aspheric optics in silicon carbide and other materials. This paper explores Zeeko robotic polishing as an effective technology for aspheric finishing.

SM4F • Fiber Gratings and Displacement Sensors—Continued

SM4F5 • 18:00

Investigation of the Directional Response of Fiber Bragg Grating-Based Acoustic Emission Sensor, Harish V. Achar¹, Rajkumar Ramakrishnan¹, Krishnan Balasubramanian², Balaji Srinivasan¹; ¹Electrical Engineering, Indian Institute of Technology, Madras, India; ²Mechanical Engineering, Indian Institute of Technology Madras, India. We investigate the directional response of fiber Bragg gratings to acoustic emissions using a home built dynamic interrogator capable of sensing acoustic emissions from few kHz to 1 MHz.

SM4F6 • 18:15

Size Effect in Fiber Optic Displacement Sensors, Garry Berkovic¹, Shlomo Zilberman¹, Ehud Shafir¹; ¹Soreq Nuclear Research Center, Israel. We explain anomalous results obtained when small core optical fibers probe the distance to some scattering surfaces, such as machined metal surfaces. Large intensity variations occur when different sections of surface are probed at constant distance.

18:30–20:00 Joint Conference Reception & Exhibit Hall Opening, The Dolphins on the Upper Plaza

NOTES

Horizontal lines for taking notes.

These concurrent sessions are grouped across two pages. Please review both pages for complete session information.

07:00–18:00 Registration, Fairway Foyer on Lower Terrace

08:00–10:00

ATu1A • Industrial Spectroscopy

Elfed Lewis; Univ. of Limerick, Ireland, President

ATu1A.1 • 08:00 **Invited**

Direct Real-Time Determination of Compositional Profiles in Structured Materials Using Laser Ablation Instruments: LIBS and LA-ICP-MS, Alexander A. Bolshakov¹, Jong H. Yoo¹, Jhanis J. Gonzalez¹, Chunyi Liu¹, Richard E. Russo¹; ¹Applied Spectra Inc, USA. Laser ablation offers rapid micro-analysis with spatial resolution ~10 nm in depth, ~3 μm lateral. Structured materials are mapped, depth-profiled for elemental and isotopic composition using LIBS or LA-ICP-MS without dissolving samples. Molecular structure can be inferred by chemometric processing.

ATu1A.2 • 08:40 **Invited**

Advances in Laser Assisted Microwave Plasma Spectroscopy (LAMPS), Philip C. Eftimion¹; ¹Envimetics, USA. LAMPS, Laser Assisted Microwave Spectroscopy, is a plasma spectroscopic technique that has higher sensitivity to LIBS using little or no laser energy. The higher sensitivity is due to microwave energy extending the duration of the micro plasma for analyzing material. The sensitivity is enhanced a factor of 10 at wavelengths < 300 nm and 40 - 200 for wavelengths > 300 nm. The lower laser energy results in no surface damage. The technique can be used to determine the composition of materials and detect biological and explosive agents. Recently, the device has been miniaturized to develop a portable hand held instrument.

08:00–10:00

CTu1B • Aperture Synthesis, Fourier Optics, Coherence 

Andy Harvey, Univ. of Glasgow, UK, President

CTu1B.1 • 08:00 **Invited**

Imaging Geostationary Satellites with a Common-Mount Optical Interferometry, Anders Jorgensen¹, David Mozurkewich², Henrique R. Schmitt³, J. T. Armstrong⁴, Robert B. Hindsley¹, Ellyn K. Baines⁴, Sergio R. Restaino⁴; ¹New Mexico Institute of Mining and Technology, USA; ²Seabrook Engineering, USA; ³Computational Physics, Inc, USA; ⁴Naval Research Laboratory, USA. We present design and preliminary performance analysis of an optical interferometer which is capable of imaging geostationary satellites. It consists of a large number of simple telescopes on a single mount fiber-feeding a beam combiner.

CTu1B.2 • 08:30 **Invited**

Aperture Synthesis in Astronomy and the Challenges of GEO Imaging, David Buscher¹; ¹Cavendish Laboratory, Univ. of Cambridge, UK. I describe the state-of-the-art in interferometric imaging in visible and near-infrared astronomy and how the lessons learned from this field can be applied to imaging of structure in deep-space satellites.

CTu1B.3 • 09:00

Experimental measurement of 4D Ambiguity functions of 2D signals, Guohai Situ¹, Laura Waller¹, Jason W. Fleischer¹; ¹Princeton Univ., USA. We present a windowed-Fourier-transform-based technique for measuring the 4D Wigner distribution function and Ambiguity function of 2D signals. Experimental results agree very well with numerical simulation.

08:00–10:00

ITu1C • Military Applications

Ken Barnard, US Air Force Research Lab, USA, President

ITu1C.1 • 08:00 **Invited**

Navy Intelligence, Surveillance, and Reconnaissance Systems, Michael Wilson¹; ¹Naval Research Laboratory, USA. Navy ISR crosses the full spectrum of ISR technologies and draw on support from novel multi-sensor architectures that are also under current development. Together these technologies are enabling sensor-sensor collaboration and automated information discovery.

ITu1C.2 • 8:30

Pixel Scaling in Infrared Focal Plane Arrays, Peter B. Catrysse¹, Torbjorn Skaul^{1,2}; ¹E. L. Ginzton Laboratory, Stanford Univ., USA; ²Norwegian defence research establishment (FFI), Norway. We discuss challenges that arise in infrared focal plane arrays when pixel size scales down to approach the wavelength. We also explore opportunities that emerge for controlling light with subwavelength optics in very small pixels.

ITu1C.3 • 08:45

Generating 3D Reflectance Images of the Shallow Water Seafloor from Airborne Lidar Data, Grady Tuell¹, Joong Y. Park², Viktor Feygels², Vinod Ramnath³; ¹Georgia Tech Research Institute, USA; ²Optech Inc., USA. Bathymetric lidar waveforms may be inverted to estimate seafloor reflectance, and rasterized to generate 3D reflectance images. These images compare favorably to diver measurements, and may be used for seafloor classification and target detection.

ITu1C.4 • 9:00

Formation of Wide-FOV Active Image Mosaics, Samuel T. Thurman¹, Andrew Bratcher¹; ¹Lockheed Martin Coherent Technologies, USA. The field-of-view (FOV) for active imaging systems typically is matched to the illumination-beam width. We describe a registration algorithm that forms wide-FOV image mosaics by taking the illumination-beam profile into account.

These concurrent sessions are grouped across two pages. Please review both pages for complete session information.

07:00–18:00 Registration, Fairway Foyer on Lower Terrace

08:00–10:00

OTu1D • Optical Testing I

Ulf Griesmann; NIST, USA, Presider

OTu1D.1 • 08:00 **Invited**

Light Scattering & Complex Optical Components: Modelization and Characterization, Myriam Zerrad^{1,3}, Michel Lequime^{1,4}, Claude Amra^{1,2}; ¹Institut Fresnel, France; ²CNRS, France; ³Aix Marseille Université, France; ⁴Ecole Centrale Marseille, France. Limitation and quantification of scattering losses are new challenges to enhance optical components performances. Last numerical and metrological platforms involved at Institut Fresnel and dedicated to light scattering characterization and modelization will be presented.

OTu1D.2 • 08:30

Light Scattering-based Measurement of Relevant Surface Roughness, Sven Schröder¹, Marcus Trost¹, Luisa Coriand¹, Angela Duparré¹; ¹Fraunhofer IOF, Germany. Light scattering measurements are used to determine surface PSD functions and application-specific roughness values in different relevant spatial frequency ranges. A new method is presented for area covering investigations of the high-spatial frequency roughness.

OTu1D.3 • 08:45

Apparent wave front aberration in the «Cat's Eye» configuration at high apertures, Hans-Martin Heuck¹, Joachim Wesner¹, Joachim Heil¹, Andreas Dorbach¹; ¹Optic Technology, Leica Microsystems CMS GmbH, Germany. Within the "Cat's Eye" configuration the reflected phase depends on the incident angle on the return mirror, particular for high NA lenses. This phase-error is derived from Fresnel's law and compared with interferometric measurements.

OTu1D.4 • 09:00

Lateral resolution and instrument transfer function as criteria for selecting surface metrology instruments, Xavier Colonna De Lega¹, Peter de Groot¹; ¹Zygo Corporation, USA. We review definitions of optical resolution and how they relate to the Instrument Transfer Function of surface profiling interferometers. The corresponding optical cutoff provides a selection criterion for a given metrology application (PSD, waviness).

08:00–10:00

RTu1E • Sensor Fusion and Lidar I

Christopher Parrish; NOAA, NGS, Remote Sensing Div, USA, Presider

RTu1E.1 • 08:00

A Multi-Sensor Approach to Coastal Characterization, Charles M. Bachmann¹, Andrei Abelev¹, William Philpot^{3,1}, C. Reid Nichols², Geoff Smith¹, Dan Korwan¹, Joan Gardner¹, Mark Sletten¹, Joseph A. Musser², Robert A. Fusina¹, Michael Vermillion¹, Christopher E. Parrish⁴, Rong-Rong Li¹, Jon Sellars⁴, Stephen White⁴, Elena van Roggen², Katarina Doctor^{6,1}; ¹US Naval Research Laboratory, USA; ²Marine Information Resources Corporation, USA; ³Cornell Univ., USA; ⁴NOAA NGS, USA; ⁵Stephen F. Austin State Univ., USA; ⁶George Mason Univ., USA. Our multi-sensor experiments are focused on coastal characterization from hyperspectral, thermal, LiDAR, and SAR. Cal/val activities include new instrumentation such as a field portable hyperspectral goniometer.

RTu1E.2 • 08:15 **Invited**

First Results From a High-Resolution Full Waveform Airborne Bathymetric LiDAR System, Craig Glennie¹, William E. Carter¹, Ramesh L. Shrestha¹; ¹Civil and Environmental Engineering, Univ. of Houston, USA. An airborne LiDAR system that integrates design characteristics of terrestrial and bathymetric sensors to enable high-resolution mapping of land and shallow bathymetry simultaneously is discussed. We also present early test results and outline future work.

RTu1E.3 • 08:45

Calibration of a Frequency Agile, Mixed Vapor-Aerosol LiDAR, David Stoker¹, Eunice Li¹, Jan van der Laan¹, Russel Warren², Richard Vanderbeek³; ¹SRI International, USA; ²ECBC, USA; ³Eo-Stat, USA. We model LiDAR backscattering from outdoor mixed vapor-aerosol (MVA) detonation tests and show that we are able to correctly separate MVA components into silica and TEP (tri-ethyl phosphate) using a novel aerosol partitioning algorithm.

RTu1E.4 • 09:00

Withdrawn

08:00–10:00

STu1F • Temperature and Photonic Crystal Fiber Sensing

John Canning, Univ. of Sydney, Australia, Presider

STu1F.1 • 8:00 **Invited**

Withdrawn

STu1F.2 • 8:30

A Compact Temperature Sensor Based on Micrometric Optical Fiber Coupler Tip, Ming Ding¹, Pengfei Wang^{1,2}, Gilberto Brambilla¹; ¹Optoelectronics Research Centre, Univ. of Southampton, UK; ²Photonics Research Centre, Dublin Institute of Technology, Ireland. A compact temperature sensor based on a coupler tip with micrometric size is demonstrated. This sensor can measure a temperatures as high as 1283 oC with an average sensitivity of ~12 pm/oC.

STu1F.3 • 8:45

Double Cladding Fiber Interferometer Suitable for Measuring Thermo-Optic Coefficient of Liquid, Young Ho Kim¹, Seong Jun Park¹, Chanki Lee¹, Se-Jong Baik², Byeong Ha Lee¹; ¹School of Information and Communications, Gwangju Institute of Science and Technology, Republic of Korea; ²Department of Physics [S] Photonics co.,Ltd, Industry foundation of Chonnam National Univ., Republic of Korea. A double cladding fiber interferometer for obtaining the thermo-optic coefficient (TOC) of liquid was demonstrated by simultaneously measuring the refractive index and temperature. The TOC of water at 1550 nm was about -1.485 x 10⁻⁴ RIU/degree.

STu1F.4 • 9:00

Temperature Monitoring of Bend Insensitive Fibers After the Fuse Effect Propagation, Mária Domingues^{1,2}, Ana Rocha^{1,2}, Paulo S. Andre^{1,2}, Ana Frias², Maria Andre^{2,3}; ¹Instituto de Telecomunicacoes, Portugal; ²Physics, Univ. of Aveiro, Portugal; ³CICECO, Univ. of Aveiro, Portugal. In this work we study the thermal behavior of bend insensitive fibers after the fuse effect. The region where the fuse effect has stopped reveals a high burning risk for optical power above 1.0 W.

These concurrent sessions are grouped across two pages. Please review both pages for complete session information.

ATu1A • Industrial Spectroscopy— Continued

ATu1A.3 • 09:20 **Invited**

In-line Characterization of Highly Concentrated Industrial Dispersions by Photon Density Wave Spectroscopy, Lena Bressel¹, Roland Hass¹, Marvin Münzberg¹, Oliver Reich¹; ¹Institute for Chemistry, Univ. of Potsdam, Germany. Photon Density Wave (PDW) spectroscopy is well suited for monitoring processes in industrial dispersions, where other optical techniques fail due to multiple light scattering. Fabrication of nanoemulsions as well as nano- and microparticles is discussed.

CTu1B • Aperture Synthesis, Fourier Optics, Coherence—Continued

CTu1B.4 • 09:15

Quartic Optimization for Coherence Retrieval, Zhengyun Zhang¹, Zhi Chen¹, George Barbastathis^{1,2}; ¹Singapore-MIT Alliance for Research and Technology, Singapore; ²Mechanical Engineering, MIT, USA. We propose optimization of a quartic function for mutual intensity recovery from intensity measurements of quasi-monochromatic sources. We prove that this function has no detrimental local minima and apply it to capturing a Schell-model source.

CTu1B.5 • 09:30

Coherence synthesis with Spatial Light Modulators, Laura Waller¹, Jason W. Fleischer¹; ¹Princeton Univ., USA. We demonstrate a simple method for designing local coherence effects in 4D, by using time and space multiplexing on a Spatial Light Modulator (SLM) acting as a dynamic diffuser element. Results are measured experimentally in 4D phase space via the spectrogram.

CTu1B.6 • 09:45

Fundamental Limits of Wavefront Sensing using Microlens Arrays, Sean Quirin¹, Rafael Piestun¹; ¹Univ. of Colorado, USA. The information theoretic bounds of Shack-Hartmann type wavefront sensors is evaluated. A tradeoff analysis among the photon count, the number of aberration coefficients to estimate, and the array size leads to optimal sensor architectures.

ITu1C • Military Applications—Continued

ITu1C.5 • 09:15

Autonomous Networked Multi-Sensor Imaging Systems, Dale C. Limne von Berg¹; ¹US Naval Research Laboratory, USA. A demonstration of automated networked multiple sensor operation in airborne environments was performed. This presentation describes the diverse sensors and imagery processing used to demonstrate autonomously interactive detection and tracking of multiple ground targets.

ITu1C.6 • 09:30 **Invited**

Real-World Lessons Learned and Future Technology Drivers for Multi-INT Imagery Exploitation Systems, Darin Partridge¹; ¹CAISR Systems Division, Space Dynamic Laboratory, USA. Tactical Multi-INT Imagery Exploitation Systems continue to evolve at a rapid pace. Key game changing technologies are combined and then demonstrated to create a robust and processing rich environment for the emerging battle-space.

10:00–10:30 Exhibit Hall & Coffee Break, The Dolphins on the Upper Plaza

10:30–12:30

ATu2A • Micro-Optical Systems

Sapna Shroff; Ricoh Innovations, Inc., USA, President

ATu2A.1 • 10:30 **Invited**

Integrated Polymer Optofluidic Chips, Heidi Ottevaere¹, Jürgen Van Erps¹, Michael Vervoake¹, Hugo Thienpont¹; ¹Department of Applied Physics and Photonics, Vrije Universiteit Brussel, Belgium. We developed integrated plastic micro-optical detection units for absorbance and fluorescence measurements in various types of microfluidic channels. For each system we present the complete development process from optical design, to fabrication and proof-of-concept demonstration.

ATu2A.2 • 11:10 **Invited**

MEMS Deformable Mirrors: From Retinal Imaging to Industrial Laser Systems, Michael Helmbrecht¹; ¹IrisAO, USA. Advances in the manufacture of MEMS deformable mirrors make them suitable for a wide range of adaptive and active optics applications. This paper presents recent developments that make them applicable to laboratory grade retinal imaging systems as well as industrial lasers.

10:30–12:00

CTu2B • Image Restoration

David Tyler; Univ. of Arizona, USA, President

CTu2B.1 • 10:30 **Invited**

Numerical Restoration of Imagery Obtained in Strong Turbulence, Douglas A. Hope¹, Stuart M. Jefferies^{1,2}, Michael Hart³, Keith Hege³; ¹Institute for Astronomy, USA; ²Steward Observatory, Univ. of Arizona, USA. A combination of approaches for overcoming the challenges faced when imaging in strong turbulence is presented. These approaches use WFS measurements, multiple telescope data with temporal signatures and spectral nulls that exist in the data.

CTu2B.2 • 11:00 **Invited**

Measuring and Improving Low-Level Image Quality, Neel Joshi¹; ¹Research, Microsoft Corporation, USA. Low-light images often suffer from noise or blur artifacts. By estimating the degradation process, it is possible to improve image quality. I will discuss recent work in both measuring and improving image quality.

10:30–11:45

ITu2C • Hyperspectral Imaging

Torbjorn Skauli; Norwegian Defence Research Establishment (FFI), Norway, President

ITu2C.1 • 10:30 **Invited**

Hyperspectral Imaging as a Tool for Fluorescence Imaging and Characterization of Skin Bruises, Lise L. Randberg¹, Julio Hernandez-Palacios^{2,3}; ¹Norwegian Univ. of Science and Technology, Norway; ²Norsk Elektro Optikk AS, Norway; ³University of Oslo, Norway. Hyperspectral systems should be specially fitted for bio-applications to achieve optimal results and avoid sample damage. Experiences from developing and using such imaging systems for characterization of bruised skin and fluorescence imaging are described.

ITu2C.2 • 11:00

Advances in Active Near-Infrared Sensor Systems for Material Classification, Holger Steiner¹, Oliver Schwaneberg¹, Norbert Jung¹; ¹Computer Science, Bonn-Rhine-Sieg Univ. of Appl. Sc., Germany. Different materials and human skin can be classified by their characteristic reflection spectra. Advanced multi-spectral sensors and imaging systems can use this for safety and security applications and provide additional value to users.

These concurrent sessions are grouped across two pages. Please review both pages for complete session information.

OTu1D • Optical Testing I—Continued

OTu1D.5 • 9:15

Minimizing Artifacts in Analysis of Surface Statistics, Peter Z. Takacs¹; ¹Instrumentation Div, Brookhaven National Laboratory, USA. Measurements from interferometers and profilometers contain information about surface figure and finish over a wide range of spatial frequencies. Proper detrending and windowing are necessary to avoid contaminating the true nature of the PSD function.

OTu1D.6 • 09:30

Characterizing Optical Surfaces using the Area Structure Function, Liangyu He¹, Chris J. Evans¹, Angela Davies¹; ¹Univ. of North Carolina at Charlotte, USA. The area structure function (ASF) spatially characterizes surfaces of any arbitrary aperture over all frequencies, while retaining information on the isotropic nature of the surface. Calculation and interpretations of ASFs are shown

OTu1D.7 • 9:45

SAGUARO: Data Analysis Software for Optical Engineering, Greg A. Smith¹, Benjamin J. Lewis¹, Dae Wook Kim¹, Michael Palmer¹, Adrian R. Loeffl¹, James H. Burge¹; ¹College of Optical Sciences, Univ. of Arizona, USA. SAGUARO software is written for the optical engineer and designed to simplify data analysis and visualization. SAGUARO is easy for the end-user processing optical test information as well as the developer adding new functionalities.

RTu1E • Sensor Fusion and Lidar I—Continued

RTu1E.5 • 09:15

Feasibility Study for the Remote Detection of Atmospheric Xenon Using a DIAL LIDAR System, Michael DeAntonio¹, Mazen Nairat¹; ¹Physics, New Mexico State Univ., USA. We describe a study of the feasibility of detecting atmospheric Xenon by modifying a DIAL LIDAR system currently used for the detection of methane. We will determine the signal levels for mid-IR Xenon absorption.

RTu1E.6 • 09:30 **Invited**

Active-Passive Data Fusion Strategies for Classification of the Shallow-water Seafloor, Grady Tuell¹; ¹Georgia Tech Research Institute, USA. The newest generation of airborne coastal mapping systems routinely produces simultaneous lidar and hyperspectral data. Recent investigations into fusion-based seafloor classification strategies indicate improved accuracies are achieved with high-level algorithms, as compared to pixel-based approaches.

STu1F • Temperature and Photonic Crystal Fiber Sensing—Continued

STu1F.5 • 9:15 **Invited**

New Platforms for Chemical, Biological and Radiation Sensing based on Emerging Micro and Nanostructured Optical Fibres, Tanya M. Monro¹; ¹Univ. of Adelaide, Australia. Emerging optical materials and structures are driving the development of new optical fibre sensors, with applications ranging from new radiation dosimeters to in-vivo biosensors. Advances in fluorescent based, label-free and nanoscale volume sensors will be presented.

STu1F.6 • 09:45

Raman Probe Based on Optically-Poled Double-Core Fiber, Anna Chiara Brunetti^{1,2}, Walter Margulis², Karsten Rottwitz¹; ¹DTU Fotonik, Denmark; ²Fiber Photonics, Acreo AB, Sweden. A Raman probe based on an optically-poled double-core fiber. In-fiber SHG allows for Raman spectroscopy of DMSO at 532nm when illuminating the fiber with 1064nm light. The fiber structure provides independent excitation and collection paths.

10:00–10:30 Exhibit Hall & Coffee Break, The Dolphins on the Upper Plaza

10:30–12:00

OTu2D • Optical Testing II

Chris Evans; Univ. of North Carolina at Charlotte, USA, Presider

OTu2D.1 • 10:30 **Invited**

Interferometric Measurements of Aspheres with No Axial Symmetry, Piotr Szwajkowski¹; ¹Engineering Synthesis Design Inc, USA. We would like to present an approach based on a Computer Generated Reference (CGR) to test a variety of aspheric surfaces including standard axially symmetric parts as well as toric, bi-conic and "free forms

OTu2D.2 • 11:00

Self-Aligning Telescope With Off-Axis And Aspheric Mirror Segments, Kent Weed¹; ¹LightWorks Optics, Inc., USA. Creating the alignment with off-axis segments of aspheric surfaces in a telescope assembly requires high precision and positive references. This paper addresses techniques that essentially create a self-aligning assembly even with complex mirror segments.

10:30–11:45

RTu2E • Sensor Fusion and Lidar II

Christopher Parrish; NOAA, NGS, Remote Sensing Div, USA, Presider

RTu2E.1 • 10:30

Extraction of Rooftops from LiDAR and Multispectral Imagery, Angela M. Kim^{1,2}, Fred A. Kruse^{1,2}, Richard C. Olsen^{1,2}, Chris C. Clasen²; ¹Naval Postgraduate School, USA; ²Remote Sensing Center, Naval Postgraduate School, USA. A rooftop extraction scheme based on statistical analysis of the LiDAR point cloud is presented. Spectral data are incorporated to reduce false alarms due to vegetation and to provide spectral discrimination of rooftop materials.

RTu2E.2 • 10:45

Withdrawn

RTu2E.3 • 11:00

NASA's High-altitude, Swath-mapping Laser Altimeter Capability, Sensor Fusion, and the Development of Technologies to Enable Space-based Lidar Mapping of the Earth's Surface, Bryan Blair¹; ¹Laser Remote Sensing Laboratory, NASA/GSFC, USA. NASA's Land, Vegetation, and Ice Sensor (LVIS) is a high-altitude, wide-swath laser altimeter. Recent data examples, sensor fusion examples, a Global Hawk version of LVIS, and technology advancements for a space-based mapping capability will be presented.

10:30–12:00

STu2F • Gas and Voltage Sensing

Anna Chiara Brunetti; DTU Fotonik, Denmark, Presider

STu2F.1 • 10:30 **Invited**

Gas Sensing using Material and Structural Slow Light Systems, Luc Thevenaz¹, Isabelle Dicaire¹, Sanghoon Chin¹, Alfredo De Rossi²; ¹Ecole Polytechnique Federale de Lausanne, Switzerland; ²Thales Research and Technology, France. Slowing light is expected to enhance light-matter interaction, leading to more compact sensing devices. By simple tests we show that the reality is more complex and the only relevant quantity is the wave electric field.

STu2F.2 • 11:00

Hollow Core Photonic Crystal Fibers for Quantitative Measurements of Fractional Amounts of Gases, Anders Simonsen¹, Jan Hald¹, Jens Lyngsø², Jan C. Petersen¹; ¹Danish Fundamental Metrology Ltd, Denmark; ²NKT Photonics, Denmark. Hollow-core photonic bandgap fibers have the potential as sensors for molecular gases. Based on measured transmission properties as a function of laser frequency the potential accuracy with which the amount of substance can be determined is estimated

These concurrent sessions are grouped across two pages. Please review both pages for complete session information.

13:20–15:10

ATu3A • Optical Systems for the Food IndustryMarion O'Farrell; SINTEF Norway, *Presider***ATu3A.1 • 13:20 Invited**

Automatic Sorting of Meat Cuts using NIR Interactance Imaging, Vegard Segtnan¹, Ingrid Måge¹, Martin Kermit², Froydis Bjerke⁴, Jens T. Thielemann³, Jon Tschudi³, Jens P. Wold¹; ¹Food Division, Nofima AS, Norway; ²Tomra Sorting Solutions, Norway; ³SINTEF ICT Solutions, Norway; ⁴Animalia, Norway. A fat and weight sorting system for heterogeneous meat trimmings has been developed. The system is based on a non-contact NIR interactance scanner, a flow weight and a sorting belt, combined with multiresponse optimization algorithms.

ATu3A.2 • 14:10 Invited

Low Cost Real-Time Sorting of In-Shell Pistachio Nuts from Kernels, Ron Haff¹, Eric S. Jackson¹; ¹Agricultural Research Service, USDA, USA. A simple, low cost optical system for separating in-shell pistachio nuts and kernels is reported. Testing indicates 95% accuracy in removing kernels from the in-shell stream with no false positive results.

ATu3A.3 • 14:50 Invited

Dairy & Optics - Blurring the Boundaries, Chris Pundmann¹; ¹Daisy Brand, USA. For decades, the food and especially the dairy industry has steered processes largely in manual control. In recent years; however, the emergence of affordable and reliable optics technologies has made a wide array of instrumentation available for automating operations and vastly improving product consistency.

13:30–15:00

CTu3B • Compressive ImagingSudhakar Prasad; Univ. of New Mexico, USA, *Presider***CTu3B.1 • 13:30 Invited**

Statistical Performance Bounds for Coded-Aperture Compressive Spectral-Polarimetric Imaging, Sudhakar Prasad¹, Robert J. Plemmons², Qiang Zhang², David J. Brady³; ¹Univ. of New Mexico, USA; ²Wake Forest Univ., USA; ³Duke Univ., USA. We apply statistical information and Bayesian estimation theories to calculate certain fundamental bounds on the reconstruction of segment boundaries, material type, and surface texture of sparse objects from their coded-aperture, compressive spectral-polarimetric image data.

CTu3B.2 • 14:00

Advances in the Design, Calibration and Use of a Static Coded Aperture Compressive Tracking and Imaging System, Phillip Poon¹, Esteban Vera², Michael E. Gehm^{1,2}; ¹College of Optical Sciences, Univ. of Arizona, USA; ²Department of Electrical and Computer Engineering, Univ. of Arizona, USA. We present our latest results in static compressive tracking and imaging. We have developed a design methodology using the compressed sensing concept of mutual coherence. We also elucidate a modified calibration scheme that boosts compressive imaging capabilities.

CTu3B.3 • 14:15

Information Optimal Static Measurement Design for Compressive Imaging, Amit Ashok¹, Mark Allen Neifeld¹, James Huang¹; ¹Univ. of Arizona, USA. We present an information-theoretic framework for measurement basis design in compressive imaging. Simulation results show that the reconstruction error obtained with information-optimal projections is nearly an order of magnitude lower than that for random projections.

CTu3B.4 • 14:30

Compressive Reflectance Field Acquisition using Confocal Imaging with Variable Coded Apertures, Ryoichi Horisaki¹, Yusuke Tampa¹, Jun Tanida¹; ¹Osaka Univ., Japan. We propose a scheme for acquiring an eight-dimensional reflectance field based on compressive sensing. The reflectance field is modulated and observed multiple times with variable coded apertures. The proposed scheme was verified in numerical experiments.

CTu3B.5 • 14:45

HoloCam: Low-power wide-field incoherent target detector, Sri Rama Prasanna Pavani¹, Jonathan Hull¹, Sergey Chemishkian¹, Kathrin Berkner¹, Ken Gudan¹; ¹Ricoh Innovations, Inc., USA. The combination of a computer generated target hologram and a large-area detector leverages optical correlation with a novel single-pixel spot/blur classifier to achieve low-power high-speed target detection with a wide field-of-view in room light.

13:30–15:00

ITu3C • Phase Space in ImagingJohn Sheridan; Univ. College Dublin Ireland, *Presider***ITu3C.1 • 13:30 Invited**

A Phase Space Tour of Optical Imaging, Markus E. Testorf¹; ¹Thayer School of Engineering, Dartmouth College, USA. The phase-space instrument function is used to analyze optical systems. The Wigner distribution function and the ambiguity function of a lenslet array are constructed to interpret imaging systems as forms of phase-space tomography.

ITu3C.2 • 14:00

New Challenges for Sampling Theory for Linear Canonical Transforms in Optics, John J. Healy¹; ¹National Univ. of Ireland, Maynooth, Ireland. The linear canonical transforms are a popular model for the paraxial propagation of scalar wave fields through first order optical systems. We examine some new sampling problems arising at the boundaries of existing knowledge.

ITu3C.3 • 14:15 Invited

Generalized Wigner Functions in Classical Optics, Miguel A. Alonso¹; ¹The Institute of Optics, Univ. of Rochester, USA. We give a prescription for defining generalized Wigner functions that extend the property of conservation along paths to a wider range of problems, including nonparaxial field propagation and pulse propagation within general transparent dispersive media.

ITu3C.4 • 14:45

The Condition Number and First Order Optical Systems, John T. Sheridan¹, Liang Zhao¹, John J. Healy¹; ¹EE&C Engineering, Univ. College Dublin, Ireland. The condition number is used to explore the characteristics of several matrices and the associated transforms used in propagation problems in Luneberg's optical systems. These include ABCD/Collins matrices and discrete linear canonical transform matrices.

15:00–15:30 Exhibit Hall & Coffee Break, *The Dolphins on the Upper Plaza*

These concurrent sessions are grouped across two pages. Please review both pages for complete session information.

13:30–15:00

OTu3D • Assembly, Alignment and Control

Weiyao Zou; ASML Optics LLC, USA, Presider

OTu3D.1 • 13:30 **Invited**

New Joining Technologies for High Stable and Smart Optical Systems, Ramona Eberhardt¹, Gerhard Kalkowski¹, Andreas Tünnermann¹, Erik Becker¹, Steffen Böhme¹; ¹Precision Engineering, Fraunhofer IOF, Germany. The presentation gives an overview about joining technologies for next generation optics. New concepts for polymer-free, precise and cost efficient manufacturing and assembly processes of modern optical sub-systems are illustrated.

OTu3D.2 • 14:00 **Invited**

Lab-on-a-chip Applications Enabled by Acousto-opto-fluidics, Xiaole Mao^{1,2}, Tony Jun Huang¹; ¹The Pennsylvania State Univ., USA; ²P & G Mason Business Center, USA. In this work we discuss novel lab-on-a-chip applications such as liquid lens and on-chip cell detection and manipulation that are enabled by combining the principles of acoustics, optics, and microfluidics.

OTu3D.3 • 14:30 **Invited**

Mass Production of 100° Field of View Helmet Mounted Display, Paul Townley-Smith¹; ¹Zygo Corporation, USA. Production of a stereoscopic, see-through, wide field of view head mounted display presents many design, assembly and test challenges. Presented here are the strategies employed to overcome these challenges to enable mass production.

13:30–14:45

STu3F • Distributed and Acoustic Sensors

Gilberto Brambilla, Univ. of Southampton, USA, Presider

STu3F.1 • 13:30 **Invited**

Miniature Fiber Acoustic Sensors and Sensor Array Using Photonic-Crystal Membranes, Michel J. Digonnet¹, Onur Akkaya¹, Gordon Kino¹, Olav Solgaard¹; ¹Stanford Univ., USA. We report a low-profile acoustic fiber sensor array incorporating ten miniature fiber Fabry-Perot acoustic sensors utilizing a reflective photonic-crystal diaphragm with exhibit high sensitivity, broad bandwidth, high thermal stability, and nearly identical operating wavelengths.

STu3F.2 • 14:00 **Invited**

Fiber Optic Distributed Sensing with Active Self-heating, Tong Chen¹, Kevin P. Chen¹, Qingqing Wang¹, Botao Zhang¹, Rongzhang Chen¹; ¹Electrical and Computer Engineering, Univ. of Pittsburgh, USA. We report distributed sensing with active control using self-heated optical fibers. The heat loss profile along the fiber is spatially interrogated with Rayleigh backscattering to perform gas flow, liquid level and hydrogen gas leakage measurements.

STu3F.3 • 14:30

Carrier Suppressed Modulation for Brillouin Gain Spectrum Analysis, Vemula Venkat Achuth¹, Ramalakshmi Agasthi¹, Deepa Venkatesh¹, Balaji Srinivasan¹; ¹Electrical Engineering, Indian Institute of Technology Madras, India. We characterize the temperature dependent gain spectrum of Stimulated Brillouin scattering in an optical fiber by using a probe signal generated through carrier suppressed modulation. Probe amplification with pulsed pump is analyzed using these results.

15:00–15:30 Exhibit Hall & Coffee Break, The Dolphins on the Upper Plaza

These concurrent sessions are grouped across two pages. Please review both pages for complete session information.

15:30–17:30

ATu4A • Optical Design and Packaging

Jess Ford; *Weatherford International Ltd, USA, President*

ATu4A.1 • 15:30 Invited

Rugged Micro-Optic Packaging for Extreme Environments, Thomas L. Haslett¹, Joseph L. Dallas¹; ¹*Avo Photonics Inc, USA*. Optical assemblies are being deployed in increasingly harsh environments from the high-vacuum cold environment of space to the high pressure, high temperature environment of down-hole applications. Challenges and resolution approaches to harsh environment optical packaging will be discussed.

ATu4A.2 • 16:10 Invited

Optical Design Considerations of Polarization and Fluorescence Imaging Systems, Rongguang Liang¹; ¹*Univ. of Arizona, USA*. This talk will use a medical device as an example to discuss optical design considerations of polarization and fluorescence imaging systems.

ATu4A.3 • 16:50 Invited

Rapid Low Cost Electro-Optic Prototyping for Space Through Use of Cubesats, Renny A. Fields¹, David Hinkley¹; ¹*The Aerospace Corporation, USA*. High function EO space missions are being demonstrated on a rapid schedule from concept to implementation using cubesat hosts. The low total satellite mission cost enables use of cutting edge COTS components and multiple missions to achieve mission assurance. Examples will be presented.

15:30–17:30

CTu4B • Computational Imaging

Rafael Piestun; *Univ. of Colorado, USA, President*

CTu4B.1 • 15:30

Low-complexity Noise-Resilient Recovery of Phase and Amplitude from Defocused Intensity Images, Jingshan Zhong¹, Justin Dauwels¹, Manuel Vazquez², Laura Waller³; ¹*School of Electrical and Electronic Engineering (EEE), Nanyang Technological Univ. (NTU), Singapore*; ²*Depto. de Teoria de la Señal y Comunicaciones, Universidad Carlos III de Madrid, Spain*; ³*Department of Electrical Engineering, Princeton Univ., USA*. A low-complexity augmented Kalman filter is proposed to efficiently recover the phase from a series of noisy intensity images. The proposed method is robust to noise, has low complexity, and may enable real-time phase recovery.

CTu4B.2 • 15:45

3D Automatic Target Recognition of Passive Photon Counting Integral Imaging using Advanced Correlation Filters, Myungjin Cho¹, Abhijit Mahalanobis², Bahram Javidi¹; ¹*Electrical and Computer Engineering, Univ. of Connecticut, USA*; ²*Lockheed Martin, USA*. We overview 3D automatic target recognition of passive photon counting integral imaging using advanced correlation filters.

CTu4B.3 • 16:00

Computational Lightcurve Imaging, Keith J. Dillon¹, Yeshaiahu Fainman¹; ¹*Electrical and Computer Engineering, Univ. of California San Diego, USA*. We consider lightcurve inversion, the reconstruction of an object given a single pixel measurement over a range of angles. We demonstrate an approach using nonlinear optimization, giving an example in two dimensions using Lambertian reflectance.

CTu4B.4 • 16:15

Analysis of Linear Non-Adaptive Projective Visual Signal Sampling, Kshitij Marwah¹, Ashok Veeraraghavan², Ramesh Raskar²; ¹*Media Lab, Massachusetts Institute of Technology, USA*; ²*Electrical Engineering, Rice Univ., USA*. We present a first empirical analysis on the best sampling strategy, progressive or random for sensing unknown visual signals of which we can have no more than m linear, non-adaptive measurements.

CTu4B.5 • 16:30

Focusing through Dynamic Disordered Media using a MEMS Spatial Light Modulator, Thomas Bifano¹, Christopher Stockbridge¹, Yang Lu¹, John Moore¹, Samuel Hoffman¹, Kimani Toussaint², Richard Paxman³; ¹*Boston Univ., USA*; ²*Univ. of Illinois, USA*; ³*Paxman Consulting, USA*. Experiments demonstrating controlled optical propagation through a dynamic, highly scattering medium are described. The phase of a coherent beam is controlled both spatially and temporally using a reflective, 1020-segment MEMS spatial light modulator.

CTu4B.6 • 16:45

High-speed Focusing of Light through Dynamic Turbid Media, Donald B. Conkey¹, Antonio M. Caravaca-Aguirre¹, Rafael Piestun¹; ¹*Univ. of Colorado, USA*. We demonstrate a high-speed phase-control holographic technique to focus light through temporally dynamic scattering media. The system generates computer-generated holograms implemented via a binary amplitude deformable mirror device.

15:30–17:30

ITu4C • Image Sensors ▶

Pierre Magnan; *Inst Sup de l'Aéronautique de l'Espace, France, President*

ITu4C.1 • 15:30 Invited

SPAD Image Sensors: From Architectures to Applications, Samuel Burri¹, Edoardo Charbon¹; ¹*Technische Universiteit Delft, Netherlands*; ²*Ecole Polytechnique Federale de Lausanne, Switzerland*. We present the challenges of using single-photon avalanche diodes in large arrays and the architectures employed in the readout systems. We also discuss the elements that make these imagers appealing for some applications and why.

ITu4C.2 • 16:00

CMOS Image Sensor with on-chip Intelligence for Lightning Detection and Imaging, Sébastien Rolando¹, Vincent Goffion¹, Pierre Magnan¹, Michel Tulet², Michel Bréart-de-Boisanger², Olivier Saint-Pé², Saiprasad Guiry², Franck Corbière¹, Romain Molina¹, Franck Larnaudie², Bruno Leone², Leticia Perez-Cuevas¹, Igor Zayer³; ¹*Image Sensor Research Team, ISAE, Université de Toulouse, France*; ²*EADS Astrium, France*; ³*ESTEC, European Space Agency, Netherlands*. We present a CMOS image sensor dedicated to lightning detection and imaging. The detector has been designed for the lightning detector pre-development phase of the European Space Agency Meteosat Third Generation Imager satellite.

ITu4C.3 • 16:15

High Dynamic Range 4Mpixel CMOS Image Sensor for Scientific Applications, Boyd Fowler¹, Paul Vu¹, Chiao Liu¹, Steve Mims¹, Peter Bartkovjak¹, Hung Do¹, Wang Li¹, Jeff Appelbaum¹, Angel Lopez², Angel Lopez²; ¹*BAE Systems Imaging Solutions, USA*. We describe a low noise 2048(H) x 2048(V) CMOS image sensor. The quantum efficiency is 73% at 600nm, the read noise is 1.1e- RMS at 100 fps data rate, the full well capacity is > 36ke-, and the dark current is < 7pA/cm² at 200C.

ITu4C.4 • 16:30

Image Sensor with 20-nm Resolution based on Uniformly Redundant Arrays, Ryan Miyakawa¹, Patrick P. Naulleau¹; ¹*Lawrence Berkeley National Laboratory, USA*. In this paper we present an image sensor based on uniformly redundant arrays that have customizable pixel resolution below 20 nm. This sensor has applications in lithography tools that produce image intensities that cannot be resolved by conventional CCDs.

ITu4C.5 • 16:45 Invited

Quantum Dot Image Sensors, Edward H. Sargent¹; ¹*Univ. of Toronto, Canada*. Colloidal quantum dots are semiconductors synthesized in, and applied from, the solution phase. They enable wide tuning of their sharp spectral response via the quantum size effect. I will present advances in colloidal quantum dot light sensing materials and devices and their application in imaging.

These concurrent sessions are grouped across two pages. Please review both pages for complete session information.

15:30–17:30

OTu4D • Nanostructures and Films

Stephen Jacobs, Univ. of Rochester, USA, Presider

OTu4D.1 • 15:30 **Invited**

Glass Ductility and Fracture at the 50 to 100 - nm Scale, *John C. Lambropoulos^{1,2}, Karan Mehrotra¹, Heather P. Howard^{2,4}, Stephen Jacobs^{2,3}, Department of Mechanical Engineering, Univ. of Rochester, USA; ²Laboratory for Laser Energetics, Univ. of Rochester, USA; ³The Institute of Optics, Univ. of Rochester, USA; ⁴Materials Science Program, Univ. of Rochester, USA. We discuss the ductile-brittle transition in optical glass either as ductility occurring at a sufficiently low indenting load (or depth of cut) or nanoindentation of patterned surfaces with features in the range 50-250 nm.*

OTu4D.2 • 16:00 **OF&T Student Paper Contest Participant**

Optical Design with Gradient-Index Elements Constrained to Real Material Properties, *Peter McCarthy¹, Duncan T. Moore¹; ¹The Institute of Optics, Univ. of Rochester, USA. An approach for designing and optimizing optical systems with gradient-index elements constrained to real material properties is detailed. Any two-component GRIN system can be modeled with these tools, providing a way to explore new design spaces.*

OTu4D.3 • 16:15 **OF&T Student Paper Contest Participant**

Nondestructive Metrology of Layered Polymeric GRIN Materials Using Optical Coherence Tomography, *Jianing Yao¹, Panomsak Meemon^{1,2}, Jannick P. Rolland¹; ¹The Institute of Optics, Univ. of Rochester, USA; ²School of Laser Technology and Photonics, Institute of Science, Suranaree Univ. of Technology, Thailand. Based on swept-source OCT technology, we investigated the unique capability of OCT for nondestructive three-dimensional characterization of the sub-surface textures and layer thickness profiles of layered polymeric GRIN samples in micrometer scale.*

OTu4D.4 • 16:30

Withdrawn

OTu4D.5 • 16:45

Improved Modeling of Grid Structures on Optics: Transmission, Sheet Resistance and Diffraction Effects, *Matthew W. Pieratt¹, Ian B. Murray¹, Doug Hibbard¹; ¹Exotic Electro-Optics, USA. Metallic grid layers are used for EMI-shielding and heating on aerospace windows and domes. The authors demonstrate the capability to accurately model the optical transmission, EMI attenuation and diffraction effects of such sub-mm-scale grid structures.*

15:30–17:30

STu4F • Micro and Nano-Engineered Sensors

Limin Tong; Zhejiang Univ. China, Presider

STu4F.1 • 15:30 **Invited**

Micro-engineered Optical Fiber Sensors Fabricated by Femtosecond Laser Micromachining, *Dong Ning Wang¹; ¹Hong Kong Polytechnic Univ., Hong Kong. Micro-structures in optical fiber created by femtosecond laser micromachining can function as the sensing elements. Different types of micro-structures can be combined together in single optical fiber to perform multiple parameter measurement without ambiguity.*

STu4F.2 • 16:00 **Invited**

Waveguiding Polymer Single-Nanofibers for Optical Sensing, *Fuxing Gu¹; ¹Optical Engineering, Zhejiang Univ., China. We report highly versatile nanosensors using polymer single nanofibers (PSNFs). Based on optical response of waveguiding PSNFs to specimens, gas and strain sensing are demonstrated with fast response and high-sensitivity.*

STu4F.3 • 16:30 **Invited**

Gas Detection with Micro and Nano-engineered Optical Fibers, *Wei Jin¹, Lifeng Qi¹, Hoi Lut Ho¹, Yingchun Cao¹; ¹Department of Electrical Engineering, Hong Kong Polytechnic Univ., Hong Kong. The prospects for realization of all-fiber gas sensors with hollow-core photonic bandgap fibers and tapered micro/nano optical fibers are investigated. Issues such as high background level and slow response time are discussed.*

17:30–19:00

JTu5A • Joint Poster Session

JTu5A.1

Collaborative work within Optical Engineering: Ethnography and curricular development, Donna M. Lanclos¹, Angela M. Ferrara¹, Matthew A. Davies¹, Chris J. Evans¹, Thomas J. Suleski¹; ¹Univ. of North Carolina at Charlotte, USA. Ethnographic research is used to reveal the nature of collaborative optical engineering work between team members of different backgrounds. Observations in an academic environment are combined data derived from interviews with industry professionals.

JTu5A.2

UFF Belt Characterization, Philip Katz¹, Timothy Lynch¹, Alexander Magill¹, Jakob Maag-Tanchack¹, Jonathan D. Ellis^{1,2}; ¹Department of Mechanical Engineering, Univ. of Rochester, USA; ²Institute of Optics, Univ. of Rochester, USA. Research was conducted on the belts used in OptiPro's UltraForm Finishing (UFF) system to better understand the fundamental mechanics of wear and material removal rates during belt polishing.

JTu5A.3

Nano-Structured Optics for Surface Metrology Research at the National Institute of Standards and Technology, Ulf Griesmann¹, Quandou Wang¹, Johannes Soons¹; ¹NIST, USA. Metrology holograms are critical for interferometric testing of precision aspheric and free-form surfaces with low uncertainty. We describe a new facility for fabrication and research of metrology holograms at NIST.

JTu5A.4

Step-height measurement by low-coherence interferometry based on wavelet transform, Takamasa Suzuki¹, Satoshi Atsumi¹, Osami Sasaki², Samuel Choi²; ¹Graduate School of Science and Technology, Niigata Univ., Japan; ²Faculty of Engineering, Niigata Univ., Japan. This study proposes low-coherence interferometry based on wavelet transform. This method can simultaneously detect the peak position and frequency of a signal. The use of this method for step-height measurement is demonstrated.

JTu5A.5

Withdrawn

JTu5A.6

Optical Testing Applied to a 6.5-Meter Mirror, Rafael Izazaga Pérez¹, Fermin S. Granados-Agustin¹, Ma. Elizabeth Percino-Zacarias¹, Esperanza Carrasco-Licea¹; ¹Instituto Nacional de Astrofísica, Óptica y Electrónica, INAOE, Mexico. We present an optical testing method for the fabrication of a hyperbolic mirror of 6.5-m diameter using a small aperture interferometer. A conic that best fits an off-axis conic section of the mirror is analyzed in order to implement an optical testing method by using sub-apertures.

JTu5A.7

Model For Frictional Forces to Reproduce the Dragging Forces in the Polishing Process, Jorge González-García¹, Alberto Cordero-Davila², Rafael Izazaga³; ¹Instituto de Física y Matemáticas, Universidad Tecnológica de la Mixteca UTM, Mexico; ²Facultad de Ciencias Físico Matemáticas, Benemerita Universidad Autónoma de Puebla BUAP, Mexico; ³Posgrado de Óptica, Instituto Nacional de Astrofísica, Óptica y Electrónica INAOE, Mexico. Dragging forces exerted on a fixed Teflon tool, for several relative velocities of the tool center and polisher densities were measured. Therefore a model for frictional forces that reproduces the dragging forces results is described

JTu5A.8 OF&T Student Paper Contest Participant

Modernizing and Unification of Optical and Mechanical Constructions of Micro-objectives, Alexey Frolov¹, Svyatoslav M. Latyev¹, Alexey G. Tabachkov², Dmitriy N. Frolov², Olga A. Vinogradova², Anatoliy S. Reznikov¹; ¹NRU ITMO, Russian Federation; ²Labor-Microscopes, Russian Federation. Microobjective is one of the main and most principal functional units of the microscope. A variety of methods and techniques work for the microscope determines demand for a wide range of lenses with different characteristics.

JTu5A.9

Precision Glass Molding of Lenses by using the Nanotech Molding Process - A Practical Summary, Michael Fuchs¹, Rolf Rascher¹, Alois Kasberger¹, Christian Wistl¹; ¹Univ. of applied sciences Deggendorf, Germany. Practical review of precision glass molding in usage of the nanotech gpm process for aspheres with form accuracy lower than 1 micron.

JTu5A.10

Quality assessment of precision optical surfaces through light scattering techniques, Sven Schröder¹, Alexander von Finck¹, Tobias Herfurth¹, Angela Duparré¹; ¹Fraunhofer IOF, Germany. Light scattering methods are extremely capable for the characterization of optical surfaces. This will be demonstrated for different applications ranging from anisotropic diamond-turned surfaces to polished surfaces exhibiting defects.

JTu5A.11 OF&T Student Paper Contest Participant

Birefringence Dispersion Measured by Low-coherence Spectral Interferometry Using a Spectrophotometer, Zhigang Han^{1,2}, Lei Chen¹, Zhi Xu^{2,3}; ¹School of Electronic and Optical Engineering, Nanjing Univ. of Science and Technology, China; ²Department of Chemistry & Biochemistry, Univ. of Missouri-St.Louis, USA; ³Center for Nanoscience, Univ. of Missouri-St.Louis, USA. Transmittance spectral interferograms were obtained to understand the birefringence dispersion of quartz crystal with fast axis orientation unknown. The interferograms have uniform background and modulation and were taken with 0.5 nm spectral resolution.

JTu5A.12 OF&T Student Paper Contest Participant

Physical, Structural, and Optical Changes in Infrared Glasses as Prepared by Precision Glass Molding (PGM), Benn Gleason¹, Peter Wachtel¹, J. David Musgraves¹, Kathleen A. Richardson¹; ¹COMSET - Clemson Univ., USA. The physical, structural, and optical properties of Schott IG5 were quantified and compared prior to and following precision glass molding.

JTu5A.13

Applying Ronchi test to evaluate local and global surface errors without both approximations and integration, Alberto Cordero-Davila¹, Juana Rosaura Kantún-Montiel¹, Jorge González-García¹; ¹Instituto de Física y Matemáticas, Universidad Tecnológica de la Mixteca UTM, Mexico; ²Facultad de Ciencias Físico Matemáticas, Benemerita Universidad Autónoma de Puebla BUAP, Mexico. A new method to evaluate local and global errors on freeform surfaces is reported. The experimental birronchigram image is reproduced by simulating birronchigrams images. We do not use fringe interference orders neither any integration methods.

JTu5A.14

LANDSAFE® Precision Flight Instrumentation System, Pri Mamidipudi¹, Elizabeth Dakin¹, Daniel Dakin¹; ¹Optical Air Data Systems, USA. Helicopter hover and landing in dust, fog, rain, and high winds is an integral part of military & commercial flight operations. This paper presents capabilities and flight-test results of a standalone LADAR Precision Flight Instrumentation System.

JTu5A.15

Intracavity Terahertz Optical Parametric Oscillator for Stand-off Spectroscopy Applications, Nils Hempler¹, Keith Ruxton¹, Gordon Robertson¹, Marc Châteauneuf¹, Francis Théberge², Gareth T. Maker¹, Graeme P. Malcolm¹; ¹M Squared Lasers Ltd, UK; ²Defence R&D Canada, Canada. M Squared Lasers Firefly-THz, a pulsed, high peak power (>1W) intracavity optical parametric oscillator, will be discussed in terms of its performance and design features. Its application to stand-off detection of explosives will be presented too.

JTu5A.16

Withdrawn

JTu5A.17

Polarization Sensitivity Allows Novel Sensing Opportunities in Terahertz Time-Domain Spectroscopy, Enrique Castro Camus¹; ¹Centro de Investigaciones en Óptica AC, Mexico. The introduction of novel polarization-sensitive photoconductive sensors has considerably broadened the information that can be obtained in single-scan time-domain spectroscopy measurements

JTu5A.18

Morphological Analysis of Bovine Sperm Head in Quantitative Phase-Contrast Holographic Microscopy, Pietro Ferraro^{1,2}; ¹cnr, Istituto Nazionale di Ottica Applicata, Italy; ²Istituto Spallanzani, Italy. Two different algorithms have been developed for in vitro bull sperm head morphometry analysis. Estimation of several morphological parameters has been performed and is demonstrated that semen analysis can be accomplished.

JTu5A.19

Measurement and Analysis for Biological Tissue from a Ring-scanning-based NIR Optical Imaging System, Min-Cheng Pan¹, Liang-Yu Chen², Jhao-Ming Yu³, Hung-Chih Chiang², Jian-Jhong Ciou², Min-Chun Pan², Sheng-Yih Sun³, Chia-Cheng Chou³, Ya-Fen Hsu⁴; ¹Department of Electronic Engineering, Tung-Nan Univ., Taiwan; ²Department of Mechanical Engineering, National Central Univ., Taiwan; ³Tao-Yuan General Hospital/National Central Univ., Taiwan; ⁴Department of Surgery, Landseed Hospital, Taiwan. System verification and the reconstructed optical-property images of breast-like phantoms and biological tissue are presented using a ring-scanning-based imaging system of frequency-domain near infrared diffuse optical tomography with a high degree of spatial flexibility.

JTu5A.20

Radial Slope Measurement of Transparent Samples, David-Ignacio Serrano-García², Noel-Ivan Toto-Arellano^{1,2}, Gustavo Rodríguez-Zurita¹; ¹Facultad de Ciencias Físico-Matemáticas, Benemerita Universidad Autónoma de Puebla, Mexico; ²Centro de Investigaciones en Óptica, A.C., Mexico. An method to measure the radial slope of transparent samples is presented. We have implemented a Mach-Zehnder Radial-Shear interferometer. The experimental results are presented, as well as the experimental evidence for the generation of spiralgrams

JTu5A.21

Design and Comparison for a Ring-scanning-based NIR Optical Imaging System, Jhao-Ming Yu¹, Liang-Yu Chen¹, Min-Chun Pan¹, Hung-Chih Chiang¹, Min-Cheng Pan², Sheng-Yih Sun³, Chia-Cheng Chou³, Ya-Fen Hsu⁴; ¹Department of Mechanical Engineering, National Central Univ., Taiwan; ²Department of Electronic Engineering, Tung-Nan Univ., Taiwan; ³Tao-Yuan General Hospital, Taiwan; ⁴Department of Surgery, Landseed Hospital, Taiwan. Comparison is made among several different imaging configurations in order to evaluate how the source-and-detector arrangement affects the resulting image. Results show that the 3ZIS design is the optimal design for the scanning mechanism.

JTu5A.22

Simulator in Augmented Reality Environment for Natural Interaction for Assembling Electrical Equipment, Nelson Sosa Macmahon¹; ¹Electronic, OSA INAOE, Mexico.

JTu5A.23

An Estimation Theoretic Framework for Structured Illumination Microscopy, David Stoker¹, Erik Matlin¹; ¹SRI International, USA. We propose an estimation theoretic framework for Structured Illumination Microscopy (SIM). Simulation results suggest that SIM can be made less susceptible to noise and illumination modulation error.

JTu5A • Joint Poster Session—Continued

JTu5A.24

Ringier Reduction for Radially Restored Images, Yupeng Zhang¹, Toshitsugu Ueda¹; ¹Graduate school of information, production and systems, Waseda Univ., Japan. This paper demonstrates a ringier reduction method for radially restored images, whose blurred versions are produced by a spherical single lens imaging system (SSLIS) embedded in an experimental camera module.

JTu5A.25

Quasi-optical Terahertz Devices, Benedikt Scherger¹, Martin Koch¹; ¹Philipps Universität Marburg, Germany. We present a collection of new low cost quasi-optical terahertz (THz) devices. Including wave plates made from ordinary copy paper, lenses made from micro powders and liquid filled lenses with variable focus length.

JTu5A.26

Parallel Shot Noise Reduction of Phase Reconstruction in Digital Holographic Microscopy, Bryan Hennelly bryanh@cs.nuim.ie¹, John J. Healy¹; ¹Department of Computer Science, NUIM, Ireland. Digital Holographic Microscopy enables capture of quantitative phase images. With low exposure time the phase is significantly effected with a noise preventing efficient unwrapping. We demonstrate an algorithm to reduce this noise in the phase image.

JTu5A.27

A High Magnification Light-Field Telescope for Extended Depth-of-Field Biometric Imaging, David Stoker¹, Jonathan Wedd¹; ¹SRI International, USA. We developed a light field telescope to simultaneously increase magnification and depth-of-field for biometric applications at large (>20 m) standoff distance. We discuss infrared performance and limitations due to microlens diffraction.

JTu5A.28

Withdrawn

JTu5A.29

Improving Layered 3D Displays with a Lens, Stefan Muenzel¹, Laura Waller¹, Jason W. Fleischer¹; ¹Princeton Univ., USA. We enhance layered 3D displays using a lens placed in front of or in between attenuation layers, which improves resolution or field-of-view of the display. In addition, we significantly reduce memory requirements for layer calculations.

JTu5A.30

Withdrawn

JTu5A.31

3-Point LPG with High Temperature Sensitivity, Paulo Lopes¹, Pedro Simões¹; ¹Physics, Universidade de AVEIRO, Portugal. We report the fabrication of 3-point only Long Period Gratings (LPG) with a CO₂ Laser. Using a high precision translational system, short LPG are obtained, while keeping good sensing parameters: 30dB peak loss and sensitivity of 109 pm/C.

JTu5A.32

Withdrawn

JTu5A.33

Withdrawn

JTu5.34

Spectral Models of Non-optical Water Quality Parameters of Urban Lakes: A case Study in Guangzhou, China, Xiuzhi Chen^{1,2,3}, Shuisen Chen^{1,5}, Yongxian Su^{1,2,3}, Dan Li^{1,2,3}, Weiqi Chen⁴, Liusheng Han^{1,2,3}; ¹Guangzhou Institute of Geography, China; ²Guangzhou Institute of Geochemistry, China; ³Graduate School of Chinese Academy of Sciences, China; ⁴Department of Geography, Oklahoma state university, USA; ⁵College of Earth, Ocean and Atmosphere Sciences, Oregon State University, USA. Derivative indices may be successfully applied to estimate concentrations of optical water constituents from remotely sensed data. Reflectance, spectral derivative and spectral ratio technologies are used to evaluate the potentiality of developing spectral models for the prediction of three water quality parameters. Results indicate that derivative spectra and spectral ratio are more effective in simulating pH, NH₄-N concentrations and DO than original reflectance. Multiple bands combination models of first-derivative spectra and second-derivative spectra can greatly improve NH₄-N simulation accuracies. Comparison with derivative spectra, spectral ratio models are much simpler methods to derive pH, NH₄-N and DO while not losing of the simulation accuracies.

NOTES

These concurrent sessions are grouped across two pages. Please review both pages for complete session information.

07:00–18:00 Registration, Fairway Foyer on Lower Terrace

08:00–10:00

JW1A • Resolution Limits & Spectral Imaging (IS & COSI) 

Kathrin Berkner; Ricoh Innovations, Inc., USA & Michael Gehm; Univ. of Arizona, USA, Presiders

JW1A.1 • 08:00 

Overcoming the Classical Limits Imposed by Diffraction and Multiple-scattering via Computational Optical Imaging, Rafael Piestun¹; ¹Univ. of Colorado, USA. Imaging beyond the resolution limit with subwavelength resolution as well as imaging through strongly scattering media have been recently accomplished overcoming classical limitations. These techniques share the need for wavefront engineering/modulation and matched algorithms.

JW1A.2 • 08:30

Some Topics in Quantum Imaging, Mikhail I. Kolobov^{1,2}; ¹Mathematics, Stanford Univ., USA; ²Laboratoire PHLAM, Université Lille 1, France. This talk will give an overview of quantum imaging which investigates ultimate performance limits in optical imaging imposed by the quantum nature of the light. I will discuss several topics of quantum imaging such as noiseless image amplification, quantum limits of super-resolution, etc.

JW1A.3 • 08:45

System Model and Performance Evaluation of Spectrally Coded Plenoptic Camera, Lingfei Meng¹, Kathrin Berkner²; ¹Ricoh Innovations, Inc., USA. We introduce an end-to-end imaging system model for a spectrally coded plenoptic camera. The model includes a system-dependent spectral demultiplexing algorithm and is used to evaluate spectral quality and classification performance of a spectrally coded plenoptic camera.

JW1A.4 • 09:00 

Field Distribution Techniques for Multi-Dimensional Snapshot Imaging, Tomasz Tkaczyk¹; ¹Rice Univ., USA. Imaging techniques e.g. field slicing and mapping, pinhole or lens field arrays to rapidly acquire multi-dimensional data are discussed. They allow recording and display of spectral, polarization or 3D spatial information in a snapshot mode.

JW1A.5 • 9:30

Random-access Spectral Imaging, Patrick Kelleher¹, Andrew R. Harvey²; ¹School of Physics and Astronomy, Univ. of Glasgow, UK. Real-time high resolution spectral imaging is prevented by various bottlenecks in data acquisition and processing. Discussed here is a prototype instrument based on a random-access approach to data collection that circumvents these limitations.

JW1A.6 • 09:45

Low-cost multi-spectral imaging camera array, James Downing^{1,2}, Andrew A. Murray¹, Andrew R. Harvey²; ¹Imaging, STMicroelectronics, UK; ²Physics and Astronomy, Glasgow Univ., UK. Snap-shot multi-spectral imagers remain prohibitively expensive for many applications. A 5x5 array of miniature, low-cost camera modules record discrete spectral bands from which, with aid of calibration, a co-registered spectral data-cube may be reconstructed.

08:00–10:00

AW1B • Energy and Applied Optics

Sean Christian; Weatherford International Ltd, USA, Presider

AW1B.1 • 08:00 

A Real-time Gas Cloud Imaging Camera for Fugitive Emission Detection and Monitoring, Robert T. Kester¹; ¹Rebellion Photonics, Inc., USA. Rebellion Photonics has developed a new snapshot spectral imaging technology for continuous monitoring of fugitive gas emissions. Its advantages include elimination of motion artifacts due to gas plume movement, high sensitivity, and low maintenance.

AW1B.2 • 08:40 

Rapid Determination of Hydrocarbon Reservoir Quality Properties at the Wellsite by Energy Dispersive X-ray Fluorescence Spectroscopy (ED-XRF), Christopher Smith¹; ¹Weatherford International Ltd, USA. Elemental analysis of reservoir cuttings can be obtained by ED-XRF in near real-time during oil and gas drilling. Elemental data can be used in stochastic models to predict lithology, mineralogy and brittleness of the reservoir formations.

AW1B.3 • 09:20 

Wireless Infrared Gas Sensor, Håkon Sagberg¹, Britta Fismen¹, Knut Sandven¹, Pål Nordbryhn¹, Niels Aakvaag¹, Lars Borgen¹, Jon Tschudt¹, Kari Anne Bakke², Ib-Rune Johansen²; ¹GasSecure, Norway; ²SINTEF, Norway. Infrared hydrocarbon gas detectors are essential for safety, but the requirement for cabled power complicates installation. A new low-power optical design based on a micro-opto-electromechanical system gives reliable battery operation over several years.

10:00–10:30 Exhibit Hall & Coffee Break, The Dolphins on the Upper Plaza

These concurrent sessions are grouped across two pages. Please review both pages for complete session information.

07:00–18:00 Registration, Fairway Foyer on Lower Terrace

08:00–10:00

SW1C • THz Sensors I

Jason Deibel; Wright State Univ., USA, Presider

SW1C.1 • 08:00 **Invited**

Terahertz Imaging and Spectroscopy of Large-Area Single-Layer Graphene, Michael J. Paul¹, Joseph L. Tomaino¹, Andrew Jameson¹, Joshua W. Kevek², Tristan A. Deborde³, Zachary J. Thompson¹, Arend van der Zande², Robert A. Barton³, Paul L. McEuen^{2,4}, Ethan Minot¹, Yun-Shik Lee¹; ¹Physics Department, Oregon State Univ., USA; ²Laboratory of Atomic and Solid-State Physics, Cornell Univ., USA; ³School of Applied and Engineering Physics, Cornell Univ., USA; ⁴Kavli Institute at Cornell for Nanoscale Science, Cornell Univ., USA. THz imaging and spectroscopy using broadband THz pulses map out the THz carrier dynamics of large-area single-layer graphene. Non-contacting, non-destructive THz probing reveals the local sheet conductivity of the graphene samples.

SW1C.2 • 08:30

Analytical Chemical Sensing in the THz Spectral Range, Benjamin L. Moran¹, Alyssa M. Fosnight¹, Ivan R. Medvedev¹; ¹Wright State Univ., USA. Highly sensitive and selective Terahertz sensor utilized to quantitatively analyze a complex mixture of Volatile Organic Compounds is reported. This study serves as basis for our research in environmental sensing and analysis of expired breath.

SW1C.3 • 08:45 **Invited**

New Sources and Schemes for Terahertz Spectroscopy, Martin Koch¹; ¹Philipps Universität Marburg, Germany. We review recent advances in terahertz spectroscopy and the generation of THz waves, which were achieved by the terahertz group at Marburg Univ. in close collaboration with other research groups.

SW1C.4 • 09:15

Fabrication of Terahertz Gradient-index Components via 3D Rapid Prototyping, Wei-Ren Ng¹, Dathon R. Golishi¹, Hao Xin¹, Michael E. Gehm¹; ¹Univ. of Arizona, USA. New advancements in 3D rapid prototyping have allowed us to explore the development of terahertz gradient-index components. We report on our progress with designing and fabricating terahertz computer generated volume hologram gradient-index components.

SW1C.5 • 09:30 **Invited**

Metamaterials for Terahertz Sensing and Detection, Richard D. Averitt¹; ¹Boston Univ., USA. I will discuss metamaterials for enhanced terahertz detection and chemical sensing. The integration of metamaterials with conventional materials offers unique approaches including designed absorption, polarization sensitivity, field enhancement, and dynamically reconfigurable properties.

08:00–10:00

OW1D • Process Engineering

Katie Schwert; Edmund Optics, USA, Presider

OW1D.1 • 08:00 **Invited**

Application-oriented Testing of Coatings for Precision Glass Molding Tools, Kyriakos Georgiadis^{1,2}, Julia Dukwen¹, Olaf Damboni¹, Fritz Klocke^{1,2}; ¹Fraunhofer Institute for Production Technology IPT, Germany; ²Fraunhofer Project Center for Coatings in Manufacturing PCCM, Germany. Analysis of the precision glass molding process and identification of possible application-specific testing methods. Application of contact angle measurement and annealing testing methods in exemplary case studies and evaluation of the results.

OW1D.2 • 08:30 **OF&T Student Paper Contest Participant**

Optics Fabrication with a Laser Based Process Chain, Sebastian Heidrich¹, Annika Richmann², Edgar Willenborg¹; ¹Fraunhofer Institute for Laser Technology ILT, Germany; ²Chair for Technology of Optical Systems TOS, RWTH Aachen Univ., Germany. The presented laser based process chain is currently under development and focuses on the fabrication of non-spherical optics, since conventional manufacturing methods tend to be comparatively slow and expensive in this field.

OW1D.3 • 08:45

Super Polishing of SiC Aspheric Optics, John Kong¹, Kevin W. Young¹; ¹Precision Asphere, Inc, USA. The method offers higher material removal rates, a deterministic approach to achieving the desired figure, minimizing contact area and the resulting load on the optical structure, and low surface micro-roughness and low mid-spatial frequency error.

OW1D.4 • 09:00 **Invited**

Aspheric and Freeform Hybrid Glass-polymer Optics: The Properties, Implementation and Performance, Valentina V. Doushkina^{1,2}; ¹N2 Imaging Systems, USA; ²Doushkina Optics, USA. Hybrid glass-polymer optical solutions unravel most of the polymer optics limitations. Furthermore, they enhance optical performance, offer compact packaging, low weight, thermal stability, and high volume low manufacturing cost by utilizing freeforms and aspherics.

OW1D.5 • 09:30 **Invited**

Bending Large Glass Plates with Local Heat and Flexible Mold, Tobias Rist¹, Matthias Gremmlspacher¹, Rainer Kübler¹, Manfred Krauss²; ¹Fraunhofer Institute for Mechanics of Materials IWM, Germany; ²Fraunhofer Institute for Silicate Research ISC, Germany. A new automated bending process for flat glass plates is introduced producing high quality bent glass that may be tempered as well. Development was supported by simulations and tested with a new glass bending machine.

10:00–10:30 Exhibit Hall & Coffee Break, The Dolphins on the Upper Plaza

These concurrent sessions are grouped across two pages. Please review both pages for complete session information.

10:30–12:15

JW2A • Sensing with Optical Fiber (AIO & SENSORS) ▶

Hans-Peter Looock; Queen's Univ., Canada, Presider

JW2A.1 • 10:30

Fiber-coupled Fluorescence and Absorption Spectroscopy for Oil and Fuel Characterization, Hengameh Omrani^{1,2}, Alexander Dudelzak^{2,1}, Hans-Peter Looock¹; ¹Chemistry, Queen's Univ., Canada; ²GasTOPS Ltd., Canada. We combined two fiber-optic techniques to permit real-time monitoring of machinery fluids. Excitation emission matrix spectroscopy and fiber-loop cavity ring-down absorption spectroscopy were used to characterize jet fuel and aero-turbine lubrication oil.

JW2A.2 • 10:50 **Invited**

Optical Fibre Chemical Sensors for Process and Environmental Monitoring, Antoine Proulx¹, Serge Caron¹, Claude Pare¹, Sebastien Dubus¹, Nolwenn Le Bouch¹, Patrick Paradis¹, Chiara Meneghini¹, Pierre Galarneau¹; ¹INO, Canada. Ion-selective optodes offer potential for in-line monitoring of various processes. Fibre sensors were developed for H⁺, Ca²⁺, K⁺, Na⁺, NH₄⁺ and NO₃⁻. Applications in hydroponic culture optimization, soil characterization and anaerobic digester process control were demonstrated.

JW2A.3 • 11:30 **Invited**

Optical Microfibers for Fast Current Sensing, Gilberto Brambilla¹; ¹Univ. of Southampton, UK. Issues and benefits of using optical microfibers for current sensing are discussed.

JW2A.4 • 12:00

Strong Bragg grating inscription in microfibers with 193 nm excimer laser, Bai-Ou Guan¹; ¹Jinan Univ., China. Strong Bragg gratings are high effectively inscribed using 193 nm excimer laser in microfibers drawn from multimode fiber. The enlarged photosensitive region offered by multimode fiber significantly enhances grating inscription efficiency.

10:30–12:00

IW2B • Digital Imaging

Francisco Imai; Canon USA, Inc., USA, Presider

IW2B.1 • 10:30 **Invited**

Image Chain Modeling and Applications, Robert D. Fiete¹; ¹ITT Exelis Geospatial Systems, USA. Modeling the imaging chain of digital cameras is necessary to relate the camera design parameters to the resulting image quality. Applications include designing cameras to meet image quality requirements as well as identifying fake images.

IW2B.2 • 11:00

Pixel Count Wars Revisited, Michael A. Kriss¹; ¹MAK Consultants, USA. This paper explores why larger pixels and sensors are key to the future of DSCs. It also looks at how aliasing artifacts are created as a function of the relationship between the optical spread function of the lens, the pixel size and the presence of a color filter array.

IW2B.3 • 11:15

A Critical Review of the Slanted-edge Method for Color SFR Measurement, Prasanna V. Rangarajan¹, Indranil Sinharoy¹, Marc P. Christensen¹, Predrag Milojkovic²; ¹Southern Methodist Univ., USA; ²US Army Research Laboratory, USA. Critical examination of the slanted-edge method for color SFR measurement reveals inaccuracies in the estimated SFR, due to the use of demosaicing. The proposed method resolves these inaccuracies by eliminating the need for demosaicing during SFR measurement.

IW2B.4 • 11:30 **Invited**

Color Imaging for Mobile Displays, Ricardo J. Motta¹; ¹NVIDIA Corporation, USA. We will discuss how changes in technology and viewing conditions require new thinking about color encoding and image processing for mobile displays.

12:00–13:30 Lunch, on your own

These concurrent sessions are grouped across two pages. Please review both pages for complete session information.

10:30–12:00

CW2C • COSI Postdeadline Paper Session

10:30–12:00

OW2D • Freeform Optics

Matthew Jenkins; Raytheon Company, USA, Presider

OW2D.1 • 10:30 **Invited**

Freeforms about to Lift Off - Standardization of Freeform Optics, *Sven Kiontke¹; ¹Asphericon, Germany*. With growing demands in optics the complexity of optical surfaces is increasing. Together with the world wide optical market we depend on understanding technical definitions and descriptions internationally. Standardization for freeforms is an important tool and it helps to remain competitive.

OW2D.2 • 11:00 **OF&T Student Paper Contest Participant**

Interferometric Null Configurations for Measuring ϕ -polynomial Surfaces, *Kyle Fuerschbach¹, Kevin P. Thompson^{2,1}, Jannick P. Rolland¹; ¹The Institute of Optics, Univ. of Rochester, USA; ²Synopsys Inc., USA*. Interferometric null configurations are presented for measuring the form error of two nonsymmetric, Zernike polynomial based optical surfaces designed for use in an off-axis, reflective imaging system.

OW2D.3 • 11:15

Withdrawn.

OW2D.4 • 11:30 **Invited**

Diamond Machining of Freeform Infrared Optics, *Thomas J. Suleski¹, Matthew A. Davies², Brian S. Dutterer²; ¹Physics and Optical Science, Univ. of North Carolina at Charlotte, USA; ²Mechanical Engineering and Engineering Science, Univ. of North Carolina at Charlotte, USA*. We discuss the application of diamond machining to the fabrication of freeform infrared optical components and structures. Fabrication approaches, challenges, and experimental results are presented for several novel optical designs.

12:00–13:30 Lunch, on your own

These concurrent sessions are grouped across two pages. Please review both pages for complete session information.

13:30–15:30

JW3A • Computational Imaging Sensors (COSI & IS) ▶

David Brady; Duke Univ., USA & Gisele Bennett; Georgia Tech, USA, Presiders

JW3A.1 • 13:30 **Invited**

Validation and Clinical Deployment of a Spatial Frequency Domain Imaging (SFDI) System for Wide-field, Quantitative Subsurface Analysis of Tissue Health, David J. Cuccia¹; ¹Modulated Imaging Inc., USA. We present instrument validation and clinical results using a novel spatial frequency domain imaging system, which utilizes structured light projection and wide-field camera detection for quantifying subsurface, spatially-resolved tissue scattering and absorption properties and chromophores.

JW3A.2 • 14:00 **Invited**

Combining Digital Holographic Microscopy with Optical Manipulation: A New Tool in Bio-Microfluidics, Pietro Ferraro¹, L. Miccio¹, P. Memmolò¹, M. Paturzo¹, F. Merola¹; ¹Istituto Nazionale di Ottica Applicata, Italy. Here we show a completely new concept of a compact holographic microscope can ensure the multi-functionality by accomplishing by the same configuration, trapping, manipulation, quantitative phase-contrast maps and accurate 3D tracking in microfluidic environment.

JW3A.3 • 14:30 **Invited**

Scaling Properties of Well-Tiled PFCAs, Patrick Gill¹, Alyosha C. Molnar¹; ¹Univ. of Toronto, Canada; ²Cornell Univ., USA. Planar Fourier Capture Arrays (PFCAs) are imaging devices made from unmodified CMOS Angle-Sensitive Pixels (ASPs). PFCAs require no external imaging optics to photograph distant objects. Here, we explore PFCAs miniaturization in two analyses. First, we show an efficient method of tiling Fourier space with ASPs. Second, we show that the area of an optimally-tiled PCFA scales as the square of the effective number of pixels.

JW3A.4 • 15:00

Challenges in Gigapixel Multiscale Image Formation, Dathon R. Golish¹, Esteban Vera¹, Kevin Kelly², Qian Gong¹, Peter Jansen¹, John Hughes¹, David S. Kittle², David J. Brady¹, Michael E. Gehm^{1,2}; ¹Department of Electrical and Computer Engineering, Univ. of Arizona, USA; ²College of Optical Sciences, Univ. of Arizona, USA; ³Department of Electrical and Computer Engineering, Duke Univ., USA. We present new results from the image formation team on the AWARE Wide-Field project. We will report on new strategies prompted by new challenges encountered in experiments with two prototype AWARE Wide-Field systems.

JW3A.5 • 15:15

CoDAC: Compressive Depth Acquisition using a Single Time-resolved Sensor, Ahmed Kirmani¹, Andrea Colaco¹, Franco N C Wong¹, Vivek K. Goyal¹; ¹EE, MIT, USA. We present a method for compressive acquisition of scene depth with high spatial and range resolution using a single, omnidirectional, time-resolved photodetector and no scanning components by applying novel signal processing to time-of-flight imaging.

13:30–15:30

AW3B • What's next in Applied Imaging

Sapna Shroff; Ricoh Innovations, Inc., USA, Presider

AW3B.1 • 13:30 **Invited**

Structured Light Optical Super-Resolution: Encoding for Limited Optical Bandwidth, Marc P. Christensen¹, Prasanna V. Rangarajan¹, Indranil Sinharoy¹, Predrag Milojkovic²; ¹Department of Electrical Engineering, Southern Methodist Univ., USA; ²Army Research Laboratory, USA. Structured illumination finds widespread use in microscopy and optical profilometry. A marriage of the principle underlying these methods promises novel solutions to the resolution problem that plagues consumer cameras.

AW3B.2 • 14:10 **Invited**

Use of Hyperspectral Imaging for Pharmaceutical Formulation Development, Gabor Kemeny¹, Gina Stuessy¹; ¹Middleton Research, USA. Push-broom hyperspectral imaging based in-situ pharmaceutical blend monitor was developed to aid solid formulation development. Aggregates of the API or excipients are identified using chemometrics and can be monitored with 30 um spatial resolution.

AW3B.3 • 14:50 **Invited**

Wave-field Imaging with Partially Coherent Light, Laura Waller¹, Lei Tian², George Barbastathis², Jason W. Fleischer¹; ¹Princeton Univ., USA; ²Massachusetts Institute of Technology, USA. Coherent (laser) light is fully determined by its amplitude and phase, whereas partially coherent light must involve higher-order statistical descriptions, offering inherently more degrees-of-freedom. Here, we describe practical methods for measurement of partially (spatially) coherent beams.

15:30–16:00 Exhibit Hall & Coffee Break, The Dolphins on the Upper Plaza

These concurrent sessions are grouped across two pages. Please review both pages for complete session information.

13:30–15:30

SW3C • THz Sensors II

Ivan Medvedev; Wright State Univ., USA, Presider

SW3C.1 • 13:30 **Invited**

Terahertz Quantum Cascade Lasers and Applications, Qing Hu¹; ¹MIT, USA. We report our development of record-performance THz quantum cascade lasers and their applications in sensing and imaging.

SW3C.2 • 14:00

Terahertz Excitation of Three-level A-Type Exciton-Polariton Modes in Quantum-Well Microcavity, Yun-Shik Lee¹, Joseph L. Tomaino¹, Andrew Jameson¹, Galina Khitrova², Hyatt Gibbs², Andrea Klettke³, Mackillo Kira³, Stephan Koch³; ¹Oregon State Univ., USA; ²Optical Science Center, Univ. of Arizona, USA; ³Fachbereich Physik and Material Sciences Center, Philips Univ., Germany. Interactions of strong few-cycle THz pulses with the induced optical polarization in a QW microcavity reveal that the exciton-polariton modes and the 2p-exciton state form a unique A-type three-level system of the coupled light-matter modes.

SW3C.3 • 14:15 **Invited**

Image Plane Coding for Terahertz Imaging, Eddie Jacobs¹, Orges Furxhi¹; ¹Electrical and Computer Engineering, Univ. of Memphis, USA. Image plane coding is an alternative to focal plane arrays in terahertz imaging devices. A device for terahertz image plane coding is described. Analysis shows that line imaging devices are favored as opposed to two-dimensional imaging.

SW3C.4 • 14:45

Terahertz Ellipsometry of Vertically Grown Carbon Nanotubes, Michael J. Paul¹, Nicholas Kuzhta¹, Joseph L. Tomaino¹, Andrew Jameson¹, Tal Sharf¹, Nalin Rupasinghe², Kenneth Teo³, Viktor Podolskiy³, Ethan Mino⁴, Yun-Shik Lee¹; ¹Oregon State Univ., USA; ²AIXTRON Ltd., UK; ³Physics and Applied Physics, Univ. of Massachusetts, USA. THz ellipsometry with broadband THz pulses reveals anisotropic THz responses from closely packed, vertically grown CNTs. Non-negligible conductivity in a direction normal to the CNT axis indicates carrier transport between adjacent CNTs.

SW3C.5 • 15:00 **Invited**

Coherent Terahertz Holographic and Tomographic Imaging, Henry O. Everitt^{1,2}, Martin Heimbeck¹, Daniel Marks², David J. Brady²; ¹Army AMRDEC WSD, USA; ²Duke Univ., USA. This talk will survey the application of digital holographic and tomographic techniques to highly coherent, single frequency terahertz sources and extremely sensitive heterodyne receivers for high resolution three dimensional reconstructions of extended, visibly opaque objects.

13:30–15:30

OW3D • Large Optics

Dae Wook Kim; Univ. of Arizona, USA, Presider

OW3D.1 • 13:30 **Invited**

UK Developments Towards Rapid Process Chains for Metre Scale Optics, Paul Shore¹, Renaud Jourdain¹, Marco Castelli¹, Paul Morantz¹; ¹CUPE, Cranfield, UK. Need of large scale optics is increasing. Previous low demand meant effective mass production approaches were not developed, consequently prices remained unduly high. This presentation will introduce UK developments to produce optics >400mm more efficiently.

OW3D.2 • 14:00

Mapping Distortion Correction for GMT Interferometric Test, Ping Zhou¹, Hubert Martin², Chunyu Zhao¹, James H. Burge¹; ¹College of Optical Sciences, Univ. of Arizona, USA; ²Steward Observatory, Univ. of Arizona, USA. The interferometric test for the 8.4m off-axis segment of the GMT primary mirror uses a complex null corrector that introduces a large amount of mapping distortion. This paper discusses the mapping correction for this test.

OW3D.3 • 14:15 **OF&T Student Paper Contest Participant**

Dependence of Thermal Stresses on Substrate Thickness During Wet Processing of Large Coated Optics, Heather Howard^{1,2}, John C. Lambropoulos^{1,3}, Stephen Jacobs^{1,4}; ¹Laboratory for Laser Energetics, Univ. of Rochester, USA; ²Materials Science Program, Univ. of Rochester, USA; ³Department of Mechanical Engineering, Univ. of Rochester, USA; ⁴Institute of Optics, Univ. of Rochester, USA. Stresses developed in oxide coatings during wet-cleaning at elevated temperatures were modeled. We demonstrate that coating stresses depend on substrate thickness, suggesting that small witness samples may not accurately represent the behavior of large optics.

OW3D.4 • 14:30 **Invited**

X-ray Optics for Astronomy, Giovanni Pareschi¹; ¹INAF - Osservatorio Astronomico di Brera, Italy. In the year of the 50th anniversary of the discovery of SCO X-1, the first extra solar X-ray source, we will review the technologies, applications and main achievements of X-ray focusing optics used in astronomical satellites.

OW3D.5 • 15:00

Light-weighting, Polishing, Bonding and Testing for the SEOSAT/Ingenio Telescope Mirrors, Emmanuelle Harel¹; ¹Space & Astronomy Program, Sagem, France. Sagem presents its recent developments in light-weighting, polishing, bonding and testing of Zerodur space mirrors equipped with pads and fixation devices. The presentation is based on Sagem's recent successful project for the SEOSAT/Ingenio satellite.

OW3D.6 • 15:15

Stress polishing of E-ELT segments: LAM demonstrator, Emmanuel Hugot¹, Johan Floriot¹, Nicolas Rousselet¹, Marc Ferrarri¹, Marie Laslandes¹, Sebastien Vives¹, Anais Bernard¹, Gerard Lemaître¹; ¹CNRS/Aix Marseille Univ., Laboratoire d'Astrophysique de Marseille, France. LAM is manufacturing a 1.45m diameter off axis segment for the E-ELT primary mirror. The optimised stress polishing process will allow reaching less than 0.5µm RMS of surface error, prior to finishing.

15:30–16:00 Exhibit Hall & Coffee Break, The Dolphins on the Upper Plaza

Cypress 1 & 2

Joint AIO & IS

16:00–18:05

JW4A • Applied Imaging (AIO & IS)

Sri Rama Prasanna Pavani; Ricoh Innovations, Inc., USA; Laura Waller; Princeton Univ., USA, Presider

JW4A.1 • 16:00 **Invited**

Lensfree On-Chip Microscopy and Tomography Toward Telemedicine Applications, *Aydogan Ozcan^{1,2}; ¹Electrical Engineering Department, UCLA, USA; ²Bioengineering Department, UCLA, USA*. We review our recent progress on lensfree holographic on-chip microscopy and tomography techniques that are aimed at telemedicine applications.

JW4A.2 • 16:40 **Invited**

CMOS Angle Sensitive Pixels for 3-D Imaging, *Alysha C. Molnar¹, Albert Wang¹, Patrick Gill¹; ¹Cornell Univ., USA*. Angle Sensitive Pixels (ASPs) are micro-scale diffractive structures sensitive to the angular distribution of incident light. Arrays of ASPs built in standard CMOS, are able to image 3-D structures with or without a lens.

JW4A.3 • 17:20

Deviations in Long Exposure Laser Speckle Contrast Imaging: Accounting for Static Scatterers, *Yaaseen Atchia^{1,2}, Hart Levy^{1,2}, Ofer Levi^{1,2}; ¹Electrical Engineering, Univ. of Toronto, Canada; ²Bio-medical and Biomaterials Engineering, Univ. of Toronto, Canada*. The long exposure speckle imaging model exhibits discrepancies in high velocity vessels. It is shown that static scatterers affect higher velocities more, and multi-exposure imaging may be implemented to account for these deviations.

JW4A.4 • 17:35 **Invited**

Fast, Automatic, Photo-realistic, 3D Modeling of Building Interiors, *Avidel Zakhor; ¹Univ. of California Berkeley, USA*. We develop an architecture and associated algorithms for fast, automatic, photo-realistic 3D models of building interiors using a human operated backpack system made of a suite of sensors such as laser scanners, gyros and cameras.

Cypress 4

Optical Sensors

16:00–17:30

SW4C • SENSORS Postdeadline Paper Session

Point Lobos

Optical Fabrication and Testing

16:00–17:30

OW4D • OF&T Postdeadline Paper Session

17:30–19:30

OSA Corporate Associates: Executive Speaker Series

Michael Silver, CEO of American Elements

The Dolphins on the Upper Plaza

NOTES

Wednesday, 27 June

07:00–15:00 Registration, Fairway Foyer on Lower Terrace

08:00–09:40

ATH1A • Spectroscopy, Lasers, and Imaging, Oh My! *Jess Ford; Weatherford International Ltd, USA, President***ATH1A.1 • 08:00**

Proposal of a Three-dimensional and Long Range Tomography using Optical Frequency Comb Interferometry, Tuan Q. Banh¹, Tatsutoshi Shioda¹, Kohei Suzuki¹, Munehiro Kimura¹, ¹Nagaoka Univ. of Technology, Japan. Coherence property of a broadband, near-infrared light is enhanced to construct a 3-dimensional tomography with the consideration of the measurement depth expansion, the measurement time reduction, and the sample scattering problem.

ATH1A.2 • 08:20 

Trace Gas Detection Using a Broadband Continuous Wave- Cavity Ringdown Spectrometer, Erika Coyne¹, Yu Chen¹, HongBing Chen¹, ¹Tiger Optics, USA. Cavity ring-down spectroscopy is a field-proven analytical technique for trace gas detection. Tiger Optics' newest instrument, the Prismatic, utilizes Brewster's angle prism retro-reflectors creating a broadband cavity for multi-species detection with high sensitivity.

ATH1A.3 • 09:00 

Compact and Portable Spectroscopy Systems for Counterfeit and Illicit Materials Detection, Jason M. Eichenholz¹, ¹Ocean Optics Inc., USA. To make optics based anti-counterfeit systems effective, they need to be small, compact, and portable. We will discuss our latest ultracompact Raman and Absorption spectroscopy optical engine developments as well as their systems architectures.

08:00–10:00

STh1B • Optical Chemical and Biological Sensors: I*Ken Ewing; US Naval Research Lab, USA, President***STh1B.1 • 08:00** 

Spectroscopic Techniques for Proximal Hazard Detection, Paul M. Pellegrino¹, John J. Brady¹, Ellen Holthoff¹, ¹US Army Research Laboratory, USA. Recent hazards both in the civilian and military settings have exposed the necessity to develop sensor systems with increased sensitivity and selectivity for use at proximal ranges. This talk will examine new efforts dedicated towards these goals.

STh1B.2 • 08:30

Immuno-SERS Microscopy: From the Design of Metal Nanoparticle Probes to Histopathology, Sebastian Schluucker¹, Mohammad Salehi¹, Dennis Steingeweg¹, Max Schütz¹, Jens Packeisen², Alexander Marx³, Philipp Ströbel³, ¹Univ. of Osnabrueck, Germany; ²Medical Center, Germany; ³Institute of Pathology, Univ. Hospital, Germany. This contribution covers the most recent developments in our laboratories, in particular the design of SERS nanoparticle probes with defined optical and chemical properties, together with their application for tissue imaging of prostate cancer biopsies.

STh1B.3 • 08:45 

Aerosol Threat Detection: Single Particle Scattering and Spectroscopy, Jay D. Eversole¹, ¹US Naval Research Laboratory, USA. Achieving low detection thresholds for biological/chemical agent aerosols, drives sensor designs to single-particle classification approaches, and short response times suggests optical, on-the-fly interrogation. Spectroscopic methods discussed include fluorescence and IR absorption.

STh1B.4 • 09:15

Biofilm Growth Monitoring on a-Si:H Based Mach-Zehnder Interferometric Biosensors, Eva Melnik^{1,2}, Paul Muellner¹, Roman Bruck¹, Michael Laemmerhofer², Rainer Hainberger¹, ¹AIT Austrian Institute of Technology, Austria; ²Univ. of Vienna, Austria. We characterize the deposition of a multi-layer biotinylated bovine serum albumine/streptavidin biofilm directly on an optical MZI biosensor. From the measurement results we determine the refractive index and layer height of this proteinogenic biofilm.

STh1B.5 • 09:30

Colorimetric Detection of Ultratrace Cholesterol by Free Standing Inverse Opal Hydrogel Films, Xiaomei Zeng¹, Zehui Du¹, Jan Ma¹, ¹School of Materials Science and Engineering, Nanyang Technological Univ., Singapore. Free-standing inverse opal hydrogel films were constructed to colorimetrically detect ultratrace cholesterol. The detection level at 10⁻⁹ M has been demonstrated striking color change with 26nm shift of reflectance peak.

STh1B.6 • 09:45

Coupled Mode Analysis of a Distributed Bragg Reflector Laser for Hydrogen Detection, Benjamin Griffin¹, Amir Arbabi¹, Lynford L. Goddard¹, ¹Electrical and Computer Engineering, Univ. of Illinois at Urbana-Champaign, USA. Simulation results for a DBR laser hydrogen sensor formed using periodic strips of palladium are presented. Due to palladium's sensitivity to hydrogen gas, the laser's output wavelength and power shift in response to hydrogen concentration.

10:00–10:30 Coffee Break, Cypress Foyer on Lower Terrace

Cypress 3

Applied Industrial Optics: Spectroscopy,
Imaging, & Metrology

10:30–12:30

ATH2A • Pharmaceutically and Medically Applied Optics

Sri Rama Prasanna Pavani; Ricoh Innovations, Inc., USA, *Presider*

ATH2A.1 • 10:30 **Invited**

Chemical and Topographic Sample Analysis for the Milli- and Micrometer Range, Jianyong Yang¹, Wei Liu¹, Thomas Dieing², Ute Schmidt², Olaf Hollricher²; ¹WITec Instruments Corp, USA; ²WITec GmbH, Germany. High Confocality in Raman imaging always results in high focus sensitivity and this can make measurements difficult with rough/inclined samples. Here we present solutions for true confocal Raman imaging on microscopic rough and inclined samples.

ATH2A.2 • 11:10 **Invited**

Photo-cosmetic Applications Using Semiconductor Diode Lasers, Stewart Wilson¹; ¹Palomar Medical Technologies, Inc., USA. Semiconductor diode laser devices are well known to be used in a variety of industries; such as telecommunication, military, medical and industrial such as car manufacturing. They are also seeing applications in photo-cosmetic industry as well. Historically, the photo-cosmetic applications have been limited to professional use only, but now some are making their way into home use consumer applications as well. I will present an overview of both professional and home use applications.

ATH2A.3 • 11:50 **Invited**

Model Guided Multi-modal Multi-scale Image Integration for Head and Neck Anatomy, Anand Santhanam¹, Jannick P. Rolland², Kye S. Lee², Huimin Zhao², Daniel Ennis¹, Daniel Low¹, Sherif Ibrahim¹, Patrick Kupelian¹; ¹Univ. of California, Los Angeles, USA; ²The Institute of Optics, Univ. of Rochester, USA; ³Univ. of Rochester, USA. Biomechanical models are employed for guiding the image integration of macro-scale images obtained from Magnetic Resonance Imaging (MRI) with micro-scale images obtained from Optical Coherence Microscopy (OCM) designed for use in image-guided clinical interventions for the head and neck region.

Cypress 1 & 2

Optical Sensors

10:30–12:00

STh2B • Optical Chemical and Biological Sensors: II

Ken Ewing; US Naval Research Lab., USA, *Presider*

STh2B.1 • 10:30 **Invited**

Infrared Optical Fibers for Sensors, J. S. Sanghera¹, L. B. Shaw¹, R. Gattass¹, L. E. Busse¹, W. Kim, S. Bayya¹, D. Gibson¹, V. Nguyen¹, F. Kung², G. Chin², C. Baker², K. Ewing² and I. D. Aggarwal³; ¹Naval Research Laboratory, USA; ²Sotera Defense Solutions, USA; ³Univ. of North Carolina at Charlotte, USA.

STh2B.2 • 11:00

Inkjet-Fabricated SERS-Active Swab-Dipstick, Wei W. Yu¹, Ian M. White¹; ¹Fischell Department of Bioengineering, Univ. of Maryland at College Park, USA. We demonstrate detection of 250 attomoles of Rhodamine 6G using an inkjet-fabricated SERS-active paper-based surface swab-dipstick. The fabrication simplicity and ease of use of this device is unprecedented for SERS-based analytics.

STh2B.3 • 11:15

Illuminating Epidermal Growth Factor Receptor Densities on Filopodia through Plasmon Coupling, Jing Wang¹, Svetlana V. Boriskina¹, Hongyuan Wang¹, Björn M. Reinhard¹; ¹Department of Chemistry and The Photonics Center, Boston Univ., USA. We designed a multivalent immune-labeling strategy using Au nanoparticles and investigated the distribution of the epidermal growth factor receptor density on filopodia and dorsal cell membrane of A431 human epidermoid carcinoma cells through plasmon coupling.

STh2B.4 • 11:30

CO₂ Sensing with a 2005 nm Thulium Holmium Co-doped Fiber Laser, Renjie Zhou¹, Steve McKeown¹, Benjamin G. Griffin¹, Bussaba Amnuaypornsakul¹, Haibo Huang², Steven Eckhoff², Dan Wasserman¹, Lynford L. Goddard¹; ¹Micro and Nanotechnology Laboratory, Univ. of Illinois, USA; ²Department of Agricultural and Biological Engineering, Univ. of Illinois, USA. We demonstrate an all-fiber thulium holmium co-doped fiber laser emitting at 2005 nm. By modulating the temperature of its fiber Bragg grating mirrors, we performed wavelength modulation spectroscopy and quantified CO₂ concentration down to 2%.

STh2B.5 • 11:45

Palladium Based Fabry-Pérot Etalons for Hydrogen Sensing, Manan Raval¹, Steve McKeown¹, Amir Arbabi¹, Lynford L. Goddard¹; ¹Univ. of Illinois at Urbana-Champaign, USA. We present simulations and measurements of palladium coated etalon sensors for detection of hydrogen gas. Hydrogen concentration can be determined by the shift in the wavelength or amplitude of the minima in the interference pattern.

12:00–13:30 **Lunch**, on your own

13:30–15:00

STh3B • Imaging

Sebastian Schluucker; Universitat Osnabrück, USA, *Presider*

STh3B.1 • 13:30 **Invited**

Medical Diagnostics and Prognostics via Infrared and Raman Spectral Imaging, Max Diem¹, Benjamin Bird¹, Miloš Miljković¹, Jennifer Schubert¹, Antonella Mazur¹; ¹Northeastern Univ., USA. We report results of Infrared and Raman spectral imaging studies of tissue microarrays and exfoliated cells to classify cancers and detect early dysplasia and viral infections, respectively. These results indicate high sensitivity and specificity.

STh3B.2 • 14:00 **Invited**

Imaging the Assembly and Dynamics of Individual Protein Complexes in Living Cells, Jacob Piehler¹; ¹Universität Osnabrück, Germany. We have employed multicolor single molecule imaging techniques for probing the assembly of cytokine receptor complexes in the plasma membrane of living cells. Thus, the diffusion and interaction dynamics of individual signaling complexes were unraveled.

STh3B.3 • 14:30 **Invited**

Real-Time Blood-Flow Characterization Using Laser Speckle Imaging, Bernard Choi¹; ¹Univ. of California Irvine, USA. Analysis of the contrast in laser speckle images, is a growing area of interest in the biomedical community. Here, I discuss recent work designed to translate laser speckle imaging concepts from the laboratory to the clinic.

Key to Authors and Presiders

A

Aakvaag, Niels - AW1B.3
 Abelev, Andrei - RTu1E.1
 Achar, Harish V. - SM4F.5
 Achtsnick, Marcel - OM4D.4
 Achuth, Vemula Venkat - STu3F.3
 Agasthi, Ramalakshmi - STu3F.3
 Aggarwal, Ishwar D. - STh2B.1
 Aikens, Dave - OTu2D.5, OM3D
 Akira, Sato - SM3F.4
 Akkaya, Onur - STu3F.1
 Alonso, Miguel A. - ITu3C.3
 Amanzadeh, Mohammad - STu2F.3
 Amarloo, Hadi - JTu5A.16
 Aminossadati, Saiied M. - STu2F.3
 Amnueypornsakul, Bussaba - STh2B.4
 Amra, Claude - OTu1D.1, OTu4D.7
 Anderson, Christopher N. - OTu2D.4
 André, Maria - STu1F.4
 Andre, Paulo S. - SM4F.4, STu1F.4
 Antunes, Paulo - SM4F.4
 Arbabi, Amir - STh1B.6, STh2B.5
 Arce, Gonzalo - CM4B.5, CM4B.6
 Arguello, Henry - CM4B.5
 Armstrong, J. T. - CTu1B.1
 Ashok, Amit - CM4B.3, CTu3B.3
 Atchia, Yaaseen - JW4A.3
 Atsumi, Satoshi - JTu5A.4
 Averitt, Richard D. - SW1C.5
 Awatsuji, Yasuhiro - SM3E.2

B

Babu, S. V. - OM2D.1
 Bachmann, Charles M. - RTu1E.1, RM2
 Baik, Se-Jong - STu1F.3
 Baines, Ellyn K. - CTu1B.1
 Baker, C. - STh2B.1
 Bakke, Kari Anne - AW1B.3
 Bakke, Thor - ATu2A.3
 Balasubramanian, Krishnan - SM4F.5
 Banh, Tuan Q. - Ath1A.1
 Barbastathis, George - AW3B.3, CTu1B.4, CTu4B.7
 Barbier, Remi - ITu4C.6
 Barnard, Kenneth - ITu1C
 Barnum, Matt - CM2B.5
 Bartkovjak, Peter - ITu4C.3
 Barton, Robert A. - SW1C.1
 Batchko, Robert G. - IM2C.4
 Bayya, S. - STh2B.1
 Beadie, Guy - IM2C.3
 Becker, Elisabeth - OM4D.4
 Beckert, Erik - OTu3D.1
 Behr, Bradford B. - AM2A.2
 Bennett, Gisele - IM3C.2, JW3A
 Bennett, Keith - IM4C.3
 Bentley, Julie L. - IM2C.2
 Berkner, Kathrin - CM2B.2, CTu3B.5, JW1A.3, JW1A
 Berkovic, Garry - SM4F.6
 Bhargava, Rohit - CM4B.1
 Biazoli, Claudécir R. - STu1F.1
 Bifano, Thomas - CTu4B.5
 Bird, Benjamin - STh3B.1
 Bjerke, Frøydis - ATu3A.1
 Blair, Bryan - RTu2E.3
 Böhme, Steffen - OTu3D.1
 Bohnert, Klaus - STu2F.5
 Bolshakov, Alexander A. - ATu1A.1
 Borgen, Lars - AW1B.3
 Boriskina, Svetlana V. - STh2B.3

Bovik, Alan C. - JM1A.2
 Bowen, Warwick P. - STu2F.3, STu4E.5
 Bowles, Jeffery - RM3E.2
 Brady, David J. - CM2B.1, CTu3B.1, JW3A.4, SW3C.5, STh1B.1, JW3A
 Brambilla, Gilberto - JW2A.3, STu1E.2
 Bratcher, Andrew - ITu1C.4
 Bréart-de-Boisanger, Michel - ITu4C.2
 Brent, Joshua I. - CM2B.5
 Bressel, Lena - ATu1A.3
 Brown, Thomas D. - STu2F.4
 Bruck, Roman - STh1B.4
 Brunetti, Anna Chiara - STu1E.6
 Burge, James H. - OTu1D.7, OW3D.2, OM4D.1
 Burri, Samuel - ITu4C.1
 Buscher, David - CTu1B.2
 Busse, L. E. - STh2B.1

C

Cajgfinger, Thomas - ITu4C.6
 Canning, John - SM4F, STu4F.4
 Cao, Yingchun - STu4E.3
 Caravaca-Aguirre, Antonio M. - CTu4B.6
 Carlisle, Sarah C. - RM2E.1
 Carney, P. Scott - CM4B.1
 Caron, Serge - JW2A.2
 Carrasco-Licea, Esperanza - JTu5A.6
 Carter, William E. - RTu1E.2
 Castelli, Marco - OW3D.1
 Castro Camus, Enrique - JTu5A.17
 Catryse, Peter B. - ITu1C.2, IM2C
 Champagnat, Frédéric - CM3B.3
 Charbon, Edoardo - ITu4C.1
 Châteauneuf, Marc - JTu5A.15
 Chemishkian, Sergey - CTu3B.5
 Chen, HongBing - Ath1A.2
 Chen, Jian-Ke - AM2A.3
 Chen, Kevin P. - STu3F.2
 Chen, Lei - JTu5A.11
 Chen, Liang-Yao - AM2A.3, JTu5A.19, JTu5A.21
 Chen, Rongzhang - STu3F.2
 Chen, Tong - STu3F.2
 Chen, Yu - Ath1A.2
 Chen, Zhi - CTu1B.4
 Chesini, Giancarlo - STu1F.1
 Chiang, Hung-Chih - JTu5A.19, JTu5A.21
 Chiara Brunetti, Anna - STu2F
 Chin, G. - STh2B.1
 Chin, Sanghoon - STu2F.1
 Cho, Myungjin - CTu4B.2
 Choi, Bernard - STh3B.3
 Choi, Dawoon - SM2F.4
 Choi, Geunchang - SM2F.2
 Choi, Samuel - JTu5A.4
 Chou, Chia-Cheng - JTu5A.19
 Christensen, Marc P. - AW3B.1, IW2B.3
 Christian, Sean - AW1B
 Chung, Taerin - SM2F.4
 Ciou, Jian-Jhong - JTu5A.19
 Clasen, Chris C. - RM2E.1, RTu2E.2, RTu2E.1
 Cojoc, Dan - IM4C.4
 Colaco, Andrea - JW3A.5
 Colonna De Lega, Xavier - OTu1D.4
 Conkey, Donald B. - CTu4B.6
 Corbière, Franck - ITu4C.2
 Cordero-Davila, Alberto - JTu5A.7, JTu5A.13
 Coriand, Luisa - OTu1D.2
 Corrales, Saul - CM2B.5
 Corsetti, James - OTu2D.3

Corson, Mike - RM3E.2
 Coyne, Erika - Ath1A.2
 Craparo, Joseph - AM4A.1
 Cronin, John - AM3A.3
 Crossley, Maxwell J. - STu4F.4
 Cuccia, David J. - JW3A.1

D

Dahan, Maxime - IM4C.5
 Dakin, Daniel - JTu5A.14
 Dakin, Elizabeth - JTu5A.14
 Dallas, Joseph L. - ATu4A.1, AM2A
 Dambon, Olaf - OW1D.1
 Dandu, Veera P. - OM2D.1
 Darcie, Thomas E. - SM2F.3
 Dauwels, Justin - CTu4B.1
 Davies, Angela - OTu1D.6
 Davies, Matthew A. - JTu5A.1, OW2D.4
 Davis, Curtiss - RM2E.4, RM3E.2, RM3E.5, RM3E
 de Groot, Peter - OTu1D.4
 De Lucia, Frank C. - AM4A.3
 De Rossi, Alfredo - STu2E.1
 De Saro, Robert - AM4A.1
 DeAntonio, Michael - RTu1E.5
 Deborde, Tristan A. - SW1C.1
 Deibel, Jason - SW1C
 DeLuca, Jennifer - CM3B.2
 DeLuca, Keith - CM3B.2
 Dicaire, Isabelle - STu2F.1
 Dieing, Thomas - Ath2A.1
 Diem, Max - STh3B.1
 Digonnet, Michel J. - STu3F.1
 Dillon, Keith J. - CTu4B.3
 Ding, Ming - STu1F.2
 Ding, Nan - CM2B.5
 Do, Hung - ITu4C.3
 Doan, Quang Tuyen - ITu4C.6
 Doctor, Katarina - RTu1E.1
 Domingues, Mária - STu1F.4
 Dominjon, Agnes - ITu4C.6
 Dorbach, Andreas - OTu1D.3
 Doushkina, Valentina V. - OW1D.4
 Downing, James - JW1A.6
 Druart, Guillaume - CM3B.3
 Du, Zehui - STh1B.5
 Dubus, Sebastien - JW2A.2
 Dudelzak, Alexander - JW2A.1
 Dukwen, Julia - OW1D.1
 Dunlop, Matthew - CM4B.4
 Duparré, Angela - JTu5A.10, OTu1D.2
 Dutterer, Brian S. - OW2D.4

E

Eastwood, Michael - RM2E.5
 Eberhardt, Ramona - OTu3D.1
 Eckhoff, Steven - STh2B.4
 Efthimion, Philip C. - ATu1A.2
 Eichenholz, Jason M. - Ath1A.3
 Ellis, Jonathan D. - JTu5A.2
 Ellison, Joseph - OM4D.2
 Ennis, Daniel - Ath2A.3
 Eriksson, Göran - STu2F.5
 Evans, Chris J. - JTu5A.1, OTu1D.6, OTu2D
 Everitt, Henry O. - SW3C.5
 Eversole, Jay D. - STh1B.3
 Ewing, Ken - STh2B.1, STh1B, STh2B

- F**
 Faehnle, Oliver W. - OM3D.4, OM2D
 Fainman, Yeshiaahu - CTu4B.3
 Farrell, Joyce - IM4C
 Feldkhun, Daniel - CM3B.5
 Fernandez-Vallejo, Montserrat - SM4F.2
 Ferrara, Angela M. - JTu5A.1
 Ferraro, Pietro - JTu5A.18, JW3A.2
 Feygels, Viktor - ITu1C.3
 Fields, Renny A. - ATu4A.3
 Fiete, Robert D. - IW2B.1
 Finaurini, Sara - IM4C.4
 Fismen, Britta - AW1B.3
 Fleet, Erin F. - IM2C.3
 Fleischer, Jason W. - AW3B.3, CM3B.4, CM3B.6,
 CM3B.7, CTu1B.3, CTu1B.5, JTu5A.29
 Ford, Jess - ATH1A, ATu4A
 Ford, Joseph - CTu2B.3
 Forstner, Stefan - STu4F5
 Fosnight, Alyssa M. - SW1C.2
 Fowler, Boyd - ITu4C.3
 Frias, Ana - STu1E.4
 Frolov, Alexey - JTu5A.8
 Frolov, Dmitriy N. - JTu5A.8
 Fuchs, Michael - JTu5A.9
 Fuerschbach, Kyle - OW2D.2
 Furxhi, Orges - SW3C.3
 Fusina, Robert A. - RTu1E.1
- G**
 Gagliardi, Gianluca - AM2A.4
 Galarneau, Pierre - JW2A.2
 Gao, Bo-Cai - RM3E.3
 Gasmi, Khaled - RTu1E.4
 Gasmi, Taieb - RTu1E.4
 Gattass, R. - STh2B.1
 Gehm, Michael E. - SW1C.4, CM4B.4, CTu3B.2, JW3A.4,
 JW1A, CM2B
 George, Nicholas - IM3C.1
 Georgiadis, Kyriakos - OW1D.1
 Gerwe, David - CM4B
 Gibbs, Hyatt - SW3C.2
 Giesen, Moritz - SM2F.1
 Gill, Patrick - JW3A.3, JW4A.2
 Gleason, Benn - JTu5A.12
 Glennie, Craig - RTu1E.2
 Goddard, Lynford L. - STh1B.6, STh2B.5, STh2B.4
 Goiffon, Vincent - ITu4C.2
 Golish, Dathon R. - CM4B.4, JW3A.4, JW3A.4, SW1C.4
 Gong, Qian - JW3A.4
 Gonzalez, Jhanis J. - ATu1A.1
 González-García, Jorge - JTu5A.7, JTu5A.13
 Good, William - RM3E.5
 Goodman, Joseph W. - JM1A.1
 Gorodkin, Sergei - OM3D.3
 Gottfried, Jennifer - AM4A.3
 Goyal, Vivek K. - JW3A.5
 Gramatikov, Boris - IM3C.4
 Granados-Agustin, Fermin S. - JTu5A.6
 Green, Kate - CM2B.5
 Green, Robert O. - RM2E.5
 Gremmelspacher, Matthias - OW1D.5
 Grepstad, Jon Olav4, - IM4C.2
 Griesmann, Ulf - JTu5A.3, OTu1D
 Griffin, Benjamin - STh1B.6, STh2B.4
 Grover, Ginni - CM3B.2
 Gu, Fuxing - STu4F2
 Guan, Bai-Ou - JW2A.4, SM4F.1, STu1F
 Gudan, Ken - CTu3B.5
 Guenther, Bruce - JM1A.3, RM3E.3
 Gur, Eran - IM4C.4
 Guyton, David - IM3C.4
- H**
 Haff, Ron - ATu3A.2
 Hainberger, Rainer - STh1B.4
 Haist, Tobias . - SM2F.1
 Hajian, Arsen R. - AM2A.2
 Hald, Jan - STu2F.2
 Han, Zhigang - JTu5A.11
 Hardesty, Chuck - RM3E.5
 Harel, Emmanuelle - OW3D.5
 Hart, Michael - CTu2B.1
 Harvey, Andrew - JW1A.5, JW1A.6, CM3B, CTu1B
 Harwood, Joseph - RTu2E.4
 Hasegawa, Satoshi - SM3F.4
 Haslett, Thomas L. - ATu4A.1
 Hass, Roland - ATu1A.3
 Hawkins, Jeffrey - JM1A.3
 Hayasaki, Yoshio - SM3F.4, SM2F
 He, Liangyu - OTu1D.6
 Healy, John J. - ITu3C.2, ITu3C.4, JTu5A.26
 Hege, Keith - CTu2B.1
 Heidrich, Sebastian - OW1D.2
 Heil, Joachim - OTu1D.3
 Heimbeck, Martin - SW3C.5
 Helmbrecht, Michael - ATu2A.2
 Helvajian, Henry - JM1A.4
 Hempler, Nils - JTu5A.15
 Hennelly, Bryan - JTu5A.26
 Herffurth, Tobias - JTu5A.10
 Hernandez-Palacios, Julio - ITu2C.1
 Heshmat, Barmak - SM2F.3
 Heuck, Hans-Martin - OTu1D.3
 Hibbard, Doug - OTu4D.5
 Hindsley, Robert B. - CTu1B.1
 Hinkley, David - ATu4A.3
 Ho, Hoi Lut - STu4F3
 Hoffman, Samuel - CTu4B.5
 Hollricher, Olaf - ATH2A.1
 Holthoff, Ellen - STh1B.1
 Hope, Douglas A. - CTu2B.1
 Horisaki, Ryoichi - CM2B.4, CTu3B.4
 Howard, Heather - OTu4D.1, OW3D.3
 Hsu, Ya-Fen - JTu5A.19, JTu5A.21
 Hu, Qing - SW3C.1
 Huang, Haibo - STh2B.4
 Huang, James - CTu3B.3
 Huang, Tony Jun - OTu3D.2
 Hughes, John - JW3A.4
 Hull, Jonathan - CTu3B.5
- I**
 Idier, Jérôme - CM3B.3
 Ihrke, Ivo - CTu4B.8
 Imai, Francisco - IW2B
 Irsch, Kristina - IM3C.4
 Izazaga Pérez, Rafael - JTu5A.6
 Izazaga, Rafael - JTu5A.7
- J**
 Jackson, Eric S. - ATu3A.2
 Jacobs, Eddie - SW3C.3
 Jacobs, Stephen - OW3D.3, OTu4D.1
 Jameson, Andrew - SW1C.1, SW3C.2, SW3C.4
 Jansen, Peter - CM4B.4, JW3A.4
 Javidi, Bahram - CTu4B.2
 Jefferies, Stuart M., - CTu2B.1
 Jenkins, Matthew - OW2D
 Jeong, Yoonchan - SM2F.2, SM3F
 Jin, Long - SM4F.1
 Jin, Wei - STu4F.3
 Johansen, Ib-Rune - ATu2A.3, AW1B.3, IM4C.2
 Johnson, Eric - OTu4D.6
 Jorgensen, Anders - CTu1B.1
- Joshi, Neel - CTu2B.2
 Jourdain, Renaud - OW3D.1
 Jung, Norbert - ITu2C.2
- K**
 Kakue, Takashi - SM3F.2
 Kalkowski, Gerhard - OTu3D.1
 Kantún-Montiel, Juana Rosaura - JTu5A.13
 Kasberger, Alois - JTu5A.9
 Kaspar, Peter - IM4C.2
 Katz, Philip - JTu5A.2
 Kaylor, Brant M. - CM4B.3
 Keith, Charlie J. - CM4B.3
 Kelleher, Patrick - JW1A.5
 Kelly, Kevin - JW3A.4
 Kemeny, Gabor - AW3B.2
 Kermit, Martin - ATu3A.1
 Kester, Robert T. - AW1B.1
 Kevek, Joshua W. - SW1C.1
 Khitrova, Galina - SW3C.2
 Kim, Angela M., - RM2E.1, RTu2E.1, RTu2E.2
 Kim, Dae Wook - OM4D.1, OTu1D.7
 Kim, Hyuntai - SM2F.2
 Kim, Myung . - SM3F.1
 Kim, W. - STh2B.1
 Kim, Young Ho - STu1F.3
 Kimura, Munehiro - ATH1A.1
 Kino, Gordon - STu3F.1
 Kiontke, Sven - OW2D.1
 Kirmani, Ahmed - JW3A.5
 Kizil, Mehmet S. - STu2F.3
 Klettke, Andrea - SW3C.2
 Klocke, Fritz - OW1D.1
 Knittel, Joachim - STu4F.5
 Koch, Martin - JTu5A.25, SW1C.3
 Koch, Stephan - SW3C.2
 Kolobov, Mikhail I. - JW1A.2
 Kong, John - OW1D.3
 Kordonski, William - OM3D.3
 Korwan, Dan - RTu1E.1
 Krauss, Manfred - OW1D.5
 Kriss, Michael A. - IW2B.2
 Kruse, Fred A. - RM2E.1, RM2E.2, RM3E.4, RTu2E.1,
 RTu2E.2
 Kübler, Rainer - OW1D.5
 Kuhta, Nicholas - SW3C.4
 Kulawiec, Andrew W. - OM3D.3
 Kung, F. - STh2B.1
 Kupelian, Patrick - ATH2A.3
- L**
 Lacolle, Matthieu - ATu2A.3
 Laemmerhofer, Michael - STh1B.4
 Lambropoulos, John C. - OTu4D.1, OW3D.3
 Lanclos, Donna M. - JTu5A.1
 Lapenna, Jacob - CM3B.4
 Larnaudie, Franck - ITu4C.2
 Latyev, Svyatoslav M. - JTu5A.8
 Lawal, Oliver - AM3A.2
 Le Besnerais, Guy - CM3B.3
 Le Bouch, Nolwenn - JW2A.2
 Lee, Byeong Ha - STu1F.3, SM2F.4
 Lee, Chanki - STu1F.3
 Lee, Krista - RM2E.2
 Lee, Kye S. - ATH2A.3
 Lee, Seung Jong - SM2F.2
 Lee, Yun-Shik - SW1C.1, SW3C.2, SW3C.4
 Lemarchand, Fabien - OTu4D.7
 Leone, Bruno - ITu4C.2
 Lequime, Michel - OTu1D.1, OTu4D.7
 Levi, Ofer - JW4A.3
 Levis, Robert J. - SM3F.5

- Levy, Hart - JW4A.3
 Lewis, Benjamin J. - OTu1D.7
 Lewis, Elfed - AM3A.3, ATu1A
 Li, Eunice - RTu1E.3
 Li, Jing - AM2A.3
 Li, Rong-Rong - RTu1E.1
 Liang, Rongguang - ATu4A.2
 Lingel, Christian - SM2F.1
 Linne von Berg, Dale C. - ITu1C.5
 Linze, Nicolas - SM4F.3
 Liu, Chiao - ITu4C.3
 Liu, Chunyi - ATu1A.1
 Liu, Wei - Ath2A.1
 Livshits, Pauvel - IM4C.4
 Loeff, Adrian R. - OTu1D.7
 Loock, Hans-Peter - JW2A.1, JW2A
 Lopes, Paulo - JTu5A.31
 Lopez, Angel - ITu4C.3
 Lopez-Amo, Manuel - SM4F.2
 Low, Daniel - Ath2A.3
 Lu, Chien-Hung - CM3B.7
 Lu, Ji-Dong - AM2A.3
 Lu, We-Jie - AM2A.3
 Lu, Yang - CTu4B.5
 Lucke, Bob - RM3E.2
 Lynch, Timothy - JTu5A.2
 Lyngso, Jens - STu2F.2
- M**
 Ma, Jan - STh1B.5
 Maag-Tanchack, Jakob - JTu5A.2
 Macon, Christopher L. - RTu2E.4
 Måge, Ingrid - ATu3A.1
 Magill, Alexander - JTu5A.2
 Magnan, Pierre - ITu4C.2, ITu4C
 Mahalanobis, Abhijit - CTu4B.2
 Mainuddin, Mohammad - OM4D.5
 Maker, Gareth T. - JTu5A.15
 Mamidipudi, Pri - JTu5A.14
 Manakov, Alkhazur - CTu4B.8
 Mansell, Justin - IM2C.4
 Mao, Xiaole - OTu3D.2
 Marchese, Sergio V. - STu2F.5
 Margulis, Walter - STu1F.6
 Marks, Daniel - SW3C.5
 Martin, Hubert - OM4D.1, OW3D.2
 Maruno, Tadashi - IM4C.3
 Marwah, Kshitiij - CTu4B.4
 Marx, Alexander - STh1B.2
 Matlin, Erik - JTu5A.23, RM2E.3
 Matoba, Osamu - SM3F.2
 Mazur, Antonella - STh3B.1
 McCarthy, Denis - AM3A.3
 McCarthy, Peter - OTu2D.3, OTu4D.2
 McEldowney, Scott - AM3A.1
 McEuen, Paul L. - SW1C.1
 McKeown, Steve - STh2B.4, STh2B.5
 Meade, Jeffrey - AM2A.2
 Medvedev, Ivan R. - SW1C.2, SW3C
 Meemon, Panomsak - OTu4D.3
 Mégret, Patrice - SM4F.3
 Mehrotra, Karan - OTu4D.1
 Melnik, Eva - STh1B.4
 Melo, José - SM4F.4
 Memmolo, P. - JW3A.2
 Meng, Lingfei - JW1A.3
 Merola, F. - JW3A.2
 Miccio, L. - JW3A.2
 Mico, Vicente - IM4C.4
 Miljković, Miloš - STh3B.1
 Miller, Steven - JM1A.3
 Milojkovic, Predrag - AW3B.1, IW2B.3
 Mims, Steve - ITu4C.3
- Minot, Ethan - SW1C.1, SW3C.4
 Misawa, Kazuhiko - SM3F.3
 Miyakawa, Ryan - ITu4C.4, OTu2D.4
 Molina, Romain - ITu4C.2
 Molnar, Alyosha C. - JW3A.3, JW4A.2
 Monro, Tanya M. - STu1F.5
 Moore, Duncan T. - IM2C.1, IM2C.2, OTu2D.3, OTu4D.2
 Moore, John - CTu4B.5
 Moran, Benjamin L. - SW1C.2
 Morantz, Paul - OW3D.1
 Motta, Ricardo J. - IW2B.4
 Mouroulis, Pantazis - RM2E.5
 Mozurkewich, David - CTu1B.1
 Muellner, Paul - STh1B.4
 Muenzel, Stefan - JTu5A.29
 Mullany, Brigid A. - OM4D.5
 Münzberg, Marvin - ATu1A.3
 Murray, Andrew A. - JW1A.6
 Murray, Ian B. - OTu4D.5
 Musgraves, J. David - JTu5A.12
 Musser, Joseph A. - RTu1E.1
- N**
 Nairat, Mazen - RTu1E.5
 Nakamura, Tomoya - CM2B.4
 Naqshbandi, Masood - STu4F.4
 Naulleau, Patrick P. - ITu4C.4, OTu2D.4
 Ndiaye, Cesaire - OTu4D.7
 Neifeld, Mark Allen - CTu3B.3
 Nelson, Jessica D. - OM3D.1
 Ng, Wei-Ren - SW1C.4
 Nguyen, V. - STh2B.1
 Nichols, C. Reid - RTu1E.1
 Nikzad, Nima - CTu2B.3
 Nishio, Kenzo - SM3F.2
 Nordbryhn, Pål - AW1B.3
- O**
 O'Farrell, Marion - AM3A, ATu3A
 Ohmura, Yui - SM3F.4
 Ohodnicki, Paul - STu2F.4
 Ojeda-Castaneda, Jorge - CM3B.1
 O'Keefe, Sinead - AM3A.3
 Olivas, Stephen J. - CTu2B.3
 Olsen, Richard C. - RM2E.2, RTu2E.1
 Olson, Eric J. - AM2A.1
 Omrani, Hengameh - JW2A.1
 Osten, Wolfgang - SM2F.1
 Ottevaere, Heidi - ATu2A.1
 Ozcan, Aydogan - JW4A.1
- P**
 Packeisen, Jens - STh1B.2
 Pagano, Thomas - RM3E.1
 Pahlevaninezhad, Hamid - SM2F.3
 Palmer, Michael - OTu1D.7
 Pan, Min-Chun - JTu5A.19, JTu5A.21
 Paradis, Patrick - JW2A.2
 Pare, Claude - JW2A.2
 Pareschi, Giovanni - OW3D.4
 Park, Joong Y. - ITu1C.3
 Park, Seong Jun - STu1F.3
 Parrish, Christopher - RTu1E, RTu2E
 Partridge, Darin - ITu1C.6
 Pascal, Joris - STu2F.5
 Paturzo, M. - JW3A.2
 Paul, Michael J. - SW1C.1, SW3C.4
 Pavani, Sri Rama Prasanna - CTu3B.5, Ath2A, JW4A
 Pegard, Nicolas C. - CM3B.6, CM3B.7
 Pellegrino, Paul M. - STh1B.1
 Percino-Zacarias, Ma. Elizabeth - JTu5A.6
 Perez-Cuevas, Leticia - ITu4C.2
- Perry, Sandra - RM3E.4
 Petersen, Jan C. - STu2F.2
 Petre, Peter - CM4B.2
 Petrucci, Jonathan - CTu4B.7
 Philpot, William - RTu1E.1
 Pihler, Jacob - STh3B.2
 Pieratt, Matthew W. - OTu4D.5
 Piestun, Rafael - CM3B.2, CTu1B.6, CTu4B.6, JW1A.1, CTu4B
 Pisani, Marco - ITu2C.4
 Plemmons, Robert J. - CTu3B.1
 Podolskiy, Viktor - SW3C.4
 Poon, Phillip - CTu3B.2
 Poutous, Menelaos - OTu4D.6
 Prasad, Sudhakar - CTu3B, CTu3B.1
 Preza, Chrysanthe - CM2B.3
 Proulx, Antoine - JW2A.2
 Psaltis, Demetri - IM3C.5
 Pu, Ye - IM3C.5
 Pundmann, Chris - ATu3A.3
 Pung, Aaron - OTu4D.6
 Puschell, Jeff - RM3E.6
- Q**
 Qi, Lifeng - STu4F.3
 Quirin, Sean - CM3B.2, CTu1B.6
- R**
 Ramakrishnan, Rajkumar - SM4F.5
 Ramirez, Ana - CM4B.6
 Ramnath, Vinod - ITu1C.3
 Randeberg, Lise L. - ITu2C.1
 Rangarajan, Prasanna V. - AW3B.1, IW2B.3
 Rascher, Rolf - JTu5A.9
 Raskar, Ramesh - CTu4B.4
 Raval, Manan - STh2B.5
 Reibel, Randy R. - CM4B.3
 Reich, Oliver - ATu1A.3
 Reinhard, Björn M. - STh2B.3
 Rembe, Christian - SM2F.1
 Reshetouski, Ilya - CTu4B.8
 Reznikov, Anatoliy S. - JTu5A.8
 Richardson, Brandon - RM2E.5
 Richardson, Kathleen - OTu4D, JTu5A.12
 Richmann, Annika - OM4D.3, OW1D.2
 Rist, Tobias - OW1D.5
 Robertson, Gordon - JTu5A.15
 Robinson, Sam - IM2C.4
 Rocha, Ana - STu1F.4
 Rodrigues, Hugo - SM4F.4
 Rodriguez-Zurita, Gustavo - JTu5A.20
 Rolando, Sébastien - ITu4C.2
 Rolland, Jannick P. - Ath2A.3, OTu4D.3, OW2D.2
 Romero, Carlos - AM4A.1
 Roth, Zachary - OTu4D.6
 Rottwitz, Karsten - STu1F.6
 Rubinsztein-Dunlop, Halina - STu4F.5
 Rumpf, Raymond - OTu4D.6
 Rupesinghe, Nalin - SW3C.4
 Russo, Richard E. - ATu1A.1
 Ruxton, Keith - JTu5A.15
 Ryan, John - RM2E.4
- S**
 Sabsabi, Mohamad - AM4A.2
 Sadler, Brian - CM4B.6
 Safavi-Naeini, Safieddin - JTu5A.16
 Sagberg, Håkon - ATu2A.3, AW1B.3
 Saint-Pé, Olivier - ITu4C.2
 Salehi, Mohammad - STh1B.2
 Sandven, Knut - AW1B.3
 Sanghera, Jasbinder S. - STh2B.1

- Santhanam, Anand - ATH2A.3
 Sargent, Edward H. - ITu4C.5
 Sasaki, Osami - JTu5A.4
 Scherger, Benedikt - JTu5A.25
 Schluecker, Sebastian - STh1B.2, STh3B
 Schmidt, Bradley - AM2A.2
 Schmidt, Greg R. - OTu2D.3
 Schmidt, Ute - ATH2A.1
 Schmitt, Henrique R. - CTu1B.1
 Schnitzer, Mark - IM4C.1
 Schröder, Sven - JTu5A.10, OTu1D.2
 Schubert, Jennifer - STh3B.1
 Schütz, Max - STh1B.2
 Schwaneberg, Oliver - ITu2C.2
 Schwertz, Katie - OW1D
 Seger, Eric M. - CM4B.3
 Segtman, Vegard - ATu3A.1
 Seidel, Hans-Peter - CTu4B.8
 Sellars, Jon - RTu1E.1
 Serrano-Garcia, David-Ignacio - JTu5A.20
 Shafir, Ehud - SM4F.6
 Shapira, Alon - IM4C.4
 Sharf, Tal - SW3C.4
 Shaw, Leslie B. - STh2B.1
 Sheridan, Eoin - STu2F.3, STu4F.5
 Sheridan, John - ITu3C, ITu3C.4
 Shields, Eric A. - CTu2B.4
 Shioda, Tatsutoshi - ATH1A.1
 Shirk, James - IM2C.3
 Shore, Paul - OW3D.1
 Shrestha, Ramesh L. - RTu1E.2
 Shroff, Sapna - CM2B.2, ATu2A, AW3B
 Silny, John - RM3E.6
 Simões, Pedro - JTu5A.31
 Simonsen, Anders - STu2E.2
 Singh, Ghanshyam - OTu4D.4
 Sinharoy, Indranil - AW3B.1, IW2B.3
 Sinzinger, Stefan - IM3C.3
 Situ, Guohai - CTu1B.3
 Skauli, Torbjorn - ITu4C.2, ITu2C, ITu2C.3
 Sletten, Mark - RTu1E.1
 Smith, Christopher - AW1B.2
 Smith, Geoff - RTu1E.1
 Smith, Greg A. - OTu1D.7
 Sohn, Erika - OM3D.2, OM4D
 Solgaard, Olav - IM4C.2, STu3F.1
 Soons, Johannes - JTu5A.3
 Sorel, Michal - CTu2B.3
 Sosa Macmahon, Nelson - JTu5A.22
 Srinivasan, Balaji - SM4F.5, STu3F.3
 Steiger, Olivier - STu2F.5
 Steiner, Holger - ITu2C.2
 Steingeweg, Dennis - STh1B.2
 Stephens, Michelle - RM3E.5
 Stockbridge, Christopher - CTu4B.5
 Stoker, David - JTu5A.23, JTu5A.27, RM2E.3, RTu1E.3
 Stuessy, Gina - AW3B.2
 Sudbo, Aasmund S. - IM4C.2
 Suleski, Thomas J. - JTu5A.1, OW2D.4
 Sun, Sheng-Yih - JTu5A.21
 Suzuki, Kohei - ATH1A.1
 Suzuki, Takamasa - JTu5A.4
 Szilagyi, Andrei - IM2C.4
 Szwaykowski, Piotr - OTu2D.1
- T**
 Tabachkov, Alexey G. - JTu5A.8
 Tahara, Tatsuki - SM3F.2
 Takacs, Peter Z. - OTu1D.5
 Takke, Ralf - OM2D.2
 Tam, Hwa-Yaw - SM4F.1
 Tampa, Yusuke - CTu3B.4
 Tanida, Jun - CM2B.4, CTu3B.4
- Taylor, Keith - SM2F.3
 Testorf, Markus E. - ITu3C.1
 Théberge, Francis - JTu5A.15
 Thevenaz, Luc - STu2F.1
 Thielemann, Jens T. - ATu3A.1
 Thienpont, Hugo - ATu2A.1
 Thompson, Kevin P. - OW2D.2
 Thompson, Zachary J. - SW1C.1
 Thurman, Samuel T. - ITu1C.4
 Tian, Lei - AW3B.3, CTu4B.7
 Tihon, Pierre - SM4F.3
 Tinker, Flemming - OM4D.6
 Tkaczyk, Tomasz - JW1A.4
 Toda, Eiji - IM4C.3
 Tomaino, Joseph L. - SW1C.1, SW3C.2, SW3C.4
 Tong, Limin - STu4F
 Toto-Arellano, Noel-Ivan - JTu5A.20
 Toussaint, Kimani - CTu4B.5
 Townley-Smith, Paul - OTu3D.3
 Trost, Marcus - OTu1D.2
 Trouvé, Pauline - CM3B.3
 Tschudi, Jon - ATu3A.1
 Tuell, Grady - ITu1C.3, RTu1E.6
 Tufillaro, Nicholas - RM2E.4, RM3E.2, RM3E.5
 Tulet, Michel - ITu4C.2
 Tünnermann, Andreas - OTu3D.1
 Tyler, David - CTu2B
- U**
 Ueda, Toshitsugu - JTu5A.24
 Ura, Shogo - SM3F.2
- V**
 Valle, Tim - RM3E.5
 van der Laan, Jan - RTu1E.3
 van Dijk, Thomas - CM4B.1
 Van Erps, Jürgen - ATu2A.1
 Van Gorp, Byron E. - RM2E.5
 van Roggen, Elena - RTu1E.1
 Vanderbeek, Richard - RTu1E.3
 VanKerkhove, Steven - OM4D.2
 Varum, Humberto - SM4F.4
 Vazquez, Manuel - CTu4B.1
 Vazquez-Zuniga, Luis A. - SM2F.2
 Veeraraghavan, Ashok - CTu4B.4
 Venkitesh, Deepa - STu3F.3
 Vera, Esteban - CTu3B.2, JW3A.4
 Verlinden, Olivier - SM4F.3
 Vermillion, Michael - RTu1E.1
 Vervaeke, Michael - ATu2A.1
 Vinogradova, Olga A. - JTu5A.8
 Visconti, Anthony - IM2C.2
 von Finck, Alexander - JTu5A.10
 Vu, Paul - ITu4C.3
- W**
 Wachtel, Peter - JTu5A.12
 Wagner, Kelvin H. - CM3B.5
 Waller, Laura - AW3B.3, CTu1B.3, CTu1B.5, CTu4B.1,
 JTu5A.29, JW4A
 Waluschka, Eugene - JM1A.3
 Wang, Albert - JW4A.2
 Wang, Dong Ning - STu4F.1
 Wang, Hongyun - STh2B.3
 Wang, Jing - STh2B.3
 Wang, Pengfei - STu1F.2
 Wang, Qingqing - STu3F.2
 Wang, Quandou - JTu5A.3
 Wang, Song-You - AM2A.3
 Warren, Russel - RTu1E.3
 Wedd, Jonathan - JTu5A.27
 Weed, Kent - OTu2D.2
- Weisberg, Arel - AM4A, AM4A.1
 Wesner, Joachim - OTu1D.3
 White, Ian M. - STh2B.2
 White, Stephen - RTu1E.1
 Whitehouse, Andrew - AM4A.1
 Wiederhold, Robert - OM3D.1
 Wildermuth, Stephan - STu2E.5
 Willenborg, Edgar - OM4D.3, OW1D.2
 Wilson, Daniel W. - RM2E.5
 Wilson, Michael - ITu1C.1
 Wilson, Stewart - ATH2A.2
 Winter, Marcus - SM2F.1
 Wissenbach, Konrad - OM4D.3
 Wistl, Christian - JTu5A.9
 Wolfe, Lena - CM2B.5
 Wong, Franco N C - JW3A.5
 Wook Kim, Dae - OW3D
 Woulfe, Peter - AM3A.3
 Wu, Yi-Kai - IM3C.4
- X**
 Xia, Peng - SM3F.2
 Xin, Hao - SW1C.4
 Xin, Kai - OM4D.6
 Xu, Zhi - JTu5A.11
- Y**
 Yang, Jianyong - ATH2A.1
 Yang, Xin - IM3C.5
 Yang, Yue-Mei - AM2A.3
 Yao, Jianing - OTu4D.3
 Yao, Shun-Chun - AM2A.3
 Yao, Zheng - AM4A.1
 Yiu, Jei-Yin - IM2C.4
 Yoo, Jong H. - ATu1A.1
 Young, Kevin W. - OW1D.3
 Yu, Jhao-Ming - JTu5A.19, JTu5A.21
 Yu, Wei W. - STh2B.2
 Yuan, Shuai - CM2B.3
 Yun, Hansik - SM2F.4
- Z**
 Zakhor, Avideh - JW4A.4
 Zalevsky, Zeev - IM3C
 Zayer, Igor - ITu4C.2
 Zeng, Xiaomei - STh1B.5
 Zerrad, Myriam - OTu1D.1, OTu4D.7
 Zhang, Botao - STu3E.2
 Zhang, Qiang - CTu3B.1
 Zhang, Rong-Jun - AM2A.3
 Zhang, Yupeng - JTu5A.24
 Zhang, Zhengyun - CTu1B.4
 Zhao, Chunyu - OW3D.2
 Zhao, Huimin - ATH2A.3
 Zhao, Liang - ITu3C.4
 Zhao, Yun - JTu5A.5
 Zheng, Rong-Er - AM2A.3
 Zhong, Jingshan - CTu4B.1
 Zhou, Ping - OW3D.2
 Zhou, Renjie - STh2B.4
 Zilberman, Shlomo - SM4F.6
 Zou, Weiyao - OTu3D

Imaging and Applied Optics 2012 Update Sheet

Added Presentations

Tuesday, 26 June

RTu2E.2 • 10:45 (is not withdrawn)

Analysis of LiDAR Data for Emergency Management and Disaster Response, *Chris Clasen¹, Fred A. Kruse^{2,1}, Angela Kim^{2,1}; ¹Remote Sensing Center, Naval Postgraduate School, USA; ²Physics, Naval Postgraduate School, USA*. Light detection and ranging (LiDAR) data demonstrate how derived horizontal and vertical coordinates of the ground and objects above the ground can be used to provide detailed information for improved emergency management and disaster response.

Wednesday, 27 June

16:00-16:40 (Point Lobos)

OW4D.1, Tutorial: Recent Advances in Ion Beam and Plasma Jet Processing, *Axel Schindler, Leibniz-Institute of Surface Modification, Germany*. Tutorial will highlight recent advances in R&D of Ion beam figuring (IBF), ion Beam Smoothing (IBS), Reactive Ion Beam Etching (RIBE) and atmospheric Plasma Jet Machining (PJM) (deep aspherization, nanometer shape correction, smoothing, film deposition).

Withdraw Presentations

IM2C.3, Polymer GRIN Lens Design

RTu2E.3, NASA's High-altitude, Swath-mapping Laser Altimeter Capability, Sensor Fusion, and the Development of Technologies to Enable Space-based Lidar Mapping of the Earth's Surface

JTu5A.14, LANDSAFE® Precision Flight Instrumentation System

JTu5A.20, Radial Slope Measurement of Transparent Samples

AW3B.2, Use of Hyperspectral Imaging for Pharmaceutical Formulation Development

OW3D.6, Stress polishing of E-ELT segments: LAM demonstrator

OW1D.4, Aspheric and Freeform Hybrid Glass-polymer Optics

STh3B.1, Medical Diagnostics and Prognostics via Infrared and Raman Spectral Imaging

Presenter Changes

Brigid Mullany will present OM4D.5, **Evaluating the Effect of Single Frequency Vibrations on Pitch Polishing Outcomes**. Also, it is removed from the OF&T student paper contest.

Balaji Srinivasan will present Stu3F.3, **Carrier Suppressed Modulation for Brillouin Gain Spectrum Analysis**

Matthew Fishburn will present ITu4C.1, **SPAD Image Sensors: From Architectures to Applications**

Daniele Spiga will present OW3D.4, **X-ray Optics for Astronomy**

Andrea Colaco¹ will present JW3A.5, **CoDAC: Compressive Depth Acquisition using a Single Time-resolved Sensor**

Presider Changes

Samuel Thurman will be the presider for CTu2B, Image Restoration

Bai-Ou Guan will be the presider for STu4F, Micro and Nano-Engineered Sensors

Schedule Changes

On Tuesday, 26 June the morning COSI sessions are in Cypress 3. The morning IS sessions are in Cypress 1 & 2.

AW3B.1, Structured Light Optical Super-Resolution: Encoding for Limited Optical Bandwidth will now be presented on Wednesday, 27 June at 14:20-14:50.

The OF&T postdeadline session on Thursday, 27 June at 16:00 has been cancelled and replaced with a new Tutorial which is listed above in "Added Presentations".

4D Technology Corporation

3280 E. Hemisphere Loop Suite 146

Tucson, AZ 85706, USA

P: +1 520.294.5600

F: +1 520.294.5601

www.4dtechnology.cominfo@4dtechnology.com

4D Technology designs and manufactures dynamic laser interferometers for non-contact metrology of optical quality surfaces, even in the presence of vibration and turbulence. 4D systems provide high resolution acquisition of phase data in as little as 1microsec, at wavelengths from DUV through NIR. Applications include astronomy, aerospace, general optics, directed energy and more.

Aperture Optical Sciences Inc.

27 Parson Lane Unit G

Durham, CT 06422, USA

P: +1 860.316.2589

F: +1 860.760.6564

iinfo@apertureos.comwww.apertureos.com

Aperture Optical Sciences provides some of the world's most unique optics. We employ advanced technologies for making aspheric mirrors; sic optics, and optics for high energy lasers. AOS optics are deployed in aircraft vision systems, industrial scanners, remote sensing and in research facilities using advanced lasers.

Avo Photonics, Inc.

700 Business Center Drive Suite 125

Horsham, PA 19044 USA

P: +1 215.441.0107

F: +1 215.441.9219

mmulrine@avophotonics.comwww.avophotonics.com

Avo is the photonics industry's trusted source for exclusive, private label photonics design, development, and manufacturing. We produce confidential, client-owned optoelectronic solutions and products for [medical](#), [military](#), [industrial](#), [aerospace](#) and [communications](#) application. Our [markets](#) trust and look to us as their single source for private labeled, precision-engineered photonics solutions and products. Light. Precisely.

BAE Systems Imaging Solutions

1801 McCarthy Blvd.

Milpitas, CA 95035, USA

P: +1 408.433.2500

F: +1 408.435.7352

CAMS.sales@baesystems.comwww.fairchildimaging.com

Proudly representing the entire Fairchild Imaging line of products, BAE Systems Imaging Solutions develops and manufactures solid-state electronic imaging components, camera, and systems. We are a company devoted to the creation of electronic imaging technology, development of that technology to production practically, and manufacture to commercial success.

Bayspec, Inc.

1101 McKay Dr.

San Jose, CA 95131 USA

P: +1 408.512.5928

F: +1 408.512.5928

mfuentes@bayspec.comwww.Bayspec.com

BaySpec, Inc., founded in 1999 with 100% manufacturing in the USA (San Jose, California), is a vertically integrated spectral sensing company. The company designs, manufactures and markets advanced spectral instruments, from UV-VIS spectrometers to handheld and portable NIR and Raman analyzers, for the biomedical, pharmaceuticals, chemical, food, semiconductor, homeland security, and the optical telecommunications industries.

Checkpoint Technologies LLC

66 Bonaventura

San Jose, CA 95134 USA

P: +1 408.321.9780

F: +1 408.321.0155

sales@checkpointtechnologies.comwww.checkpointtechnologies.com

Checkpoint develops and manufactures advanced imaging systems. Our products include confocal laser scanning systems, very high numerical aperture lenses, and electrical signal extraction modules by optical means, fiber coupled EO modulators, and PC controlled multi-laser modules with continuously variable power output. Checkpoint products are used in optical diagnostic applications for semiconductor devices as well as various scientific and research applications. The company also engages in collaborative product development with other technology manufacturers.

OSA would like to THANK the following
2012 Imaging and Applied
Optics Congress:

Corporate Sponsor:



Corporate Contributor:

BAE Systems

No photography is
permitted in the
exhibit hall.

Thank you!



ESDI - Engineering Synthesis Design, Inc.

150 N. Tucson Blvd.
Tucson, AZ 85716 USA
P: +1 520.296.3068
F: +1 520.296.2897
piotr.s@esdimetrology.com
www.esdimetrology.com

ESDI is a globally recognized leader in providing innovative surface & wavefront metrology solutions for astronomical, aerospace, bio-medical, optical fabrication, data storage & production metrology applications. ESDI products include Fizeau, Shearing, sub-Nyquist and "Real Time" vibration insensitive Interferometers; the world-renowned Intellwave™ software; Interferometer Accessories & Upgrades; and Custom Metrology Solutions.

Inrad Optics

181 Legrand Ave
Northvale, NJ 07647 USA
P: +1 201.767.1910
F: +1 201.767.9644
sales@inradoptics.com
www.inradoptics.com

Inrad Optics manufactures custom optics, crystals, electro-optical devices and precision diamond turned metal optics. Our products include transmission flats, beamsplitters, harmonic generation crystals, pockels cells, aspheric mirrors, and opto-mechanical assemblies. Our optical design for manufacturability expertise allows us to execute even the most challenging custom optic designs.

Mitre Corporation

7515 Colshire Drive
McLean, VA 22102, USA
P: +1 703.983.1813
F: +1 703.983.6501
rathale@mitre.org
www.darpa.mil

Manufacturable Gradient Index Optics (MGRIN) is a program initiated by DARPA/STO (Dr. Stephanie Tompkins, PM) that aims to bring GRIN optics into main stream optical design community. As part of this program DARPA expects to initiate a foundry service, GRIN Exchange. Interested parties should contact Dr. Michael Huff at CNRI: mhuff@mems-exchange.org

Ocean Optics, Inc.

830 Douglas Ave.
Dunedin, FL 34698 USA
P: +1 727.733.2447
F: +1 727.733.3962
info@oceanoptics.com
www.oceanoptics.com

Ocean Optics is the inventor of the world's first miniature spectrometer and the industry leader in optical sensing. We provide single solutions, turnkey solutions and spectrometers for field. Ocean Optics also offers a full line of sensing accessories, light sources and optical fibers. Ask about our exclusive 3-year warranty and total technical services.

Optimax Systems, Inc.

6367 Dean Parkway
Ontario, NY 14519 USA
P: +1 585.265.1066
F: +1 585.265.1033
sales@optimaxsi.com
www.optimaxsi.com

Optimax grinds and shines optical materials to make aspheres, cylinders, spheres and prisms to customer specifications. We specialize in producing optics in small lot sizes with diameters up to 300 mm with more than 100 opticians, CNC machining and in-house coating capabilities; Optimax can deliver prototype optics in 1 week!

Photonics Media/Laurin Publishing

2 South Street
Pittsfield, MA 01201 USA
P: +1 413.499.0514
F: +1 413.442.3180
www.photonics.com

Photonics Media – the Pulse of the Industry – invites you to explore the information leader and all that we have to offer. As the publisher of Photonics Spectra, BioPhotonics and EuroPhotonics magazines, Photonics Buyers' Guide, Photonics.com, and more, we bring you the news, research and applications articles you need to succeed. Visit www.Photonics.com for your FREE subscriptions and much more.

PolarOnyx, Inc.

2526 Qume Drive, Suites 17&18
San Jose, CA 95131 USA
P: +1 408.573.0930
F: +1 408.573.0932
sales@polaronyx.com
www.polaronyx.com

World leading company in high energy/power ultrashort (fs, ps, ns) fiber lasers. Excellent for material processing, micromachining, spectroscopy, microscopy, biomedical instrumentation & optical sensing applications. OEM and instrument version are available. Wavelength ranges from UV to Mid-IR. Contact: Lihmei Yang, Director Sales & Product, lihmeiyang@polaronyx.com. New products: GHz high power ultrafast fiber lasers (UV to IR), Compact high energy ultrafast fiber laser (UV to Mid-IR)

Zygo Corporation

Laurel Brook Road
Middlefield, CT 06455 USA
P: +1 860.347.8506
F: +1 860.347.8372
inquire@zygo.com
www.zygo.com

Zygo Corporation is a worldwide supplier of optical metrology instruments, precision optics, and electro-optical design and manufacturing services serving customers in the semiconductor capital equipment, bio-medical, scientific and industrial markets. Our precision noncontact measuring instruments and systems enable manufacturers to increase operating efficiencies and product yields by identifying and collecting quantitative data on product defects during and after the manufacturing process.

4D Technology Corporation

3280 E. Hemisphere Loop Suite 146

Tucson, AZ 85706, USA

P: +1 520.294.5600

F: +1 520.294.5601

www.4dtechnology.cominfo@4dtechnology.com

4D Technology designs and manufactures dynamic laser interferometers for non-contact metrology of optical quality surfaces, even in the presence of vibration and turbulence. 4D systems provide high resolution acquisition of phase data in as little as 1microsec, at wavelengths from DUV through NIR. Applications include astronomy, aerospace, general optics, directed energy and more.

Aperture Optical Sciences Inc.

27 Parson Lane Unit G

Durham, CT 06422, USA

P: +1 860.316.2589

F: +1 860.760.6564

iinfo@apertureos.comwww.apertureos.com

Aperture Optical Sciences provides some of the world's most unique optics. We employ advanced technologies for making aspheric mirrors; sic optics, and optics for high energy lasers. AOS optics are deployed in aircraft vision systems, industrial scanners, remote sensing and in research facilities using advanced lasers.

Avo Photonics, Inc.

700 Business Center Drive Suite 125

Horsham, PA 19044 USA

P: +1 215.441.0107

F: +1 215.441.9219

mmulrine@avophotonics.comwww.avophotonics.com

Avo is the photonics industry's trusted source for exclusive, private label photonics design, development, and manufacturing. We produce confidential, client-owned optoelectronic solutions and products for [medical](#), [military](#), [industrial](#), [aerospace](#) and [communications](#) application. Our [markets](#) trust and look to us as their single source for private labeled, precision-engineered photonics solutions and products. Light. Precisely.

BAE Systems Imaging Solutions

1801 McCarthy Blvd.

Milpitas, CA 95035, USA

P: +1 408.433.2500

F: +1 408.435.7352

CAMS.sales@baesystems.comwww.fairchildimaging.com

Proudly representing the entire Fairchild Imaging line of products, BAE Systems Imaging Solutions develops and manufactures solid-state electronic imaging components, camera, and systems. We are a company devoted to the creation of electronic imaging technology, development of that technology to production practically, and manufacture to commercial success.

Bayspec, Inc.

1101 McKay Dr.

San Jose, CA 95131 USA

P: +1 408.512.5928

F: +1 408.512.5928

mfuentes@bayspec.comwww.Bayspec.com

BaySpec, Inc., founded in 1999 with 100% manufacturing in the USA (San Jose, California), is a vertically integrated spectral sensing company. The company designs, manufactures and markets advanced spectral instruments, from UV-VIS spectrometers to handheld and portable NIR and Raman analyzers, for the biomedical, pharmaceuticals, chemical, food, semiconductor, homeland security, and the optical telecommunications industries.

Checkpoint Technologies LLC

66 Bonaventura

San Jose, CA 95134 USA

P: +1 408.321.9780

F: +1 408.321.0155

sales@checkpointtechnologies.comwww.checkpointtechnologies.com

Checkpoint develops and manufactures advanced imaging systems. Our products include confocal laser scanning systems, very high numerical aperture lenses, and electrical signal extraction modules by optical means, fiber coupled EO modulators, and PC controlled multi-laser modules with continuously variable power output. Checkpoint products are used in optical diagnostic applications for semiconductor devices as well as various scientific and research applications. The company also engages in collaborative product development with other technology manufacturers.

OSA would like to THANK the following
2012 Imaging and Applied
Optics Congress:

Corporate Sponsor:



Corporate Contributor:

BAE Systems

No photography is
permitted in the
exhibit hall.

Thank you!



ESDI - Engineering Synthesis Design, Inc.

150 N. Tucson Blvd.
Tucson, AZ 85716 USA
P: +1 520.296.3068
F: +1 520.296.2897
piotr.s@esdimetrology.com
www.esdimetrology.com

ESDI is a globally recognized leader in providing innovative surface & wavefront metrology solutions for astronomical, aerospace, bio-medical, optical fabrication, data storage & production metrology applications. ESDI products include Fizeau, Shearing, sub-Nyquist and "Real Time" vibration insensitive Interferometers; the world-renowned Intellwave™ software; Interferometer Accessories & Upgrades; and Custom Metrology Solutions.

Inrad Optics

181 Legrand Ave
Northvale, NJ 07647 USA
P: +1 201.767.1910
F: +1 201.767.9644
sales@inradoptics.com
www.inradoptics.com

Inrad Optics manufactures custom optics, crystals, electro-optical devices and precision diamond turned metal optics. Our products include transmission flats, beamsplitters, harmonic generation crystals, pockels cells, aspheric mirrors, and opto-mechanical assemblies. Our optical design for manufacturability expertise allows us to execute even the most challenging custom optic designs.

Mitre Corporation

7515 Colshire Drive
McLean, VA 22102, USA
P: +1 703.983.1813
F: +1 703.983.6501
rathale@mitre.org
www.darpa.mil

Manufacturable Gradient Index Optics (MGRIN) is a program initiated by DARPA/STO (Dr. Stephanie Tompkins, PM) that aims to bring GRIN optics into main stream optical design community. As part of this program DARPA expects to initiate a foundry service, GRIN Exchange. Interested parties should contact Dr. Michael Huff at CNRI: mhuff@mems-exchange.org

Ocean Optics, Inc.

830 Douglas Ave.
Dunedin, FL 34698 USA
P: +1 727.733.2447
F: +1 727.733.3962
info@oceanoptics.com
www.oceanoptics.com

Ocean Optics is the inventor of the world's first miniature spectrometer and the industry leader in optical sensing. We provide single solutions, turnkey solutions and spectrometers for field. Ocean Optics also offers a full line of sensing accessories, light sources and optical fibers. Ask about our exclusive 3-year warranty and total technical services.

Optimax Systems, Inc.

6367 Dean Parkway
Ontario, NY 14519 USA
P: +1 585.265.1066
F: +1 585.265.1033
sales@optimaxsi.com
www.optimaxsi.com

Optimax grinds and shines optical materials to make aspheres, cylinders, spheres and prisms to customer specifications. We specialize in producing optics in small lot sizes with diameters up to 300 mm with more than 100 opticians, CNC machining and in-house coating capabilities; Optimax can deliver prototype optics in 1 week!

Photonics Media/Laurin Publishing

2 South Street
Pittsfield, MA 01201 USA
P: +1 413.499.0514
F: +1 413.442.3180
www.photonics.com

Photonics Media – the Pulse of the Industry – invites you to explore the information leader and all that we have to offer. As the publisher of Photonics Spectra, BioPhotonics and EuroPhotonics magazines, Photonics Buyers' Guide, Photonics.com, and more, we bring you the news, research and applications articles you need to succeed. Visit www.Photonics.com for your FREE subscriptions and much more.

PolarOnyx, Inc.

2526 Qume Drive, Suites 17&18
San Jose, CA 95131 USA
P: +1 408.573.0930
F: +1 408.573.0932
sales@polaronyx.com
www.polaronyx.com

World leading company in high energy/power ultrashort (fs, ps, ns) fiber lasers. Excellent for material processing, micromachining, spectroscopy, microscopy, biomedical instrumentation & optical sensing applications. OEM and instrument version are available. Wavelength ranges from UV to Mid-IR. Contact: Lihmei Yang, Director Sales & Product, lihmeiyang@polaronyx.com. New products: GHz high power ultrafast fiber lasers (UV to IR), Compact high energy ultrafast fiber laser (UV to Mid-IR)

Zygo Corporation

Laurel Brook Road
Middlefield, CT 06455 USA
P: +1 860.347.8506
F: +1 860.347.8372
inquire@zygo.com
www.zygo.com

Zygo Corporation is a worldwide supplier of optical metrology instruments, precision optics, and electro-optical design and manufacturing services serving customers in the semiconductor capital equipment, bio-medical, scientific and industrial markets. Our precision noncontact measuring instruments and systems enable manufacturers to increase operating efficiencies and product yields by identifying and collecting quantitative data on product defects during and after the manufacturing process.

**2012 OSA
OPTICS &
PHOTONICS
CONGRESS**

POSTDEADLINE PAPERS

Imaging and Applied Optics

**Applied Industrial Optics: Spectroscopy,
Imaging, and Metrology (AIO)**

**Computational Optical Sensing and Imaging
(COSI)**

Optical Fabrication and Testing (OF&T)

**Optical Remote Sensing of the Environment
(ORS)**

Optical Sensors (SENSORS)

ISBN 978-1-55752-948-5

24 – 28 June 2012

Monterey Plaza Hotel
Monterey, California, USA

www.osa.org/congresses

Photo credit: Ryan Gallagher, www.kineticphotography.net

OSA[®]

Imaging and Applied Optics: OSA Optics & Photonics Congress

Postdeadline Papers

ISBN 978-1-55752-948-5

RTu2E • ORS Postdeadline Paper

Tuesday, 26 June, 11:30 – 11:45

Big Sur Room

Christopher Parrish; NOAA, NGS, Remote Sensing Div, USA, Presider

RTu2E.5 • 11:30

Derivative Spectroscopy with HICO, *N. Tufillaro*¹; ¹*Oregon State Univ., USA*. HICO® is hyper-spectral ocean spectrometer currently in orbit on the International Space Station. We use HICO's detailed spectral resolution to examine applications of derivative spectroscopy to complex coastal waters with riverine inputs.

COSI Postdeadline Session

Wednesday, 27 June, 10:30-11:00

Cypress 4 Room

TBD, Presider

CW2C.1 • 10:30

Superresolution of Dense Quantum Dot Clusters using Independent Component Classification, *A.J. Barsic*¹, *R. Piestun*¹, ¹*Univ. of Colorado, USA*. We propose a superresolution technique to resolve dense clusters of independently blinking emitters. Experiments and numerical simulations demonstrate the ability to superresolve up to five emitters located within an area of a diffraction limited spot.

CW2C.2 • 10:45

Confidence Measures of Optical Flow for Multi-Frame Image Reconstruction, *A. Kanaev*¹, *C.W. Miller*²; ¹*US Naval Research Lab., USA*; ²*Tekla Research, USA*. Multi-frame image processing encompasses algorithms for imaging through turbulence, super-resolution, and filtering. In-scene motion remains a challenge and requires optical flow estimation. We propose confidence measure to

augment the problem of insufficient optical flow accuracy.

SENSORS Postdeadline Session

Wednesday, 27 June, 16:00-17:45

Cypress 4 Room

Enrique Castro Camus; Centro de Investigaciones en Optica A.C., Mexico, Presider

SW4C.1 • 16:00

Generation and Coherent Detection of Broadband Terahertz Radiation in Phase-Matched Waveguides, *S. Liu*¹, *X. Shou*¹, *A. Agrawal*¹, *A. Nahata*¹, ¹*University of Utah, USA*. We describe novel waveguide devices that allows for broadband generation and coherent detection of THz radiation. We achieve a system with spectral content beyond 8 THz using <10 mW total average optical power.

SW4C.2 • 16:15

Polarization Modulation Time-domain Terahertz Polarimetry, *C.M. Morris*¹, *R. Valdes Aguilar*¹, *A.V. Stier*¹, *N. Armitage*¹, *Dept. of Physics and Astronomy, Johns Hopkins University, USA*. A polarization modulation time-domain THz polarimetry technique with a precision of 0.02° (350 μrad) will be presented, along with ongoing applications to interesting material systems such as topological insulators and quantum magnets.

SW4C.3 • 16:30

Resonant Metamaterial Detectors Utilizing THz Quantum-Cascade Lasers, *A. Benz*¹, *S. Schwarz*¹, *M. Krall*¹, *D. Dietze*¹, *M. Brandstetter*¹, *C. Deutsch*¹, *K. Unterrainer*¹, *H. Detz*¹, *A.M. Andrews*¹, *W. Schrenk*¹, *G. Strasser*¹, *A. Benz*²; ¹*Technische Universität Wien, Austria*; ²*Sandia National Laboratories, USA*. We present the design, fabrication and characterization of a resonant metamaterial detector based on a THz

quantum-cascade laser. The same active region can be used to generate and detect the light leading to miniaturized and integrated optical systems in the THz spectral range.

SW4C.4 • 16:45

Non-Destructive Evaluation of Aerospace Materials using Terahertz Time-Domain Imaging, *L. Owens¹, D.T. Petkie¹, J.A. Deibel¹, D.T. Petkie², J.A. Deibel²*; ¹*Physics, Wright State University, USA*; ²*Electrical Engineering, Wright State University, USA*. THz time-domain imaging was utilized in the non-destructive evaluation of various composite materials used in aerospace structures and components for the characterization of defects and changes in material properties due to mechanical and thermal strain.

SW4C.5 • 17:00

Hydration Dynamics of Arabidopsis Thaliana under Water Deficit Conditions Monitored in-vivo by THz Spectroscopy, *E. Castro Camus¹, M. Palomar², A.A. Covarrubias²*; ¹*Centro de Investigaciones en Optica AC, Mexico*; ²*Biologia Molecular de Plantas, Instituto de Biotecnologia, Universidad Nacional Autonoma de Mexico, Mexico*. We monitored hydration dynamics of *A. thaliana* under water deficit conditions. The plant showed slow dehydration over ~17h followed by rapid loss of moisture over 3h, this might be caused by a defensive mechanism of the plant that activates water availability decreases below certain threshold.

SW4C.6 • 17:15

Recent Experimental Results of a Large Format 80x64 Pixel THz Camera Sensitive to 0.6 – 1.2 THz Radiation, *D. Burdette¹, C. Roedig¹, H.L. Mosbacker¹, J. Alverbro², P. Fay³, K. Sertel⁴, G. Trichopoulos⁴, K. Topalli⁴, Y. Ni⁵*; ¹*Traycer, USA*; ²*IRNova, Kista, Sweden*; ³*Notre Dame, USA*; ⁴*Ohio State Univ., USA*; ⁵*New Imaging Technologies, Buisson, France*. THz applications have been limited by the lack of a cost-effective, real-time, large format THz camera. This paper discusses the recent experimental results of a real-time (100 Hz), large-format (80x64 pixel), broadband (0.6 – 1.2THz) THz camera.

SW4C.7 • 17:30

Improving the Performance of Difference Frequency THz Generation in Waveguides, *P.E. Powers¹, J.W. Haus¹, P.E. Powers², J.W. Haus²*; ¹*Physics Department, University of Dayton, USA*; ²*Electro-Optics Program, University of Dayton, USA*. Improving the performance of THz generation by difference frequency generation is presented for waveguide interactions. A numerical model is used to show how to optimize THz generation and understand cascaded processes in the waveguide.

AIO Postdeadline Paper

Thursday, 28 June, 9:40 – 10:00

Cypress 3 Room

Jess Ford; Weatherford International Ltd, USA, Presider

ATh1A.4 • 9:40

Experimental Demonstration of an NIR Compressive Sensing Hyper-Spectral Imaging System, *Y. Wu¹, G.R. Arce¹, D.W. Prather¹*, ¹*Electrical and Computer Engineering, University of Delaware, USA*. We utilized the compressive sensing theory in building a hyperspectral imaging system for NIR wavelengths. This system simultaneously captures 24 spectral images for the wavelength range between 990-1450 nm without any mechanical/temporal scanning processes.

RTu2E.5 • ORS Postdeadline Paper

Tuesday, 26 June, 11:30 – 11:45

Big Sur Room

Derivative spectroscopy with HICO[®]

Nicholas B. Tuffiaro and Curtiss O. Davis

Oregon State University, 104 CEOAS Administration Building, Corvallis, OR 97331-5503

nbt@coas.oregonstate.edu

Abstract: The Hyperspectral Imager of the Coastal Ocean — HICO[®] — is a visible and near-IR grating spectrometer currently in orbit on the International Space Station (ISS) [1]. HICO's 5.7 nm (binned) spectral resolution permits the application of derivative spectroscopy to the identification of remotely sensed water constituents. We examine applications of derivative spectroscopy to complex coastal waters with riverine inputs such as the Columbia and Yangtze rivers.

© 2012 Optical Society of America

OCIS codes: 000.0000, 999.9999.

1. Background

Remote sensing ocean imagers are designed to capture a dark object (water) in a bright background (atmosphere). The current generation of ocean imagers are 'multispectral,' and product algorithms are tuned to make use of the distinct spectral channels. As demonstrated by HICO [2], however, current technology permits the design of low-noise space borne spectrometers with continuous spectral coverage, as well as enhanced spatial coverage. HICO's typical ground sampling distance is 90 meters with a native spectral resolution of 1.9 nm, which is typically binned up to 5.7 nm. Useable spectral coverage ranges from 400 nm to 900 nm.

Derivative spectroscopy is a useful technique for the routine analysis of laboratory spectra. Derivative spectroscopy is also useful in the identification of informative remote sensing channels to aid the design of multispectral imagers [3], and initial applications also show its utility in the identification of shallow water bottom types [4].

Multispectral imagers focus on the extrema spectra of water or atmospheric constituents. Hyperspectral instruments and derivative spectroscopy allows us to quantify the shape and curvature of spectral peaks as well. For instance, the half-width of a fluorescence peak is amplified by the use of derivative spectroscopy. A peak with a smaller half-width will have a larger derivative around the maximum, and this spectral feature which is emphasized in the derivative can be used to distinguish and identify spectral features.

Care must always be taken in the numerical computation of derivatives to minimize the the impact of noise amplification. We compute the derivatives using a Savitzky-Golay filter [5]. At the same time we interpolate the data to a uniform 5 nm spacing. HICO has a signal-to-noise (SNR) of about 400 in the blue and 200 in the red [2]. To further reduce the noise in the data, where appropriate, we spatially bin the data to larger pixel sizes to further increase the SNR. Spectral features are identified by first looking at the extrema and zero crossings of the derivatives, but further analysis also includes the calculation of principal components to try to match the remote sensing spectra to lab measurements of probable minerals or pigments [6].

2. Applications

As a first example we examine an image of the Columbia River from May 2012 (Fig. 1). The fourth derivative is often used since it has the same extrema as the original spectra (the second derivative also has the same extrema but with the minimums and maximums interchanged). Pixels are chosen which are thought to represent different water masses, and the derivative is examined (Fig. 1 (c)) to find features that are used to distinguish the water masses. Then these channels can be chosen for the RGB composite to highlight differences. In this example it appears that there are three distinct water masses, presumably occurring from sediments at three distinct depths due to tidal forcing. Choosing, for instance, a channel near 610 nm allows us to separate older water outflowing from the Columbia (red dot in Fig. 1 (a)) from newer water (green dot in Fig. 1(a)). Picking RGB channels to separate water masses results in the image Fig. 1(b). Thus, in this very simple application, we illustrate how a derivative signature can be used for image enhancement.

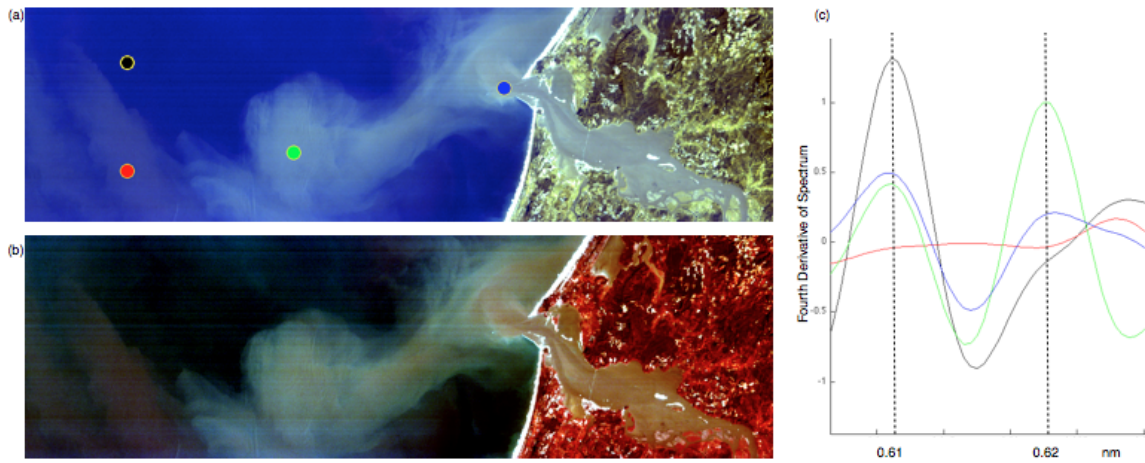


Fig. 1. HICO image of the Columbia River from 12 May 2012, 1:05 GMT. (a) RGB image of river outlet, (b) enhanced image highlighting plume structure, (c) use of derivative analysis in selection of channels sensitive to plume sediments.

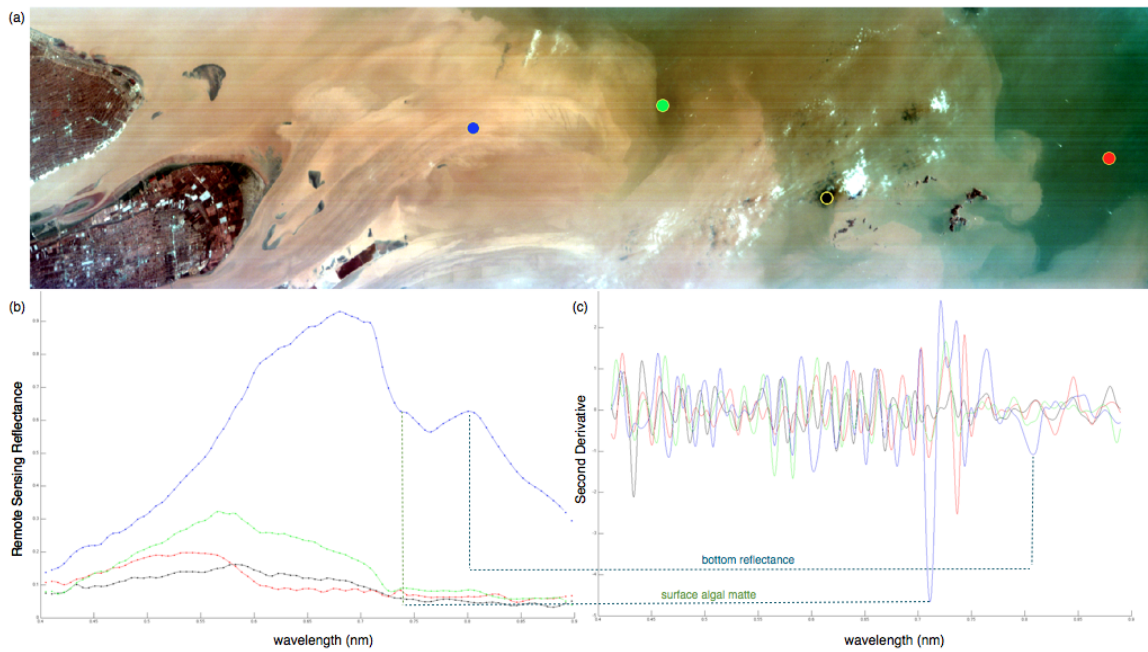


Fig. 2. HICO image of the Yangtze River from 28 March 2012, 0:47 GMT. (a) RGB image of river outlet, (b) Atmospherically corrected spectra, (c) derivative analysis highlighting channels sensitive to bottom reflectance and algal mattes.

As a second example consider the sediment rich outflow from the Yangtze river in March of 2012 (Fig. 2). The average total dissolved solids (TDS) out of the Yangtze exceeds 250 mg/L, and causes a tan colored fan shape in the East China Sea easily seen from space. Atmospherically corrected spectra are shown in Fig. 2 (b). Salient features such as a peak of 800 nm from bottom reflectance and a peak at about 710 nm from a surface algal matte are highlighted in the second derivative (Fig. 2(c)). Although the bottom reflectance is easy to see in the original spectra (Fig. 2(b)), the 710 nm peak is not readily apparent, but is prominent in the second derivative plot (Fig. 2(c)).

References

1. M. Corson and C. O. Davis, "A new view of the coastal ocean from the space station," *Eos. Trans. AGU* **92** (19), 161-162 (2011).
2. R. L. Lucke et. al., "Hyperspectral Imager for the Coastal Ocean: instrument description and first images," *Applied Optics* **50** (11), 1501-1516 (2011).
3. Z.P. Lee, K. Carder, R. Arnone, M.X. He, "Determination of primary spectral bands for remote sensing of aquatic environments," *Sensors* **7**, 3428-3441 (2007).
4. E. M. Louchard et. al., "Derivative analysis of absorption features in hyperspectral remote sensing data of carbonate sediments," *Optics Express* **10** (26), 1573-1584 (2002).
5. C. Ruffin and L. King, "The analysis of hyperspectral data using Savitzky-Golay Filtering", *IEEE IGRASS' 99 Proceedings* (1999).
6. J. D. Ortiz, D. L. Witter, K. A. Ali, N. Fela, M. Duff and L. Mills, "The influence of multiple color producing agents on chlorophyll-a estimation in the Sandusky Bay and Lake Erie's Western Basin," (preprint, 2010).

CW2C • COSI Postdeadline Session

Wednesday, 27 June, 10:30-11:00

Cypress 4 Room

Superresolution of Dense Quantum Dot Clusters using Independent Component Classification

Anthony Barsic and Rafael Piestun

*Department of Electrical and Computer Engineering, University of Colorado at Boulder
UCB 425, Boulder, CO 80309, USA
anthony.barsic@colorado.edu*

Abstract:

We propose a superresolution technique to resolve dense clusters of independently blinking emitters. Experiments and numerical simulations demonstrate the ability to superresolve up to five emitters located within an area of a diffraction limited spot.

OCIS codes: (100.6640) Superresolution; (180.2520) Fluorescence microscopy

1. Introduction

Optical microscopy has a fundamental resolution limit determined by diffraction. However, if one can assume the object consists of a collection of point-like sources, as is the case in single-molecule fluorescence imaging, the resolution paradigm is completely changed. Recent superresolution fluorescence microscopy techniques (such as PALM and STORM) rely on the ability to temporally resolve closely-spaced emitters to achieve superresolution [1,2]. The critical step is to control the experimental conditions such that unresolved emitters are switched temporally – in essence, temporal resolution is traded for spatial resolution. This allows experimentalists to spatially resolve emitters that are separated by much less than the diffraction limit. These methods still rely on the ability to resolve the emitters in time so that the diffraction limited image of each emitter does not overlap. This places a limit on the labeling density of samples.

A related technique uses a clever analysis of quantum dot blinking; by exploiting their random temporal fluctuations, two emitters spaced closer than the diffraction limit can be resolved without relying on localization [3]. This method involves performing Independent Component Analysis (ICA) on the data. The way in which ICA is able to resolve the emitters relies on the fact that the quantum dots blink randomly and independently. The ICA algorithm uses this fact to decompose the data into a small set of variables which have maximally non-Gaussian probability distribution functions. In theory, these non-Gaussian variables will correspond to the images of the independently-blinking quantum dots in the scene.

Quantum dot emitters are attractive in various types of superresolution experiments due to their high photon output, photostability, wide range of emission wavelengths, and broad absorption spectra.

Unfortunately, the ICA algorithm has one major shortcoming – in order to correctly resolve the emitters, one must know the true number of emitters in the scene (which is obviously not known in an experimental setting). This is a difficult enough hurdle to preclude the method from being implemented in any nontrivial situation. Here, we demonstrate a procedure that addresses this problem by incorporating spatial analysis of the quantum dots in addition to the stochastic temporal analysis. The algorithm uses ICA to generate a family of possible solutions and then the independent components are classified according to their spatial and temporal characteristics. The result that best matches a model of quantum dot behavior is selected – hence the name Independent Component Classification (ICC).

In this summary, we present numerical simulations to validate the superresolution capabilities of ICC. Subsequently, we apply the method to an experimental dataset in which five classically unresolvable quantum dots are successfully resolved.

2. Independent Component Classification – Numerical Simulations

In Monte Carlo simulations, several emitters were placed randomly within a diffraction limited spot, given random blinking behavior, and combined with background noise and shot noise. Then, the ICA was performed numerous times to generate a family of potential solutions. With each iteration, an increasing number of emitters was assumed. An example of such a solution set is shown in Figure 1. In this case, the true number of emitters is four. By examining the spatial characteristics of the potential solutions, a clear pattern emerges: once the number of emitters is overestimated, spurious results that do not resemble the system Point Spread Function (PSF) are returned. When the number of emitters is underestimated, the returned independent components are often a superposition of two emitters (this result is less obvious in this example where the emitters are unresolved, but simulations with easily resolved emitters clearly exhibited this tendency). ICC exploits this tendency in order to estimate the number of emitters in the scene. Each set of potential solutions is given a score that measures the maximum error of any one

of the returned components as compared to the theoretical PSF. The number of emitters in the scene is assumed to be the set of results that immediately precedes the largest first derivative of the score set. In other words, the correct solution is assumed to be the one in which no spurious components are returned. This comparison is calculated by computing the L-2 norm of the difference between the data and the ideal PSF in Fourier space; the calculation is performed in Fourier space to account for possible lateral shifts.

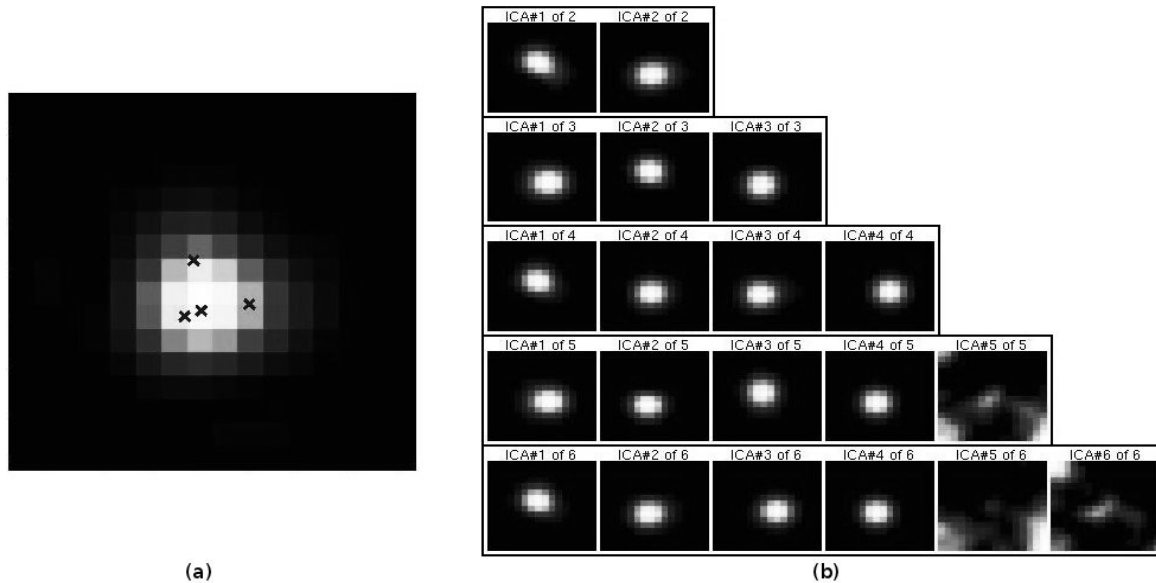


Figure 1: Simulation of Independent Component Classification: The average of the simulated video is shown in (a), with the centers of the unresolved quantum dots marked with x's. In (b), the family of potential solutions is shown. Each row is a separate result from the ICA algorithm, assuming a different number of emitters (row 1 assumes two emitters, row 2 assumes three emitters, etc).

The results of the Monte Carlo simulations are summarized in Figure 2. For each number of emitters from one to seven, a random set of unresolved locations is generated, and the ICC algorithm attempts to determine the number of emitters and their locations; this is repeated 500 times for each number of emitters. As expected, the ability to correctly estimate the number of emitters increases with the SNR. With experimentally achievable SNRs, the ICC algorithm can reliably resolve up to five emitters within a diffraction limited spot. At higher densities, the number of emitters is often underestimated.

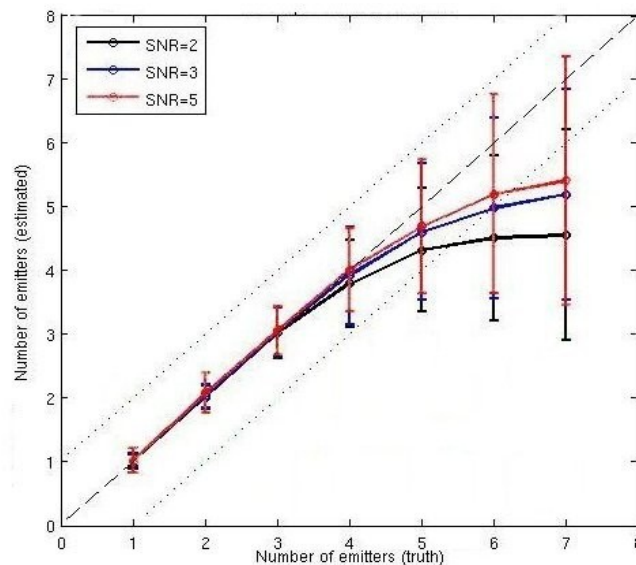


Figure 2: Results of Monte Carlo simulations for varying numbers of emitters and noise levels. Error bars show the standard deviation of the repeated simulations.

3. Experimental Superresolution Results

Experiments were performed to test this superresolution scheme. A fluorescence microscope was built using a 405nm diode laser as the excitation source, and a 1.3NA 100x Zeiss objective collected the fluorescence from the 525nm quantum dots from Invitrogen. A 100mm tube lens was selected to give 62.5x magnification on a Hamamatsu Orca-Flash 2.0 CMOS camera. This system resulted in slight over-sampling of the PSF, with 3.5 pixels across the full-width at half-maximum of the PSF. A test sample composed of quantum dots scattered across the cover slip was imaged for 500 frames with an exposure time of 200ms per frame, giving a total acquisition time of less than 2 minutes.

The results of the ICC analysis of a short video section are shown below. In the normal fluorescence image, there are no clearly-resolved emitters, but the ICC analysis suggests there are 5 unresolved emitters. Figure 3 shows the average image of the video, as well as the estimated locations of the emitters and their separated images. The distance between neighboring emitters is between 85 and 230nm in all cases, and the furthest distance between two of the emitters is 420nm. For comparison, this system's diffraction-limited spot is 493nm in diameter. Therefore, all 5 emitters have been superresolved.

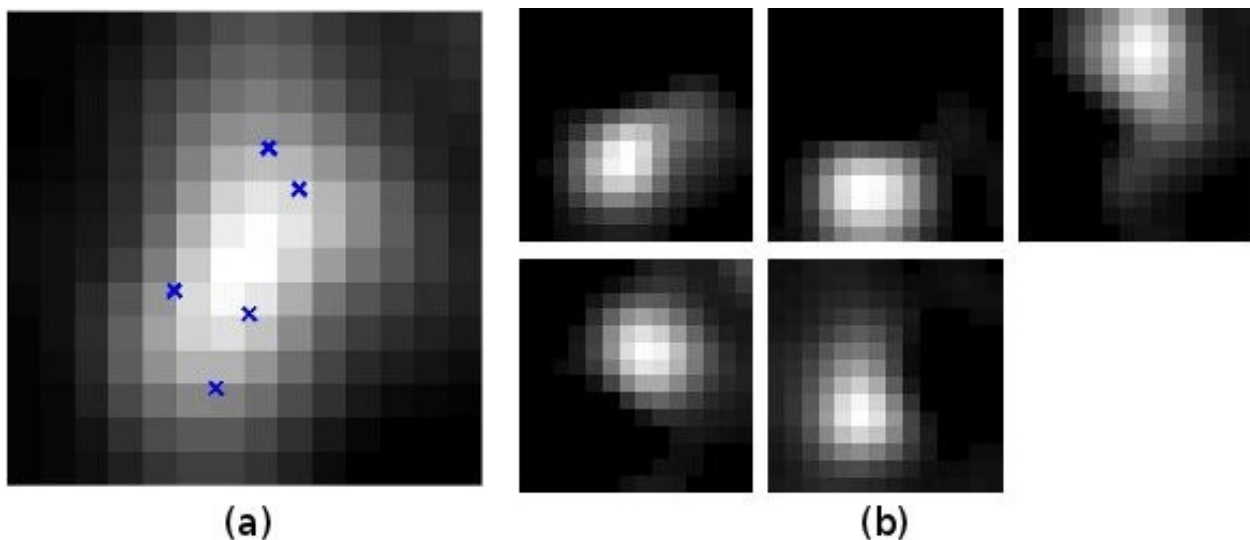


Figure 3: Experimental results: (a) shows the average of the 500-frame video of blinking quantum dots; the estimated locations of the five emitters are shown as x's. In (b), the five independent emitter images obtained with the ICC method are displayed.

4. Summary

This paper has demonstrated a superresolution technique capable of resolving dense clusters of quantum dots. The method was validated with simulations, which exhibit the ability to resolve emitters that would normally be unresolved. Experimental data was presented in which superresolution was achieved.

References

- [1] E. Betzig, G. H. Patterson, R. Sougrat, O. W. Lindwasser, S. Olenych, J. S. Bonifacino, M. W. Davidson, J. Lippincott-Schwartz, and H. F. Hess, "Imaging intracellular fluorescent proteins at nanometer resolution," *Science* 313, 1642–1645 (2006).
- [2] M. J. Rust, M. Bates, and X. W. Zhuang, "Sub-diffraction-limit imaging by stochastic optical reconstruction microscopy (storm)," *Nat. Methods* 3, 793–795 (2006).
- [3] K. A. Lidke, B. Rieger, T. M. Jovin, and R. Heintzmann, "Superresolution with quantum dots: enhanced localization in fluorescence microscopy by exploitation of quantum dot blinking," *Biophys. J.* 88, 346a–346a (2005).

Confidence Measures of Optical Flow for Multi-Frame Image Reconstruction

A.V. Kanaev¹ and C. W. Miller²

¹Naval Research Laboratory, 4555 Overlook Avenue, Washington DC 20375, USA

²Tekla Research, 3700 Fetter Park Drive, Quantico Center, Dumfries, VA 22025

Abstract: Multi-frame image processing encompasses algorithms for imaging through turbulence, super-resolution, and filtering. In-scene motion remains a challenge and requires optical flow estimation. We propose confidence measure to augment the problem of insufficient optical flow accuracy.

OSIS codes: 100.0100 (Image processing); 100.3010 (Image reconstruction techniques); 100.6640 (Superresolution)

1. Introduction

Estimation of optical flow (OF) from an image sequence represents one of the cornerstone problems in computer vision. Its major applications include super-resolution, turbulence degraded image restoration, video compression and denoising. Numerous optical flow algorithms have been developed recently and their evaluation has been unified by the Middlebury database work [1,2]. The number of papers on OF during the last several years easily tops a hundred while a considerably smaller number of papers has been devoted to OF confidence measures [3,4]. Despite the evident progress of new generation OF techniques, their test image performance has become rather saturated. In this situation, one way to qualitatively improve effectiveness of OF utilization in multi-frame image processing is to develop and implement application driven confidence measures.

2. Optical flow, error metrics, and confidence/uncertainty measures

Two components of the OF field $\mathbf{u}(u_x, u_y)$ are defined for each pixel of the pair of images I_1 and I_2 satisfying the image intensity constancy assumption relation $I_1(\mathbf{r}) = I_2(\mathbf{r} + \mathbf{u})$. Generally, the problem of finding \mathbf{u} is ill-posed so that the OF estimate is obtained by minimizing the error functional by incorporating certain assumptions about properties of the solution. Usually the functional consists of two parts, the data term and the regularization term. One approach to regularization term considers a fully nonlinear diffusion scheme cast into the L1 norm which is approximated by the Charbonnier penalty function [2],

$$E(\mathbf{u}) = \|I_1(\mathbf{r}) - I_2(\mathbf{r} + \mathbf{u})\|_{L1} + \gamma \|\nabla I_1(\mathbf{r}) - \nabla I_2(\mathbf{r} + \mathbf{u})\|_{L1} + \lambda \|\nabla \mathbf{u}\|_{L1}. \quad (1)$$

The corresponding nonlinear Euler-Lagrange equations can be solved on a multi-resolution grid using two nested fixed point linearization procedures, providing the advantage of accounting for the nonlinearized constancy assumption relation.

Several metrics for error evaluation of the obtained solution have been discussed previously [1]. The most widely used error metric is the endpoint or geometrical error \mathbf{EE} , which estimates the absolute value of the difference between estimated vector \mathbf{u} and the ground truth vector \mathbf{u}_r . The second often utilized metric is the angular error \mathbf{AE} , which represents the angle between the estimated vector \mathbf{u} and the ground truth vector \mathbf{u}_r . However, one can argue that the most important error for motion compensation is interpolation error \mathbf{IE} in which the ground truth image is compared with the motion compensated image i.e., the image warped according to OF estimation. The later metric estimates the typical result that is passed by an OF algorithm to other image processing components. In other words, for multi-frame applications where motion compensation is required, the warping operator or OF field is implicit an intermediate result while motion compensated image is the explicit final product that is used further in the processing.

Previously proposed uncertainty (or conversely confidence) measures can be divided in two large groups, the measures that estimate the error *a priori* i.e., without regard to a particular OF computation and the measures that estimate the error *a posteriori* i.e., taking into account one or more OF computations. One such metric from the first group relies on the image gradient to gauge the aperture problem prohibiting accurate estimation of OF $\psi_{gr} = 1/(1 + |\nabla I|)^2$ [4]. Other members of the same group rely on the image structure tensor eigenvalues [3]. If $\lambda_1 \geq \lambda_2 \geq \lambda_3$ are the three eigenvalues of the spatiotemporal tensor formed by an image sequence, then the total coherence of the structure tensor reflecting its anisotropy and presence or absence of noise leads to another uncertainty metric $\psi_{ct} = -([\lambda_1 - \lambda_3]/[\lambda_1 + \lambda_3])^2$. Spatial coherence of the structure tensor quantifying the extent of the aperture problem is defined by $\psi_{cs} = ([\lambda_1 - \lambda_2]/[\lambda_1 + \lambda_2])^2$. A corner measure can be computed from the two last measures

$\psi_{cc} = -([\lambda_1 - \lambda_3]/[\lambda_1 + \lambda_3])^2 + ([\lambda_1 - \lambda_2]/[\lambda_1 + \lambda_2])^2$, which accounts for both the aperture problem and the coherence motion or noise problem. The obvious flaw of all *a priori* uncertainty measures is their inability to consider propagation of local information when solving for problematic image regions. Essentially, this translates into inability of *a priori* measures to account for regularization terms of OF. One uncertainty measure from the *a posteriori* group stems naturally from the variational approach to the OF estimation [4]. Indeed, functional energy minimization residue shows how well the solution follows the underlying model. Then, the logical uncertainty measure is the final functional energy after the minimization procedure.



Fig.1 Dimetrodon image test (a) reference image; (b) interpolation error *IE*; (c) endpoint error *EE*; (d) angular error *AE*.

We propose a “warping residue” uncertainty measure which also belongs to the *a posteriori* group and which is not specific to any particular implementation of OF estimation,

$$\psi_{wr} = \sqrt{[I_1(x, y) - I_2(x + u_x, y + u_y)]^2}. \quad (2)$$

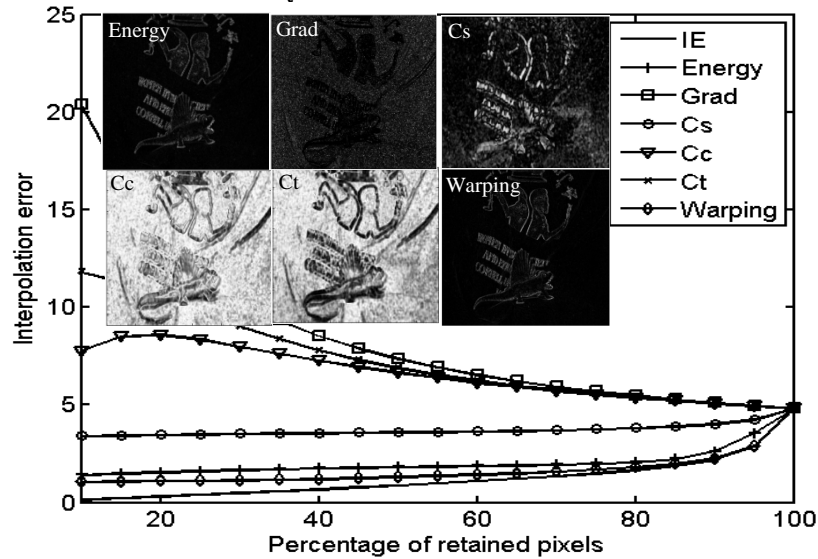


Fig. 2 Dimetrodon set confidence measure sparsification test with respect to interpolation error *IE*. Subimages display the tested measures.

3. Optical flow uncertainty measure application to multi-frame processing

A common approach to uncertainty or, conversely, confidence measure evaluation is based on sparsification [4]. The errors pertaining to each pixel are ordered according to the uncertainty measure being tested and the mean error is calculated using only a given percentile of the best values. Such a procedure estimates correctness of both the spatial distribution and the histogram of the confidence measure with respect to those of the true error. OF uncertainty measures presented here are evaluated using the sparsification test with the Dimetrodon images from Middlebury database [1]. The result for only one pair of images is presented due to the space constrains. The OF algorithm based on Eq. (1) is employed [2]. Figure 1 displays the reference image I_1 (Fig. 1a) and the absolute values of the optical flow errors *IE*, *EE*, and *AE* (Figs. 1b-d). Comparison of the three error metrics shows that the latter-two have little correlation with the former, emphasizing the fact that different OF errors require separate error measures. Uncertainty measures computed with the methods introduced in the Chapter 2 are shown on subimages of Fig. 2 also presenting sparsification test results with respect to interpolation error. The “warping residue” measure values are the closest to those of *IE* therefore they provide the most accurate representation of the interpolation error.

The proposed OF confidence measure has been incorporated into multi-frame algorithm for restoration of imagery degraded by underwater turbulence [5]. The restoration technique uses synthesis of nonlinear gain “lucky

region” fusion and optical flow based image warping. A typical underwater image distorted by extreme turbulence is presented on Fig. 3a. The sequence of ten distorted underwater images is used to obtain the final higher-resolution estimate. Imagery motion between the frames caused by extreme refraction index fluctuations underwater makes OF estimation difficult as constancy assumption often becomes invalid. This leads to spurious artifacts evident on Fig. 3b. In this case, the proposed confidence measure based on estimation of optical flow using nonlocal approach [1] is used to tune the anisotropic gain, which results in significant image quality improvement as shown on Fig. 3c.

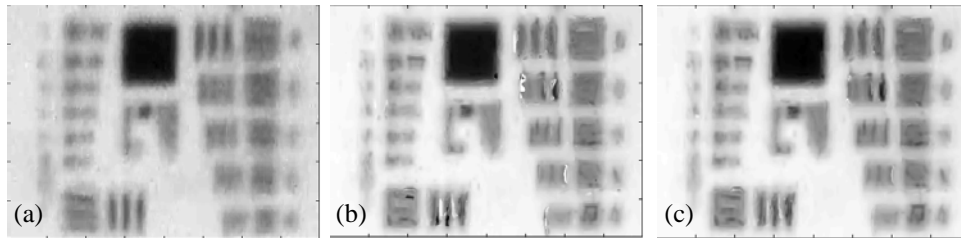


Fig. 3 Multi-frame restoration of images degraded by underwater turbulence: (a) typical frame, (b) restored image, (c) image restored with confidence measure.

Another important OF application area is multi-frame super-resolution. Multi-frame super-resolution of images containing complex motion fields remains an elusive target requiring precise estimation of such motion between the frames. Although accuracy of OF algorithms has been increasing steadily it is not yet sufficient to provide confident subpixel resolution enhancement during super-resolution reconstruction. One way to improve the super-resolved image quality is to incorporate confidence measures of OF into the processing. A variational super-resolution algorithm with anisotropic smoothness term based on local image structure tensor has been augmented with weights that depend on OF confidence level $W \sim \exp(-\psi_{wr})$. Eight low-resolution frames obtained by 4X downsampling and blurring of a high-resolution image sequence have been used for 4X super-resolution processing. A typical low-resolution image is presented on Fig. 4a and the super-resolved image is displayed on Fig. 4b. Lower accuracy of OF estimation around right hand and left leg of the man figure in the image results in artifacts that are eliminated if the confidence measure of optical flow is used (Fig. 4c).

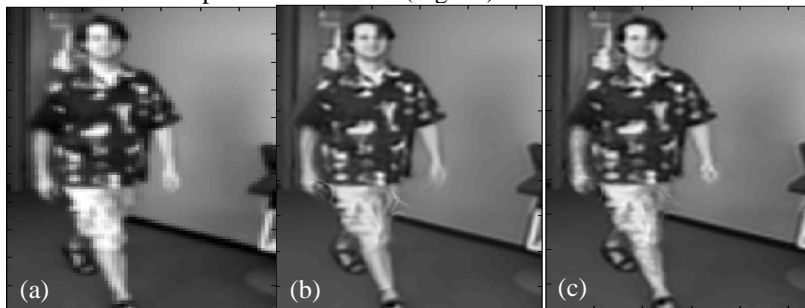


Fig. 4 Results of multi-frame super-resolution (a) typical frame; (b) 4X super-resolved; (c) 4X super-resolved using proposed confidence measure

In conclusion, a confidence measure of OF estimation suitable for multi-frame image processing is proposed. Using a sparsification test it has been proved that the proposed warping residue measure is an accurate representation of the OF interpolation error. Practical application of the confidence measure has been demonstrated for two OF algorithms ([1] and [2]) and two examples: restoration of imagery degraded by underwater turbulence, where confidence level thresholding has been used and multi-frame super-resolution of scene containing complex motion, where the confidence defined weights have been introduced into the minimization procedure.

4. References

- [1] D. Sun, S. Roth, and M. J. Black, "Secrets of optical flow estimation and their principles," Proceedings of the IEEE Int. Conf. on Computer Vision & Pattern Recognition (2010), San Francisco CA and references herein.
- [2] T. Brox, A. Bruhn, N. Papenberger, and J. Weickert, "High accuracy optical flow estimation based on a theory for warping," In Proc. 8th European Conference on Computer Vision, v. 4, pp. 25-36, Prague Czech Republic, May (2004).
- [3] H. Haussecker, H. Spies, Handbook of Computer Vision and Applications, v. 2, Academic Press, pp. 336–338 (1999).
- [4] A. Bruhn, J. Weickert, "A confidence measure for variational optic flow methods," Geometric Properties for Incomplete Data, p. 283 (2006).
- [5] A.V. Kanaev, W. Hou, S. Woods, and L.N. Smith, "Restoration of turbulence degraded underwater images," Opt. Eng., v. 51, (2012).

SW4C • SENSORS Postdeadline Session

Wednesday, 27 June, 16:00-17:45

Cypress 4

Generation and Coherent Detection of Broadband Terahertz Radiation in Phase-Matched Waveguides

Shuchang Liu, Amit Agrawal, Xiang Shou, and Ajay Nahata

Department of Electrical and Computer Engineering, University of Utah, Salt Lake City, UT 84112

Email: nahata@ece.utah.edu

Abstract: We describe novel waveguide devices that allows for broadband generation and coherent detection of THz radiation. We achieve a system with spectral content beyond 8 THz using <10 mW total average optical power.

© 2012 Optical Society of America

OCIS codes: Nonlinear optics, devices; (250.5460) Polymer waveguides; (190.7110) Ultrafast nonlinear optics.

Terahertz time-domain spectroscopy (THz TDS) is an extremely sensitive and flexible technique for determining far-infrared spectral and time-resolved properties of materials [1]. A common approach constructing such a system uses nonlinear optical materials that exhibit a macroscopic second-order nonlinearity for both generation and coherently detection of broadband terahertz (THz) radiation. This approach is attractive, because it allows one to capture a large fraction of the driving optical bandwidth. However, generation and detection processes using conventional nonlinear optical media, such as ZnTe, typically require 100's of mW in average optical power [2]. Given the dramatic advances in developing small form-factor ultrafast lasers, that often deliver relatively low average power, there is significant incentive to devices that would enable similarly small form-factor *broadband* THz time-domain spectrometers. However, the nonlinear conversion efficiency for second-order nonlinear processes, such as optical rectification and electro-optic sampling are fundamentally dependent upon the driving optical intensity and the phase-matched interaction length. Therefore, instead of using bulk crystals with freely-propagating radiation, waveguides offer the possibility of requiring significantly lower optical power over long interaction lengths. In fact, broadband THz radiation has been generated using parallel plate waveguides with embedded nonlinear optical materials [3,4]. However, such an approach only confines the radiation along one axis.

In this submission, we demonstrate novel guided-wave devices that confine both the optical and THz beams along two axes. The approach is used for generation and coherent detection of broadband THz radiation based on metal waveguide structures that allow for single-mode propagation of broadband THz radiation, as well as low-loss single-mode propagation of the optical pump and probe beams, enabling phase-matched interaction of the beams over long interaction lengths. Since the beams are strongly confined by the waveguide geometry, significantly lower optical power is required for efficient nonlinear conversion than in typical free-space geometries. *For example, we find that by using <10 mW of total average power for both waveguide structures, we are able to create a THz time-domain spectroscopy system with spectral content beyond 8 THz.* Thus, this waveguide approach overcomes the aforementioned problems of source power, detector sensitivity and THz frequency response.

In Fig. 1(a), we show a schematic diagram of the waveguide geometry using a modified microstrip structure. Conventional microstrip waveguide geometries do not allow for true TEM guided-wave propagation, because of the dielectric discontinuity at the dielectric-air interface adjacent to the upper electrode [5]. However, if we overcoat the device with the same dielectric medium (acrylate polymer), the device will support true TEM mode propagation. In the schematic, the total waveguide design thickness (top metal electrode to ground plane separation) for this prototype device is $\sim 10 \mu\text{m}$, with a 2D $3 \mu\text{m} \times 3 \mu\text{m}$ nonlinear optical (poled polymer [6]) waveguide core embedded between the metal electrodes. The core dimensions were chosen in order to ensure that the 2D waveguide allows for single mode propagation of the ultrafast optical pump beam. The basic experimental geometry for generation and coherent detection of broadband THz radiation is shown in Figure 1(b). Broadband THz pulses were generated using a waveguide emitter and coupled into the detection waveguide using a hyper-hemispherical sapphire lens and a dipole antenna that was fabricated on the end face of the waveguide. The same lens was used to couple the optical probe beam into the nonlinear core. Within this detection device, the polarization of the optical probe beam is altered through an electro-optic interaction with the broadband THz beam and measured using a conventional amplitude modulator arrangement. The measured time-domain waveform obtained using 1 mm long waveguides for generation and detection is shown in Figure 1(c). The corresponding amplitude spectrum is shown as an inset. We note that in the absence of the dipole antenna on the waveguide endface, no THz waveform was coupled into the waveguide.

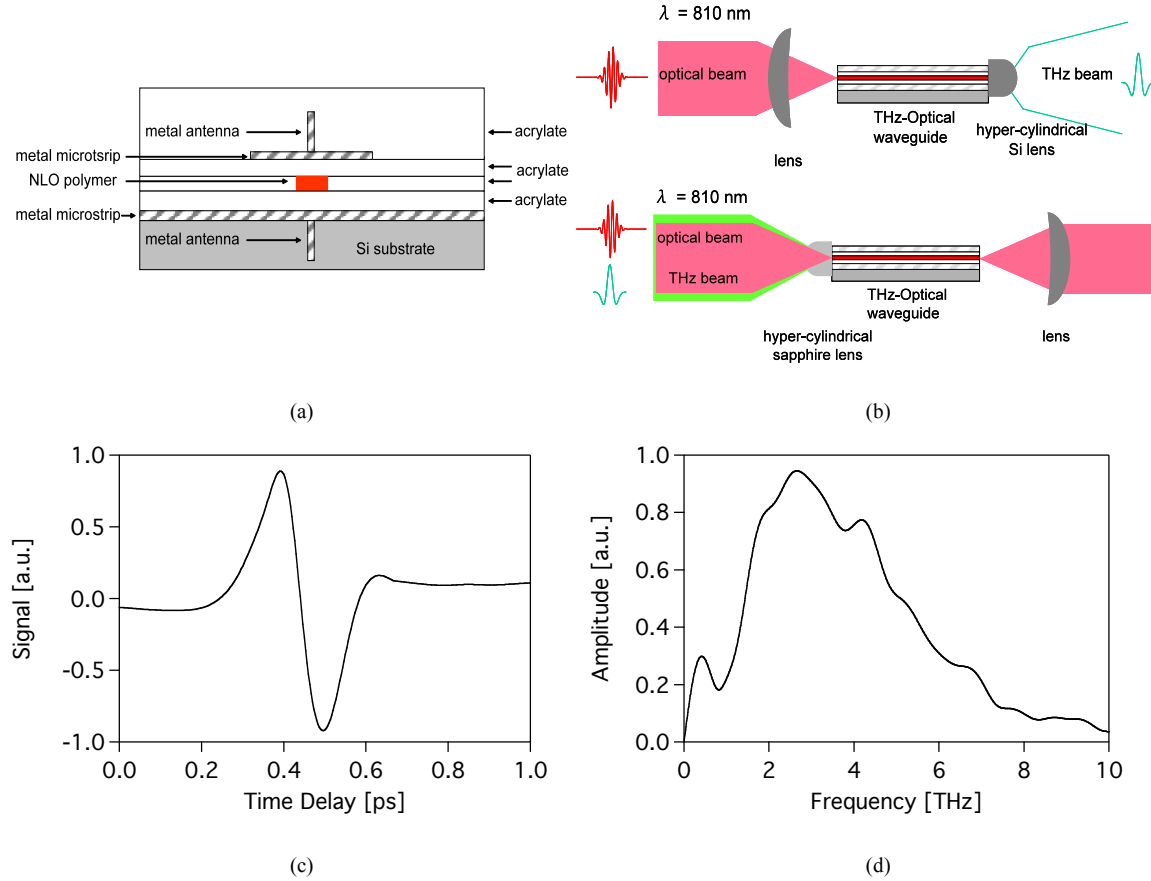


Fig. 1. (a) Schematic diagram of a single-mode THz/optical planar waveguide with integrated antenna for enhanced coupling efficiency (end view). (b) Schematic diagram of coupling into and out of the modified microstrip waveguide (c) Time-domain waveform using 1 mm long waveguides for both generation and coherent detection (d) Corresponding amplitude spectrum.

A fundamental consideration in the operation of these devices for either generation or coherent detection of broadband THz radiation is the issue of phase-matching. The general phase-matching condition for the generation of THz via difference frequency mixing and coherent detection via electro-optic sampling within this waveguide structure is given by

$$\vec{\beta}(\omega_{opt} + \omega_{THz}) - \vec{\beta}(\omega_{opt}) = \vec{\beta}(\omega_{THz}). \quad (1)$$

Here, β corresponds to the propagation vector within the waveguide structure, ω_{opt} and ω_{THz} are the optical and THz frequencies, respectively, and ω_{opt} and $(\omega_{opt} + \omega_{THz})$ both lie within the optical spectrum of the optical pulse. We will show that the resulting constraint is identical to that for free space i.e. the optical group velocity within the waveguide should equal the THz phase velocity. Correspondingly, the coherence length, $\ell_c (= \pi/\Delta\beta)$, for the generation of broadband THz via difference frequency mixing (and coherent detection of broadband THz radiation via electro-optic sampling) within this waveguide structure may approximately be written as [2]

$$\ell_c = \frac{\pi c}{\omega_{THz} |n_g - n_{THz}^{eff}|}. \quad (2)$$

Here $n_g = c/[d\omega/d\beta]$ is the group index at the optical pump frequency, and n_{THz}^{eff} is the effective refractive index of the dielectric medium within the metal waveguide at THz frequencies.

In summary, we have demonstrated that modified microstrip waveguide devices that incorporate 2D nonlinear optical cores are well suited for developing broadband THz TDS systems. By using optimized poled polymers, we expect that the total optical power required for a high sensitivity THz TDS system can be significantly <10 mW.

This work was supported through the National Science Foundation MRSEC program under grant #DMR-1121252.

References

- [1] M.C. Beard, G.M. Turner, and C.A. Schmuttenmaer, "Terahertz spectroscopy," *J. Phys. Chem. B* **106**, 7146-7159 (2002).
- [2] A. Nahata, A.S. Weling, and T.F. Heinz, "A wideband coherent terahertz spectroscopy system using optical rectification and electro-optic sampling," *Appl. Phys. Lett.* **69**, 2321-2323 (1996).
- [3] H. Cao, R.A. Linke, and A. Nahata, "Broadband generation of broadband terahertz radiation in a waveguide," *Opt. Lett.* **29**, 1751-1753 (2004).
- [4] S. Coleman and D. Grischkowsky, "Parallel plate THz transmitter," *Appl. Phys. Lett.* **84**, 654-656 (2004).
- [5] N. Marcuvitz, *Waveguide Handbook* (Peter Peregrinus, London, 1986).
- [6] A. Nahata, J. Shan, J.T. Yardley and C. Wu, "Electro-optic determination of the nonlinear-optical properties of a covalently functionalized Disperse Red 1 copolymer," *J. Opt. Soc. Am. B* **10**, 1553-1564 (1993).

Polarization modulation time-domain terahertz polarimetry

C. M. Morris, R. Valdés Aguilar, A. V. Stier, and N. P. Armitage*

*Department of Physics and Astronomy, The Johns Hopkins University, 3400 N. Charles St., Baltimore, MD 21218, USA, *npa@pha.jhu.edu*

Abstract: A polarization modulation time-domain THz polarimetry technique with a precision of 0.02° ($350 \mu\text{rad}$) will be presented, along with ongoing applications to interesting material systems such as topological insulators and quantum magnets.

Picosecond (10^{-12} s) timescales are one of the most ubiquitous in condensed matter systems. In recent years, advances in time-domain THz spectroscopy (TDS) have dramatically increased the ease of investigation of this time-scale, creating a rapidly expanding area of optical and materials research with a broad range of applications [1].

Despite the considerable progress in this field, a number of challenges remain. For example, highly accurate measurement of polarization states in the THz range is challenging [2]. Specialized multi-pole devices and calibrated wire-grid polarizer measurements have pushed the precision to $\sim 0.2^\circ$. However, investigations of fundamental effects such as extremely small Kerr and Faraday rotations in many materials at the forefront of condensed matter physics require an increased level of precision by approximately one order of magnitude [5]. Additionally, easy high precision determination of terahertz polarization states would set the stage for entirely new spectroscopic techniques such as THz ellipsometry.

Here we present a polarization modulation technique employing a fast rotator in combination with photoconductive switch based time-domain THz spectroscopy. It is capable of an unprecedentedly high angular precision of better than 0.02° and an accuracy of 0.05° in the frequency range from 0.1 to 1.25 THz, a sensitivity that opens the door to a new class of terahertz measurements. Additionally x and y direction electric fields are measured simultaneously which decreases measurement times.

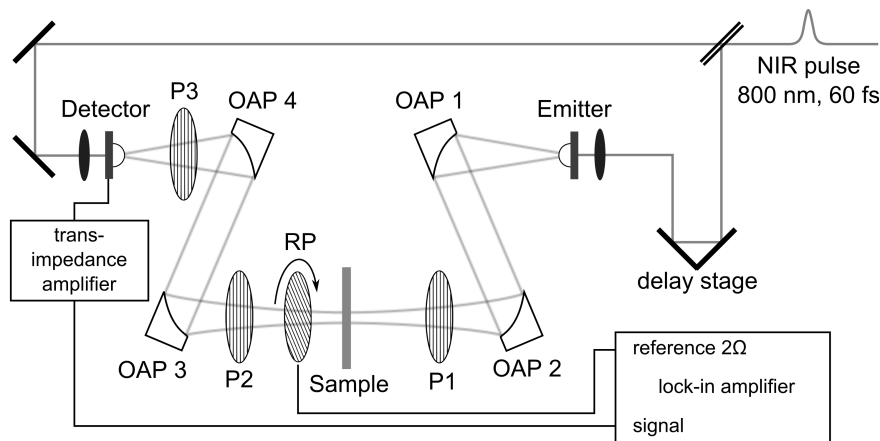


Fig. 1. a) Experimental setup. A broadband time-domain THz setup incorporating a modulation of the electric field by a rotating wire-grid polarizer (RP).

Figure 1 shows the experimental setup. The generation and detection of the terahertz waveform is accomplished by a standard time-domain terahertz spectrometer using photoconductive antennas. A femtosecond laser pulse excites a biased Auston switch THz emitter, creating a linearly polarized electromagnetic pulse a few picoseconds in duration (with THz frequency Fourier components from 0.1 to 3 THz). The pulse propagates through space and interacts with a sample under test. The linearly polarized light passing through the sample becomes elliptically polarized according to the properties of the particular sample. The elliptically polarized terahertz light passes through a rotating wire-grid polarizer, which modulates the elliptical

polarization at twice the rotation frequency Ω . A second photoexcited Auston switch is used to detect the final electric field waveform.

One can show [3] that the modulation of the polarization allows for direct detection of the x and y components of the electric field simultaneously on the in- and out-of-phase components respectively of a lock-in amplifier detecting at 2Ω . This simultaneous detection of both electric field polarizations is advantageous, as the phase sensitive nature of TDTS means that unlike conventional polarimetry, only two orthogonal directions have to be measured to resolve the complete transfer matrix for a polarized wave.

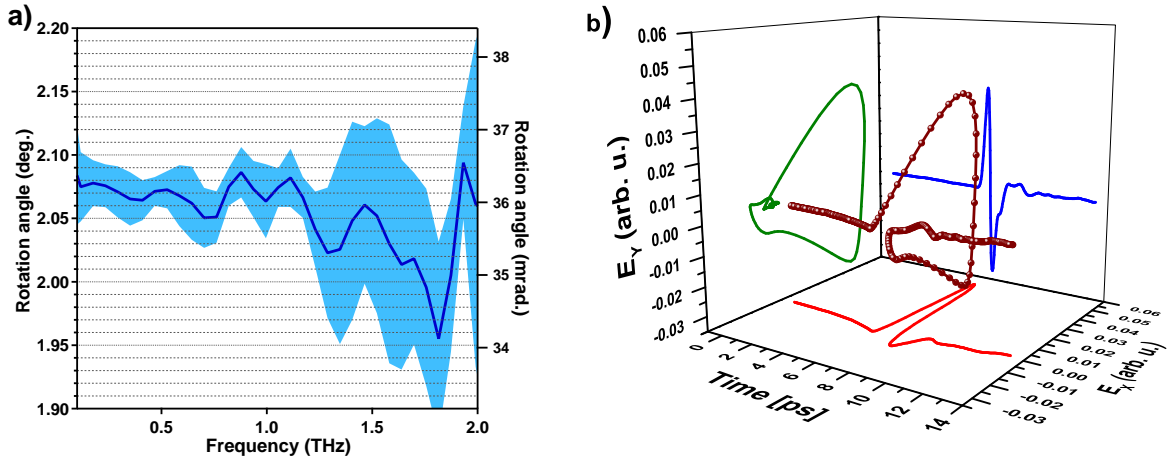


Fig. 2. a) A test polarizer angle is used in place of a sample, with an angle of $\sim 2^\circ$, showing 0.05° accuracy and 0.02° precision up to 1.25 THz. The shaded area indicates the measurement precision. b) A single polarization modulation measurement of a wafer of R-cut sapphire, oriented at 45° to the vertical x-axis. The sample birefringence of this orientation produces a time-domain electric field waveform that rotates in time.

The effect of the sample on the polarization state of the terahertz electric fields can be described by the sample transfer matrix T :

$$T(\omega) = \begin{pmatrix} \tilde{t}_{xx}(\omega) & \tilde{t}_{xy}(\omega) \\ \tilde{t}_{yx}(\omega) & \tilde{t}_{yy}(\omega) \end{pmatrix} \quad (1)$$

The elements of this matrix are determined by the physics of the investigated sample, and their measurement is the main goal of the polarimetry described here. Properties of the sample such as the complex conductivity can be directly extracted from the elements of this matrix. With the technique presented, a single measurement yields two elements of the transfer matrix with the signals on the X and Y channels of the lock-in detector [3]:

$$\begin{aligned} S_X(\omega) &\sim E_x^0(\omega) \tilde{t}_{xx}(\omega) \\ S_Y(\omega) &\sim E_x^0(\omega) \tilde{t}_{yx}(\omega) \end{aligned} \quad (2)$$

where $E_x^0(\omega)$ is the frequency domain representation of the original electric field. This single rotator measurement accomplishes the same as two static polarizer measurements. While for some samples the full matrix must be resolved, for simple effects such as Faraday and Kerr rotation only one diagonal and one off-diagonal matrix element needs to be measured.

A wire-grid polarizer in a static rotation mount was used as a reference sample to characterize the performance of the system. Figure 2(a) shows a measurement for a polarizer angle of 2° , demonstrating the ultimate accuracy and precision of the system. Note that in the Vernier scale rotation mount used here, the test polarizer angle can only be set with an accuracy of $\sim 0.1^\circ$, producing the small offset angle from 2° . Given this constraint, the measurement accuracy is instead described as the flatness of the angle over the

measurement frequencies, as the polarizer should produce the same polarization angle for all frequencies. The level of variation from this is the inaccuracy of the measurement. As usual, the precision is determined by the standard deviation of repeated measurements from the mean angle. The solid curve presented in Fig. 2(a) is the average of several scans. The standard deviation of these scans is plotted as the shaded blue area around the curve. From 0.1 – 1.25 THz, the precision is $\sim 0.02^\circ$ (350 μrad). The precision of the system is thus far only limited by the averaging time. The averaged scan shown in Fig. 2(a) accounts for 20 minutes of measurement, a reasonable time-scale for many experiments.

To test the technique on a real sample, the birefringent response of a piece of R-cut sapphire was measured. The sample was placed with the ordinary and extraordinary axes at 45° with respect to the initial vertical (x) light polarization. This crystal orientation produces a phase delay between the electric field projections on the two axes, changing the polarization from linear to elliptical. Figure 2(b) shows the measurement of the x and y electric fields that occurs in the two lock-in channels in a single measurement, which is then used to reconstruct the time domain electric field polarization state. The transfer matrix elements can then be used to directly determine the difference in the index of refraction between the two birefringent axes. As the R-cut is a somewhat complicated projection of multiple crystallographic axes, we forgoe that treatment here. This measurement clearly demonstrates the conversion of the initial linearly polarized THz pulse into a more complex elliptically polarized state.

The high precision technique for measurement of polarization states presented here will have a wide applicability to a number of materials systems at the cutting edge of condensed matter physics, such as high- T_c superconductors [4], quantum magnets, and topological insulators [5]. Many of these systems are predicted to have extremely small Kerr or Faraday rotations in the THz range that should be signatures of their fundamental materials properties, however thus far the size of such rotations has precluded measurements. We will describe our ongoing measurements using this high precision THz polarimetry to look for these effects in these interesting material systems.

This work was made possible by support from the Gordon and Betty Moore Foundation and DARPA YFA N66001-10-1-4017.

References

1. M. Tonouchi, "Cutting-edge terahertz technology," *Nat. Photonics* **1**, 97–105 (2007).
2. E. Castro-Camus, "Polarization-resolved terahertz time-domain spectroscopy," *Journal of Infrared, Millimeter and Terahertz Waves*, **33**, 418–430 (2012).
3. C. M. Morris, R. Valdés Aguilar, A. V. Stier, and N. P. Armitage, "Polarization modulation time-domain terahertz polarimetry," *Optics Express* **20**, 12303-12317 (2012).
4. J. Xia, Y. Maeno, P. T. Beyersdorf, M. M. Fejer, and A. Kapitulnik, "High resolution polar kerr effect measurements of Sr_2RuO_4 : Evidence for broken time-reversal symmetry in the superconducting state," *Phys. Rev. Lett.* **97**, 167002 (2006).
5. X.-L. Qi, T. L. Hughes, and S.-C. Zhang, "Topological field theory of time-reversal invariant insulators" *Phys. Rev. B* **78**, 195424 (2008).

Resonant Metamaterial Detectors Utilizing THz Quantum-Cascade Lasers

A. Benz*, **S. Schwarz**, **M. Krall**, **D. Dietze**,
M. Brandstetter, **C. Deutsch** and **K. Unterrainer**

*Photonics Institute and Center for Micro- and Nanostructures,
Vienna University of Technology, Gusshausstrasse 29/387, A-1040 Vienna, Austria*

**Currently: Sandia National Laboratories, PO Box 5800, MS 1314, Albuquerque, NM, 87185-1314, USA
alexander.benz@tuwien.ac.at*

H. Detz, **A. M. Andrews**, **W. Schrenk** and **G. Strasser**

Institute of Solid-State Electronics, Vienna University of Technology, Floragasse 7/362, A-1040 Vienna, Austria

Abstract: We present the design, fabrication and characterization of a resonant metamaterial detector based on a THz quantum-cascade laser. The same active region can be used to generate and detect the light leading to miniaturized and integrated optical systems in the THz spectral range.

© 2012 Optical Society of America

OCIS codes: 040.2235, 250.5300, 140.5965.

1. Introduction and Background

The terahertz (THz) spectral region shows a huge potential for applications such as spectroscopy, chemical sensing or real-time imaging. THz quantum-cascade lasers (QCLs) have become the preferred compact sources covering the frequencies from 1.2 to 5 THz. They show great potential for local chemical sensors [1]. Nevertheless, the integration of a THz source and detector is still challenging. The large wavelengths in combination with small semiconductor structures leads to divergent emission fields and extensive collection optics. A monolithic integration of both components eases the requirements on beam collimation and focusing.

Here, we present the use of conventional THz-QCLs as resonant metamaterial detectors emitting and detecting in the same spectral region. The metamaterial allows us to couple normal incidence radiation resonantly to the intersubband transitions. Furthermore, the resonance frequency of the metamaterial is defined by geometry resulting in a highly designable detector. In a second step, this approach allows the realization of integrated optical sensor systems. The source and the detector are realized on the same chip using the same active region.

2. Experimental results

The detector region is based on a GaAs/Al_{0.15}Ga_{0.85}As heterostructure grown by molecular beam epitaxy. The underlying THz-QCL exploits the longitudinal-optical phonon depopulation scheme [2] and is designed to operate at an applied field of 10 kV/cm in the frequency range from 2.6 to 3.2 THz [3]. The same structure is used as a detector at zero bias; it shows three dominant transitions at 16.8, 42.9 and 88.9 meV. Light below and above the reststrahlen band can be detected.

Metamaterials have proven to be an excellent way of coupling free-space radiation to intersubband transitions in the THz range [4, 5]. The polarization of the incoming radiation is rotated in the near-field making it compatible with the intersubband selection rules. The electric field distribution inside the active region is illustrated in Fig. 1(a). The strong z-field component for an incoming E_x polarization is clearly visible. We process the metamaterial directly into the top contact using optical lithography; a scanning electron microscope image of one single meta-atom is presented in the inset of Fig. 1(b). Throughout this work we use the complementary metamaterial which shows a similar frequency response as the conventional one [6]. The big advantage is the naturally forming uninterrupted top-contact layer; this ensures a homogeneous electric field distribution across the entire active region. To increase the optical confinement further, we process our devices into double-metal waveguides [7].

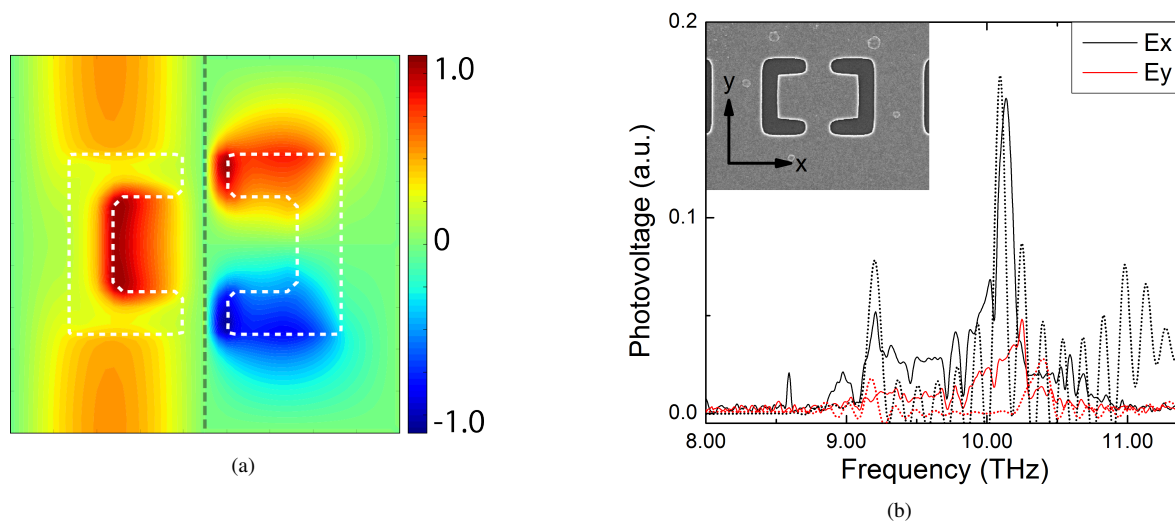


Fig. 1. Metamaterial field distribution and spectra. (a) Calculated E_z (left half) and H_y (right half) fields inside the active region for an excitation frequency of 10 THz. The white dashed lines indicate the position of the metamaterial. (b) Metamaterial spectrum for a period of $9.15 \mu\text{m}$. The solid line represents the experimental results, the dotted one the simulation. The inset shows a scanning electron microscope image of one meta-atom.

The detector response is an overlap of the intersubband energies and the metamaterial response. Since both systems, the quantum-wells and the metamaterial, are defined purely by design, the resulting devices are highly flexible and can be adopted to the problem. The theoretical and experimental results for a metamaterial with a period of $9.15 \mu\text{m}$ are presented in Fig. 1(b). The detector shows a broad response around 10 THz corresponding to one of the three dominant transitions. The double split-ring shows a polarization dependent response due to its asymmetry. At an incident E_y polarization the peaks at 9.2 and 10 THz are suppressed; the dominant peak is red-shifted to 10.2 THz. Depending on the metamaterial period we can also excite the quantum-well transitions at 16.8 and 88.9 meV.

3. Conclusion

In conclusion we have designed and realized resonant metamaterial detectors based on THz-QCLs. They are sensitive below and above the reststrahlen band. The metamaterial is processed directly into the top-contact and used to couple radiation to the intersubband transitions. It allows the realization of an integrated optical system consisting of source, waveguide and detector on the same chip.

References

1. A. Benz, C. Deutsch, M. Brandstetter, A. M. Andrews, P. Klang, H. Detz, W. Schrenk, G. Strasser, and K. Unterrainer, "Terahertz Active Photonic Crystals for Condensed Gas Sensing," *Sensors* **11**, 6003–6014 (2011).
2. B. S. Williams, H. Callebaut, S. Kumar, Q. Hu, and J. L. Reno, "3.4-THz quantum cascade laser based on longitudinal-optical-phonon scattering for depopulation," *Appl. Phys. Lett.* **82**, 1015–1017 (2002).
3. A. Benz, G. Fasching, A. M. Andrews, M. Martl, K. Unterrainer, T. Roch, W. Schrenk, S. Golka, and G. Strasser, "The influence of doping on the performance of terahertz quantum-cascade lasers," *Appl. Phys. Lett.* **90**, 101,107:1–101,107:3 (2007).
4. M. Geiser, C. Walther, G. Scalari, M. Beck, M. Fischer, L. Nevou, and J. Faist, "Strong light-matter coupling at terahertz frequencies at room temperature in electronic LC resonators," *Appl. Phys. Lett.* **97**, 191,107:1–191,107:3 (2010).
5. D. Dietze, A. Benz, G. Strasser, K. Unterrainer, and J. Darmo, "Terahertz meta-atoms coupled to a quantum well intersubband transition," *Opt. Express* **19**, 13,700–13,706 (2011).

6. F. Falcone, T. Lopetegi, M. A. G. Laso, J. D. Baena, J. Bonache, M. Beruete, R. Marques, F. Martin, and M. Sorolla, "Babinet Principle Applied to the Design of Metasurfaces and Metamaterials," *Phys. Rev. Lett.* **93**, 197,401:1–197,401:4 (2004).
7. S. Kohen, B. S. Williams, and Q. Hu, "Electromagnetic modeling of terahertz quantum cascade laser waveguides and resonators," *J. Appl. Phys.* **97**, 053,106:1–053,106:3 (2005).

Non-Destructive Evaluation of Aerospace Materials using Terahertz Time-Domain Imaging

Lindsay Owens¹, Douglas T. Petkie^{1,2}, and Jason A. Deibel^{1,2}

*1. Dept. of Physics, 2. Dept. of Electrical Engineering
Wright State University, 3640 Colonel Glenn Hwy., Dayton, OH 45435
jason.deibel@wright.edu*

Abstract: THz time-domain imaging was utilized in the non-destructive evaluation of various composite materials used in aerospace structures and components for the characterization of defects and changes in material properties due to mechanical and thermal strain.

OCIS codes: (110.6795) Terahertz imaging; (300.6495) Spectroscopy, terahertz

1. Introduction

While the use of terahertz (THz) imaging as an evaluation tool for novel materials and systems has found much success in recent years [1-3], there remain several possible application areas still in need of thorough investigation. Here, we investigate the use of terahertz imaging for the characterization and evaluation of materials and components used in advanced aerospace components. Defects present in a protective coating/paint layer covering a metal surface, a coating similar to that used on airframes, were located using THz imaging. Fiberglass composite materials were evaluated with THz light to determine and characterize defects such as voids, burns, and delamination. While suggested as a potential NDE tool for use in the field of ceramic and ceramic matrix composite materials, the use of THz spectroscopy and imaging in the examination of the effects of mechanical and thermally induced strain on ceramic composite materials is not well established. THz time-domain reflection imaging was performed to do non-destructive evaluation on ceramic composite materials in order to characterize changes in material properties due to mechanical and thermal strain [4-5].

THz time-domain images were acquired using a commercial system manufactured by Teraview. Ultrafast laser pulses with an 800 nm center wavelength and 100 fs pulse width triggered a fiber-coupled GaAs photoconductive antenna (PCA). Collimated THz light from the PC antenna transmitter was focused via a 50 mm focal length lens ($f\# = 2$) onto the samples at a near-normal incident angle. The reflected radiation was detected by a PCA receiver module, based on LT-GaAs, with an identical lens configuration. When the system is optimized and calibrated using a metal reference reflection target, the typical bandwidth of the detected THz pulse exceeds 3 THz.

2. THz NDE of Protective Coatings

The ability of terahertz radiation to penetrate obscuring materials such as paints, oils, etc. has often been cited as a primary benefit for its use as an NDE tool. The surface of a metallic plate was covered with a protective coating/paint often used in the aerospace field. An "X" pattern was scored across the sample thus providing exposure such that the ambient environment could induce corrosion (top half of Fig. 1). The rest of Fig. 1 shows a THz image, in which the magnitude of each pixel is based on the maximum amplitude of the THz pulse, of this sample with delamination and blistering present on the paint which is evident in both images. While the "X" and delamination's were clearly visible to the eye, there were several defects identified in the THz image that were not seen in the visible light image.

3. Defect Detection in Fiberglass Composite Materials

Fiberglass composite samples, designated here as the KT samples, were characterized to determine if THz imaging was a useful technique for detecting delamination's, burns, and other defects in composite materials. These materials were characterized previously using transmissive THz imaging over much smaller spatial scan areas [6]. The work described here was performed in reflection as described in the first section. Fig. 2(a) shows imaging results from three of these samples. KT2 and KT3 were both burned in isolated areas. The darkened portions of the samples seen in these THz images clearly show evidence of the defects due to burning. Fig. 2(b) shows zoomed-in views of both visible and THz images of the KT-3 sample which was burned at 830°F for 4 minutes in the circular area as marked. KT4 was a sample composed of five layers of varying thickness. By comparing the arrival time of the pulse through each of the layers, the layer thickness was able to be determined for each section.

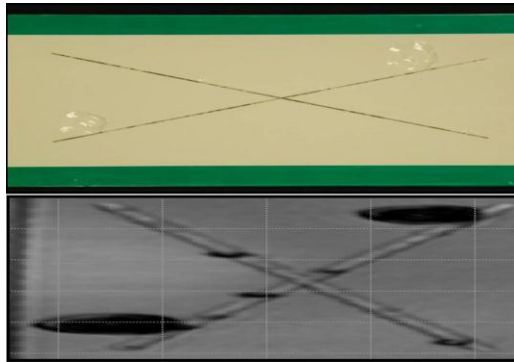


Fig. 1. Visible light image of a metal surface covered with protective paint/coating (top) and a THz image of the same sample (bottom).

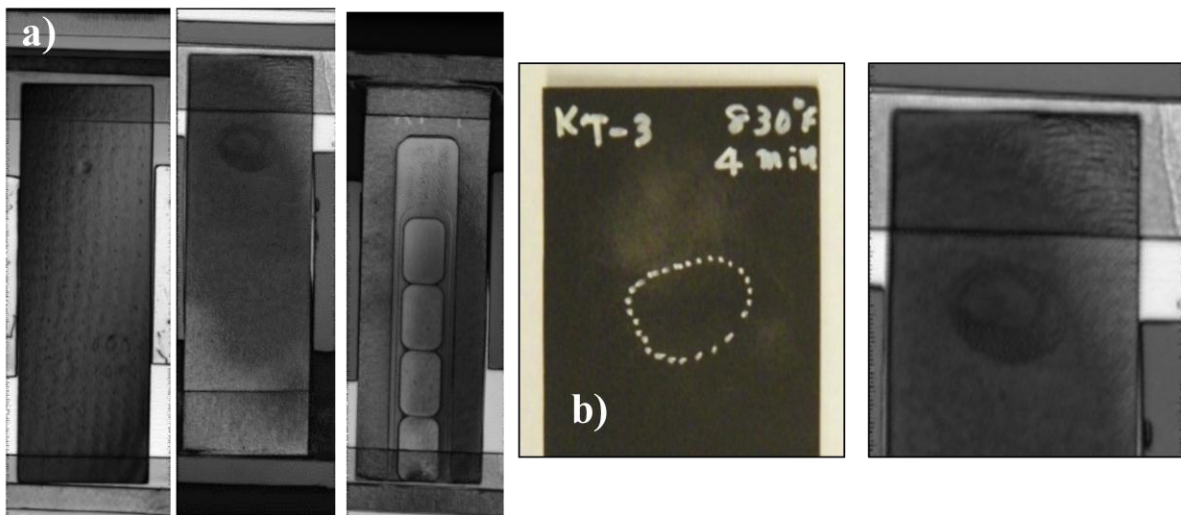


Fig. 2. (a) THz images of fiberglass composite samples KT2 (left), KT3 (center) and KT4 (right). (b) Zoomed-in visible light (left) and THz images (right) of the burned area of sample KT3.

4. Characterization of Ceramic Composite Materials using Terahertz Reflection Imaging

Tests were conducted on both oxide-based and silicon nitride carbon based ceramic matrix composite (CMC) samples [4]. A 5.9 x 17.4 cm area was scanned, containing both an aluminum reference and the CMC sample. A full time-domain waveform, 250 ps long, was acquired for each 0.5 x 0.5 mm pixel. For this comprehensive study, there were multiple rounds of data acquisition. The first round consisted of initial spectroscopic imaging of all of the samples. Additional rounds consisted of imaging of the samples following treatments of either thermally or mechanically induced stress of varying magnitudes and also combinations of the two differing types of stress. Comparison of the data both in the time-domain and frequency-domain acquired from this imaging of both the untreated and treated samples was used to assess whether or not the magnitude and extent of stress-induced changes can be monitored using terahertz imaging and spectroscopy.

Fig. 3 (a) is an image based on the frequency weighted reflectivity from an oxide CMC sample prior to any stress treatment. Note that the textured weave on the surface of the sample is clearly visible. Quantitative analysis is also accomplished by producing graphs of normalized reflectivity (averaged over the entirety of the sample) as a function of frequency. In all cases, the reflectivity is based on comparison of a THz pulse reflected from a CMC sample compared to the aluminum reference. In Fig. 3(b), Sample B-87, which was heat treated at 1200°C for 100 hours, showed no obvious variation from the baseline measurement. Sample B-60 was fatigue treated under 225 MPa of pressure at 1 Hz for 1000 cycles, and shows decreased reflectivity.

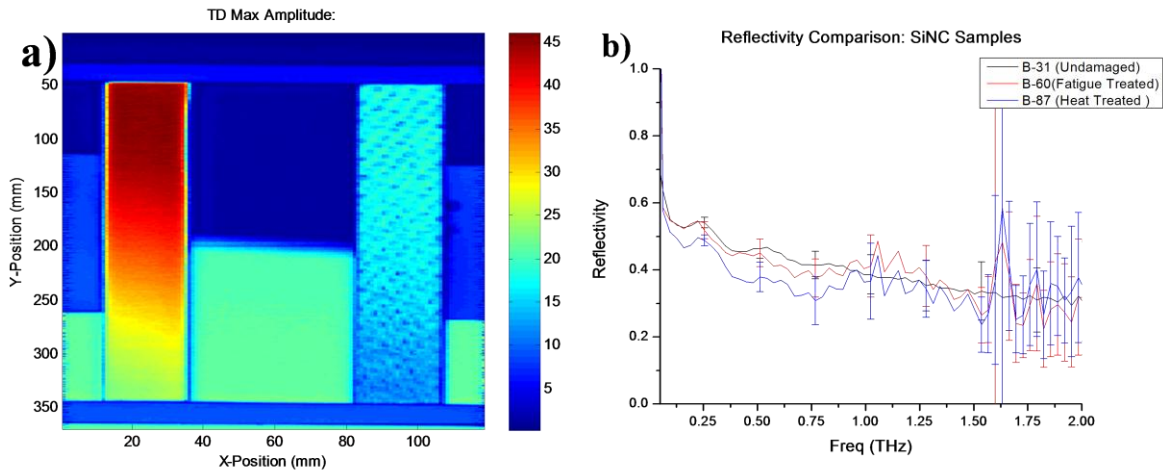


Fig. 3. (a) Frequency Weighted Reflectivity Image of Aluminum Reference Piece (Left) and A-29 Oxide CMC Sample (Right). (b) Reflectivity vs. frequency for a SiNC sample prior to treatment (black), post fatigue (red), and post heat treatments.

5. Summary

In this talk, we report on recent progress on the use of terahertz imaging for the characterization and evaluation of materials and components used in the aerospace industry. Defects hidden underneath protective coatings such as paint can be detected with THz imaging in addition to defects present in the interiors and on the surfaces of composite materials. Finally, we will update progress on efforts to demonstrate characterization of ceramic composite materials using terahertz time-domain reflection imaging.

6. References

- [1] D. T. Petkie, et. Al., "Nondestructive terahertz imaging for aerospace applications," Proceedings of SPIE: Millimetre Wave and Terahertz Sensors and Technology, **7485** (Berlin, Germany, 2 September 2009). [7485-13]
- [2] Wai Lam Chan, et. Al., "Imaging with terahertz radiation," *Reports on Progress in Physics* **70**, 1325-1379 (2007).
- [3] Naftaly M, et. Al., "Investigation of ceramic boron nitride by terahertz time-domain spectroscopy," *J. Eur. Ceram. Soc.* (2010), doi:10.1016/j.jeurceramsoc.2010.04.040
- [4] L. Owens, et. Al., "Characterization of Ceramic Composite Materials using Terahertz Reflection Imaging Technique," in *2011 36th International Conference on Infrared, Millimeter, and Terahertz Waves, Volumes 1 and 2* (IEEE 2011), paper W2C.2.
- [5] M. Bischoff, L. Owens, A. Cooney, J.A. Deibel, and D. Petkie, "Characterization of Composite Materials using Millimeter-wave Techniques," in *2011 36th International Conference on Infrared, Millimeter, and Terahertz Waves, Volumes 1 and 2* (IEEE 2011), paper W2C.3.
- [6] C. D. Stoik, et. Al., "Nondestructive evaluation of aircraft composites using transmissive terahertz time domain spectroscopy," *Opt. Express* **16**, 17039-17051 (2008)

7. Acknowledgements

The authors wish to acknowledge the Ohio Third Frontier Program for funding and other support.

Hydration dynamics of *Arabidopsis thaliana* under water deficit conditions monitored *in-vivo* by THz spectroscopy.

Enrique Castro-Camus¹, Miguel Palomar² and Alejandra A. Covarrubias²

¹ Centro de Investigaciones en Óptica A.C., Loma del Bosque 115, Lomas del Campestre, León, Guanajuato 37150, México

² Depto. Biología Molecular de Plantas, Instituto de Biotecnología,

Universidad Nacional Autónoma de México, A.P. 62210, Cuernavaca, Morelos, Mexico

Author e-mail address: enrique@cio.mx

Abstract: Terahertz time-domain spectroscopy was used to monitor the tissue hydration dynamics of *Arabidopsis thaliana* under water deficit conditions. Terahertz spectroscopy is found to be an excellent non-destructive *in-vivo* probe of hydration. The plant leaves showed very slow dehydration over the first 16 to 18 hours while a very rapid loss of moisture was seen over the following 3 hours, this transient behavior might be caused by a defensive mechanism of the organism that activates when the soil moisture decreases below certain threshold.

OCIS codes: (300.0300) Spectroscopy; (300.6495) Spectroscopy, terahertz

Water stress in plants represents an area of research that has attracted enormous attention recently [1] given the need of crops that can grow in areas where water supply is limited and capable of resisting drought periods. At present, a number of physiologic, metabolic and molecular responses have been described in various plant species when they are subjected to water deficit conditions [2]. *Arabidopsis thaliana* is a small flowering plant with a relatively short life cycle and small genome, which is considered a model system in plant biology, where many different processes have been characterized, including the plant response to environmental stress. [3] These studies and those carried out in other plant species have led to establish that the plant response to water limitation is a complex process that involves many changes at different functional levels and that depends on many different factors [4]. A better understanding of this complex response needs of more detailed analyses combining the application of different techniques, which could allow an integration of the molecular and physiological plant reactions to water deficit.

So far most of the studies requiring monitoring moisture dynamics in plant tissues have used destructive methods to quantify the amount of water present in them. In this work we present terahertz time-domain spectroscopy (THz-TDS) for dynamic *in-vivo* determination of hydration dynamics in vegetative tissue which is a non-contact and non-destructive technique.

Wild type *Arabidopsis thaliana* (*Lansberg erecta* ecotype) (AT) were grown in Petri dishes with MS 1X pH 5.7 (4.3 g/L Murashige and Skoog salts, 1% sucrose, 0.5g/L MES, 0.8% agar) in a chamber at controlled temperature of 21°C, 16/8 hrs light/dark photoperiod, 80 $\mu\text{E m}^{-2} \text{s}^{-1}$ of light intensity and a relative humidity of 60-80% for 2 weeks. Seedlings were transplanted to a low water retention substrate (Turface) and incubated for three weeks under the conditions described before and watered with nutritive solution. When plants reached reproductive stage (approximately five-weeks), plants were exposed to progressive water lose and cauline leaves were used for analyses because their location in the stem was optimal for the study.

A standard THz-TDS system was used for this study based on a Ti:Sapphire laser oscillator (33fs, 3.0nJ/pulse, 80MHz repetition rate). Terahertz transients were generated by photo-exciting a 400 μm gap semi-insulating-GaAs photo-conductive emitter biased with a square wave (120V amplitude at 12kHz). Detection was performed using a 1mm thick [110] ZnTe electro-optic crystal.

A reference terahertz waveform E_{ref} was recorded as function of the pulse delay δ before the sample was placed in the THz path. A live specimen of AT was placed next to the THz-TDS system. The stem was carefully bent and one of the cauline leaves (coming off the main stem) was fixed at the sample position using a semi-rigid card-board holder, softly pressing it to avoid any damage to plant tissues. At this moment, water supply to the plant was interrupted and a time-domain waveform E_i was recorded every 5 minutes for 24 hours. All measurements were done in normal atmospheric air in order to avoid any additional stress on the plant by CO_2 deficit.

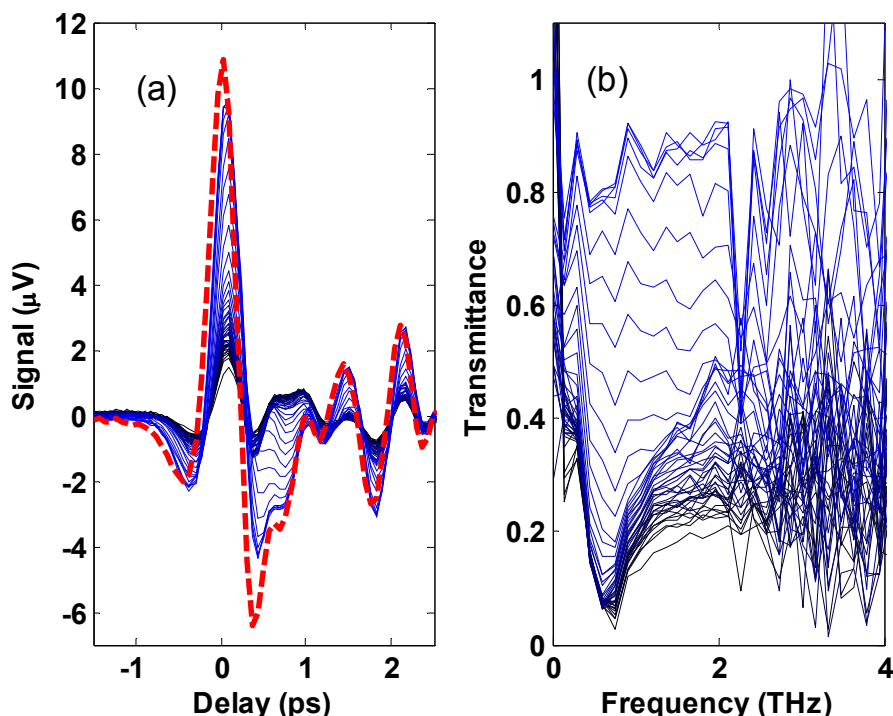


Fig. 1. (a) Continuous curves are terahertz waveforms of pulses transmitted through a AT leaf. (each curve represents 30 minute interval starting at time=0 (in darker color) and finishing at time=24 hours (in lighter color) . The dashed thick curve is the reference in absence of sample. (b) Transmittance calculated from the spectra of measurements shown in (a).

Waveforms acquired at half hour interval are shown in Fig. 1a. It is clear from the plot that the amplitude of the transmitted pulse changed significantly across the 24 hour period. Given that water presents strong absorption (causing low transmittance) these curves represent an indirect measure of the amount of water in the plant tissue at different times.

The transmittance of the leave as function of time at 0.9 THz is shown in Fig. 2. The plot presents a very slow riser in transmission over the first 16 to 18 hours. During the following 3 to 4 hours there is a very fast transmission increase from ~ 0.2 to ~ 0.85 related to a very fast moisture loss. This sudden change of the water content in the tissue might be associated to the activation of a defensive mechanism of the plant that resulted in a restriction of the water supply to the leaves in order to minimize the loss of moisture. This transient behavior could be a reaction not only to the water deficit experienced by the plant but also to the rate of change of water available, which is relatively fast in the case of the substrate used in these samples. By weighing another sample, we determined that the initial humidity in the substrate was of 0.28 ml/g (milliliters of water per gram of dry substrate) and that the loss of humidity was exponential with a time constant of 0.05 h^{-1} .

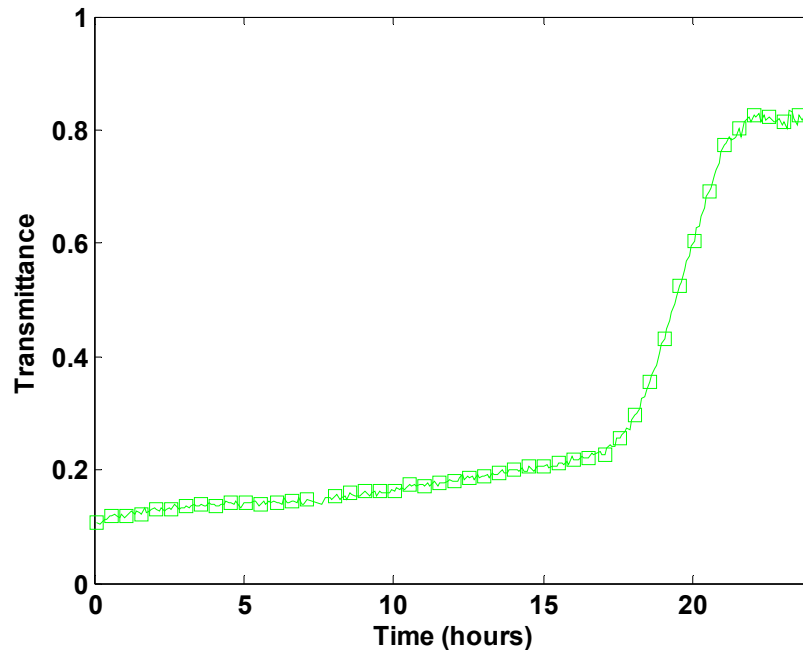


Fig. 2. Terahertz transmission as function of time at 0.9 THz from Arabidopsis leaves. There is a relatively slow change in transmission over the first ~17 hours, then a sudden change is observed and transmittance abruptly changes across the following 3 hours.

Terahertz time-domain spectroscopy was used to successfully monitor the *in-vivo* hydration dynamics in leaves of *A. thaliana* under water stress. It was observed that the leaves moisture shows very little susceptibility to the soil water contents unless the soil hydration goes below certain threshold, if this happens the moisture of the leaves rapidly decreases. This could be attributed to the reach of a threshold in which the ‘defensive’ responses in this leaf were lost or drastically reduced given the fast decrease in water availability in this organ during this experiment.

This technique is, to our knowledge, the first non-contact and non-destructive method to monitor *in-vivo* hydration dynamically in plant tissues. We believe it will be very useful in the future to understand the effects of water deficit on vegetable tissues. This at its time is of enormous importance to improve drought resistant crops.

- [1] Zhu, J.K. Salt and drought stress signal transduction in plants. *Annual Review of Plant Biology*. 53, 247 (2002)
- [2] Ingram, J. and Bartels, D. The molecular basis of dehydration tolerance in plants. *Annual Review of Plant Biology*, 47, 377 (1996)
- [3] Bray, E. Plant responses to water deficit. *Trends in Plant Science*. 2, 48 (1997)
- [4] Koorneef, M. and Meinke, D. The development of Arabidopsis as model plant. *Plant Journal* 61, 909 (2010)

We would like to thank funding from CONACyT (project 131931).

Recent Experimental Results of a Large Format 80x64 Pixel THz Camera Sensitive to 0.6 – 1.2 THz Radiation

Don Burdette, Chris Roedig, Jorgen Alverbro, Patrick Fay, Kubilay Sertel, Yang Ni, Georgios Trichopoulos, Kagan Topalli, and H.Lee Mosbacker
 Traycer, Inc. 1275 Kinnear Rd. Columbus OH, 43212
 don.burdette@traycer.com

Abstract: THz applications have been limited by the lack of a cost-effective, real-time, large format THz camera. This paper discusses the recent experimental results of a real-time (100 Hz), large-format (80x64 pixel), broadband (0.6 – 1.2THz) THz camera.

1. Introduction

THz imaging applications have been demonstrated in fields as diverse as non-destructive evaluation, security, and medical imaging [1]; however, wide-scale adoption of these applications has not occurred due to the lack of a cost-effective, large-format, real-time THz camera. Traycer has developed THEIA (THz Engine for Imaging Applications) to fill this market need, see Fig. 1. An overview of THEIA's technology and initial application results are the focus of this summary, followed by a brief outline of the work that is currently being conducted to further improve THEIA's imaging performance.

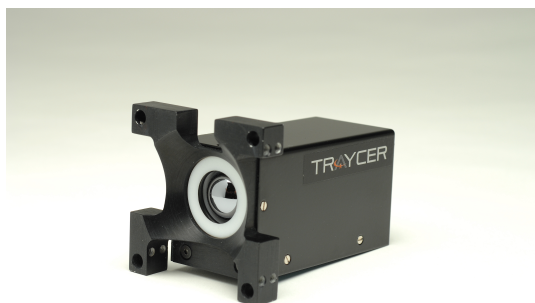


Fig. 1 Photograph of THEIA (THz Engine for Imaging Applications)

2. THEIA Technology Description

THEIA is a real-time (100 Hz), 80x64 pixel (100 μm x 100 μm pitch), broadband (0.6 THz – 1.2 THz) THz camera with a measured responsivity of 1000 V/W at 0.7 THz [2,3]. The core technological innovation that makes THEIA possible is the 80x64 pixel focal plane array (FPA) of antinode based heterostructure backward diodes (Sb-HBDs) [4]. These diodes can be uniformly fabricated and impedance matched to either narrowband or broadband antenna structures in the 0.1 THz – 2.0 THz regime (depending on the THz application). The FPA is flip-chipped bonded to a readout integrated circuit (ROIC) that multiplexes the pixel outputs to an intermediate electronics board that digitizes and converts the data to a standard CAMLINK output compatible with any off-the-shelf frame grabber. A one inch diameter, high-resistivity float-zone (HRFZ) silicon hyper-hemispherical lens is coupled to the front of the FPA to both focus the incident THz light onto the FPA and to provide the necessary boundary conditions for proper pixel operation.

3. Initial Experimental Results

The experimental set-up shown in Fig. 2 was constructed as an initial demonstration of THEIA's imaging capabilities. A backward wave oscillator (BWO) emitting 680 GHz continuous-wave THz radiation at approximately 0.75 mW is used as the THz source. The THz beam is collimated through the use of a TPX lens placed 2.5 cm from the BWO. An object is placed in the collimated beam (in this case an aluminum plate with a void spelling "THZ" – the thickness of each letter is 2 mm, see Fig. 3), blocking a portion of

the THz radiation. The THz radiation passing through the slit is spread over an image plane formed on the FPA by the combined use of a TPX lens and the HRFZ hyper-hemispherical silicon lens. The transmitted THz image is shown in Fig. 3. This image is the concatenation of three, one-second data runs created by averaging 100 frames of data. Each letter of the image was collected individually and then combined together during post processing to form the final image. These steps were necessary to create the final image due to both the limited beam-width of the BWO, and the attainable field-of-view of the THEIA using the current silicon optics [3]. However, it should be noted that a similar image at this frequency using a single-pixel raster-scanning methodology at $100\ \mu\text{m} \times 100\ \mu\text{m}$ resolution typically takes on the order of ten minutes to collect.

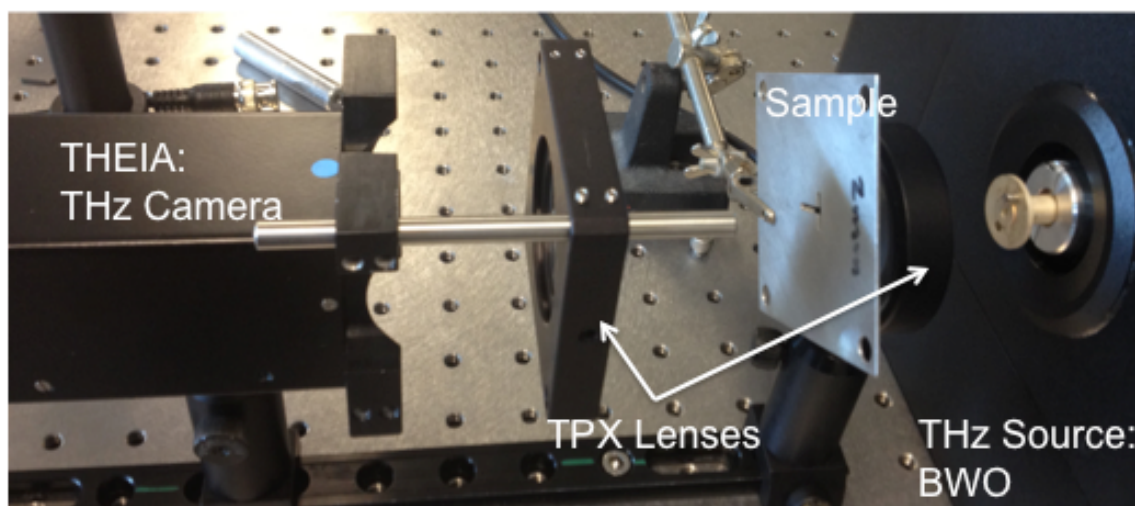


Fig. 2. Experimental set-up for transmission mode application demonstration.

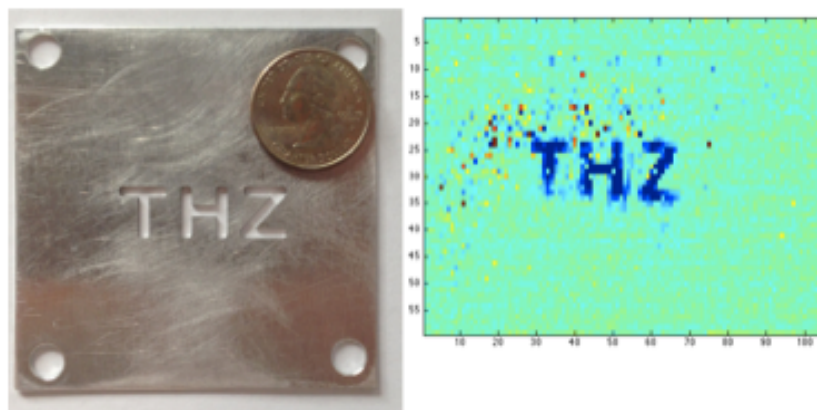


Fig. 3. (Left): A photograph of an aluminum plate with 2 mm thick letters carved out of the metal (approximately 1 cm in height). (Right): THz image collected by THEIA of a metal void in transmission mode using the experimental set-up of Fig. 2 at 680 GHz.

THEIA has also been successfully demonstrated as a beam profiler for a variety of THz sources, see Fig 4. These images were collected with THEIA positioned 1 inch in front of each respective THz source using only the HRFZ silicon hyper-hemispherical lens to focus the beam onto the FPA. Each image in Fig. 4 is the average of 100 frames of data (or 1 second of data). The image on the left is of a 0.5 mW, 610 GHz Virginia diode electronic THz source. The center image was collected from a 0.75 mW Microtech BWO operated at 680 GHz. The image on the right was collected at the NIST Free Electron Laser.

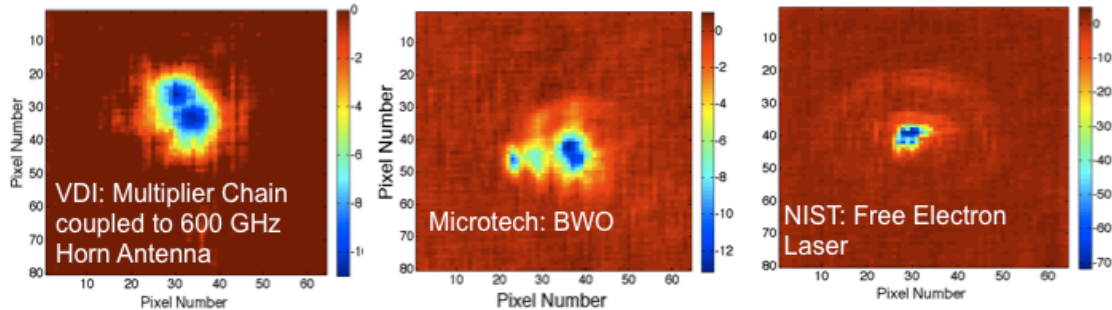


Fig. 3 Images of three THz sources collected with THEIA: (left) 600 GHz Virginia Diode Source, (center) Microtech backward wave oscillator source (680 GHz), (right) NIST Free Electron Laser.

4. Conclusions and Future Work

This work has demonstrated that THEIA is a promising THz imaging technology in the 0.1–2 THz regime. Images from beam profiling and transmissive non-destructive experiments have been successfully demonstrated.

It is important to note that the results depicted in this study were collected with the initial THEIA prototype that does not have optimized THz optics or reduced noise readout electronics. It is expected that four orders of magnitude improvement to the current signal-to-noise ratio is possible by optimizing the THz optics and the readout electronics. These improvements include the use of digital signal processing (DSP) and Digital Image Processing (DIP) algorithms, the use of a chopper to employ lock-in integration techniques, an optimized redesign of the readout ROIC and back-end intermediate electronics, and modifying the FPA antenna geometry to remove spherical aberrations inherent in the use of hyper-hemispherical lenses [5].

5. References

- [1] M. Tonouchi, "Cutting-edge terahertz technology," *Nature Photonics*, Vol. 1, pp. 97-105, Feb. 2007.
- [2] Burdette, D., J. Alverbro, Z. Zhang, P. Fay, Y. Ni, P. Potet, K. Sertel, G. Trichopoulos, K. Topalli, J. Volakis, and H. L. Mosbacker, "Development of an 80x64 pixel, broadband, real-time THz imager," *Proc. SPIE 8023*, 80230F (2011).
- [3] G.C. Trichopoulos, L. Mosbacker, D. Burdette, and K. Sertel, "A Broadband Focal Plane Array Camera for Real-time THz Imaging Applications," *IEEE Transactions on Antennas and Propagation* [Submitted April 2012 – Under Review].
- [4] Zhang, Ze, R. Rajavel, P. Deelman, and P. Fay, "Sub-Micron Area Heterojunction Backward Diode Millimeter-Wave Detectors With 0.18 pW/Hz^{1/2} Noise Equivalent Power," *Microwave and Wireless Components Letters, IEEE*, vol. 21, no. 5, pp 267-269, May 2011.
- [5] G.C. Trichopoulos, G. Mumcu, K. Sertel, H.L. Mosbacker, and P. Smith, "A Novel Approach for Improving Off-Axis Pixel Performance of Terahertz Focal Plane Arrays," *Microwave Theory and Techniques, IEEE Transactions on*, vol. 58, no. 7, pp. 2014-2021, July 2010.

Improving the Performance of Difference Frequency THz Generation in Waveguides

Peter Powers^{1,2}, Joseph Haus^{2,1}

¹ Physics Department, University of Dayton, 300 College Park, Dayton, OH45469, USA

² Electro-optics program, University of Dayton, 300 College Park, Dayton, OH45469, USA
powers@udayton.edu

Abstract: Improving the performance of THz generation by difference frequency generation is presented for waveguide interactions. A numerical model is used to show how to optimize THz generation and understand cascaded processes in the waveguide.

OCIS codes: (300.6495) THz Spectroscopy; (190.0190) Nonlinear Optics; (190.4975) Parametric Processes

THz sources, detectors, and applications have grown steadily over the past decade to the point where commercial THz systems are available from several companies. However, certain applications still require further source development. For example, stand-off imaging systems need to address power loss due to significant water vapor absorption. For this and similar applications a narrow line width THz source provides distinct advantages over broadband sources. By tuning between water lines, one is able to minimize (but not eliminate) the absorption thus allowing for larger imaging distances. THz sources based on difference frequency generation (DFG) provide narrow linewidth and tunability covering the entire THz spectral region. DFG sources can benefit from further refinement to improve the output power while simplifying the overall system architecture. Here, we focus on techniques to improve the performance of narrow band systems based on DFG in waveguides.

THz generation by means of DFG between two near-IR lasers has two main problems that stem from the large difference in the frequencies of the inputs and that of the THz output. In a typical DFG setup, one focuses the inputs into a crystal to generate the DFG output. When applied to THz generation, the THz beam has a diffraction that is approximately 100 times or greater than that of the inputs. This rapid diffraction reduces the overlap of the interacting beams and reduces the parametric gain. Another issue arising from the large frequency difference is illustrated by the expression for DFG described in terms of photon energy, $\hbar\omega_p = \hbar\omega_s + \hbar\omega_{\text{THz}}$ where ω_p and ω_s are the pump and signal input angular frequencies for the DFG process, and ω_{THz} is the output THz angular frequency. This expression shows that the maximum conversion efficiency to the THz is given by $\eta_{\text{max}} = \omega_{\text{THz}} / \omega_p = \lambda_p / \lambda_{\text{THz}}$. Because of the large wavelength differences between the THz and the pump input, the DFG process for generating THz has a large quantum defect. Both the large divergence and large quantum defect may be addressed by confining the process in a waveguide structure.

Our approach to studying THz generation in waveguides is using a numerical model. This model uses parameters that one would encounter in a laboratory setting for difference frequency generation. We assume two lasers are co-aligned and focused at the input face of the waveguide structure and these beams then are numerically propagated through the structure. This approach better simulates the laboratory setting where lasers with Gaussian beam profiles are focused into the waveguide. In this case many modes of the waveguide, including nonpropagating modes, are potentially excited depending on the mode matching of the input laser beams to the waveguide modes. In our simulations, no assumptions are made with regard to modes, instead we let the field propagate based on the wave equation and waveguide index of refraction structure.

The model uses the split-step technique [1], which has been successfully implemented to numerically model three-wave interactions for a large range of applications. Extending the model to the THz regime is straightforward with the requirement that, for bulk interactions, the numerical grid be large enough to account for the rapid THz diffraction. In the case of a THz waveguide, this criterion is relaxed to require that the grid be large enough to accurately sample the input beams as well as the guided THz field. In many cases a two-dimensional cross-sectional grid is employed to allow for asymmetric effects such as Poynting vector walk-off. However, in some cases, symmetry in the process may allow for a one-dimensional grid. In the current study, we assume cylindrical symmetry, which allows us to use a 1D grid. Figure 1 a) shows the basic geometry. Cylindrical symmetry is appropriate, for example, for LP modes in a cylindrical waveguide. These types of modes are a natural

consideration for nonlinear mixing in a waveguide where phase matching dictates linearly polarized modes. Going to a cylindrical coordinate system for these cases allows for a 1D numerical grid, but it also requires the use of Hankel transforms instead of Fourier transforms in order to model diffraction [2]. The Hankel transform is not as fast as an FFT, so the advantage of the 1D grid is lessened by the longer computation time of the Hankel transform. But overall, the computation time is decreased when compared to an equivalent 2D grid with the same point spacing. The 1D cylindrically symmetric case is especially useful for optimization since many simulation runs may be required.

The large wavelength difference for THz generation by way of DFG introduces challenges to waveguide design. Because of large THz wavelengths, on the order of one hundred to hundreds of microns, the waveguide core size will be of the same order. In this regime, the THz waveguide looks like a bulk crystal or a highly multi-mode structure to the NIR inputs. THz waveguide lengths are limited by practical considerations such as material absorption in the THz and the restriction that the waveguide is fabricated on a substrate, which in turn dictates the maximum waveguide length to several cm. For such structures, instead of launching waveguide modes for the NIR inputs, it is more appropriate to consider focusing the near-infrared inputs into the structure to maximize the nonlinear interactions while avoiding clipping on the structure. The design is then a combination of optimizing the nonlinear interaction by adjusting the THz waveguide size and input spot sizes. Figure 1 a) shows a scenario for a cylindrical waveguide, and Figure 1 b) shows the output for the ranges of input beam sizes and waveguide diameters. The waveguide consists of a core-air interface and does not have a cladding because of the difficulty in fabricating a cylindrical waveguide with a closely matched cladding for THz frequencies.

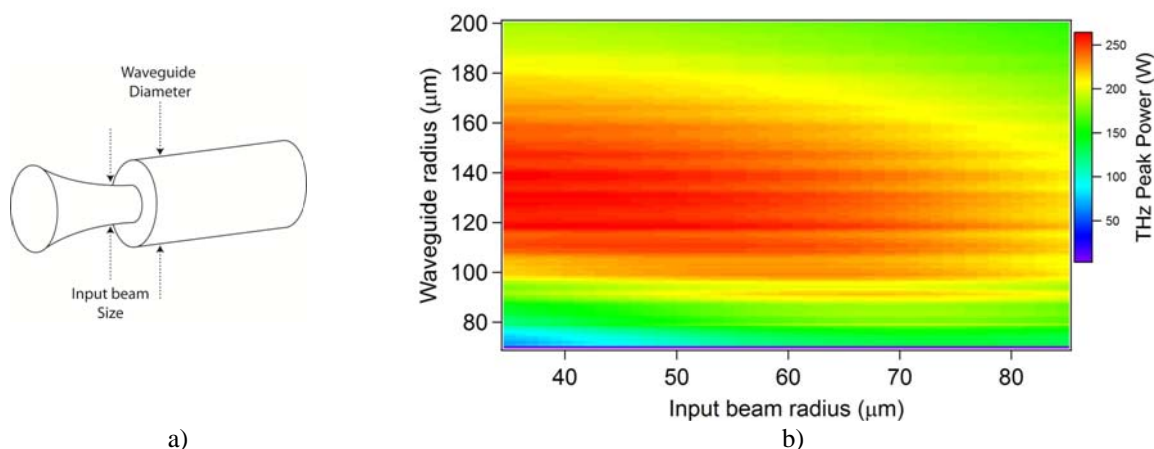


Figure 1. a) Illustration of the DFG interaction showing the input beams and cylindrical waveguide. b) Optimization results showing trends for spot size and waveguide diameter.

The particular simulation shown in Figure 1 was run for a 1 cm crystal assuming that the process was either birefringently phase matched or quasi-phase matched (QPM). The peak powers used in the simulation were 50 kW, which is a common power level for nsec pulsed lasers (approximately 500 μ J in 10 nsec). The simulation was run using a 1.8 THz DFG output (the inputs were \sim 1.8 μ m). Because the THz field sees a waveguide, it experiences waveguide dispersion. Hence as the waveguide size is decreased, the phase matching or quasi-phase matching has to be adjusted accordingly. For each point in the figure, Δk was optimized for maximum output. This figure shows that tight focusing is the best strategy for obtaining high output power. This result makes sense considering the short 1 cm length, which is smaller than the confocal parameter for the beam sizes considered here. The lower limit on the spot size was estimated to be the minimum based on material damage threshold. The figure also shows that the waveguide diameter has a large range where the performance is high. When compared with a bulk interaction, the waveguide results here are approximately 2.5 times more efficient.

It is possible in principle to achieve even higher conversion efficiency by working around the quantum defect inherent in the DFG process. Nearly all of the pump energy in THz DFG goes to amplifying the signal. A common strategy for mid-wave infrared and near-infrared is to use a second stage to amplify the DFG output at the expense of the amplified signal beam [3]. In the mid-wave infrared the phase matching condition for these two processes is

different thus requiring two phase matching regions for the principal DFG stage and the second cascaded stage. In the case of THz generation the situation is somewhat different. Here the coherence length of the DFG process and the cascaded process are nearly the same and may be a significant fraction of the overall crystal length. For example, coherence lengths on the order of 0.5 mm are typical. In this situation, the cascaded process runs in parallel with the principal DFG process. In this regard, the best strategy is to use as long a crystal as possible with a fixed quasi-phase matching period. In this way, both processes build up coherently. Such a situation only arises to a significant degree when the DFG process starts to deplete the pump. For lower energies, the cascaded processes do not become appreciable.

In the high conversion efficiency limit, as has been encountered with MW peak powers [4], we also consider multiple cascaded processes. For example, the THz field may sum-frequency mix with the pump. In our simulation we consider 6 fields as shown in the inset of Figure 2 (THz field not shown). Other cascaded orders are not included since the crystal length used here won't allow them to become appreciable. Although the coherence lengths of these processes are all similar, the coherence length for generating a second THz field at twice the frequency is significantly different. Therefore we do not include outputs at multiples of the THz frequency. As an example, we consider a GaP waveguide with a 180 μm diameter, and two inputs with 50 KW peak power, 65 μm beam radii, and wavelengths of 1.8 and 1.82 μm (yielding a 1.8 THz output). Figure 2 a) shows the NIR fields, while Figure 2b) shows the THz field. In the figure the inputs are at ω_p (pump) and ω_s (signal) while the cascaded frequencies are given by $\omega_4 = \omega_s - \omega_{\text{THz}}$, $\omega_5 = \omega_4 - \omega_{\text{THz}}$, and $\omega_6 = \omega_p + \omega_{\text{THz}}$. These relationships show that all the fields are coupled to each other via the THz field. The simulation shows that it is possible to nearly deplete both the pump and signal, and when this occurs the other cascaded frequencies grow in amplitude. For higher peak powers, the scale becomes shorter and the observation of the cascaded frequencies becomes more likely. In the higher peak power limit, there is an optimum crystal length for maximum THz output because of back conversion of the THz.

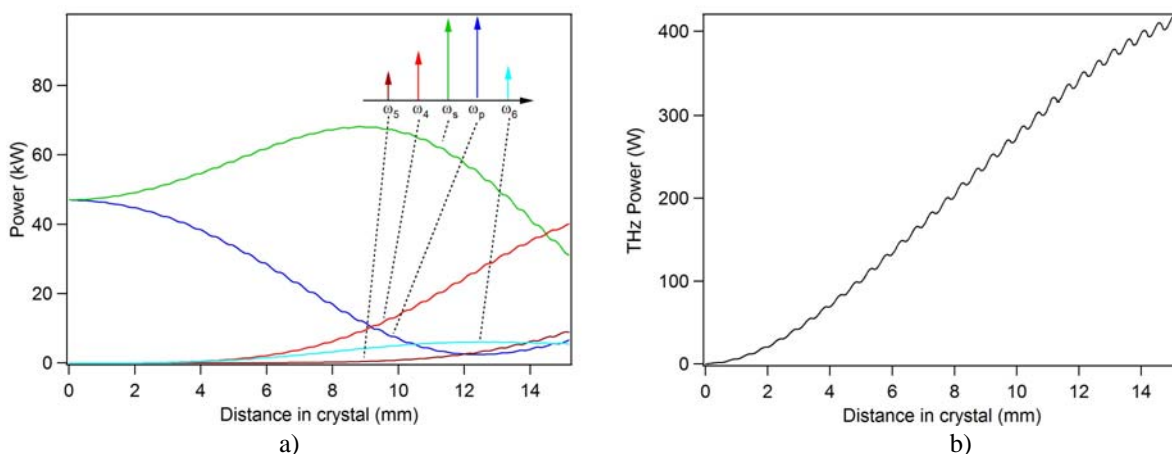


Figure 2. a) Peak-power for near-infrared wavelengths and b) THz output in the limit of high conversion efficiency showing parallel cascaded processes.

In conclusion this presentation shows a method to optimize THz generation in waveguides using a numerical model. The model is extended to include cascaded THz processes, which show shows that it is possible to nearly deplete both the pump and signal to help boost the THz output. The authors would like to acknowledge discussions with Wei Shi and Arturo Chavez-Pirson from NP Photonics that helped to give context to ideas presented in this talk.

[1] M. D. Feit and J. A. Fleck, "Light propagation in graded-index optical fibers," *Appl. Opt.* **17**, 3990 (1978).

[2] M. Guizar-Sicairos and J. C. Gutierrez-Vega, "Computation of quasi-discrete Hankel transforms of integer order for propagating optical wave fields," *J. Opt. Soc. Am. A* **21**, 53 (2004).

[3] A.R. Pandey, P.E. Powers, and J.W. Haus, "Experimental Performance of a Two-Stage Periodically Poled Lithium Niobate Parametric Amplifier," *IEEE J. Quant. Electron.* **44**, 203 (2008).

[4] Y. Jiang, D. Li, Y. Ding, and I. Zotova, "Terahertz generation based on parametric conversion: from saturation of conversion efficiency to back conversion," *Opt. Lett.* **36**, 1608 (2011).

ATh1A.4 • AIO Postdeadline Paper

Thursday, 28 June, 9:40 – 10:00

Cypress 3

Experimental Demonstration of an NIR Compressive Sensing Hyper-Spectral Imaging System

Yuehao Wu, Gonzalo R. Arce, and Dennis W. Prather

Department of Electrical and Computer Engineering, University of Delaware, Newark, DE, USA19716
wyh@udel.edu

Abstract: We utilized the compressive sensing theory in building a hyperspectral imaging system for NIR wavelengths. This system simultaneously captures 24 spectral images for the wavelength range between 990-1450 nm without any mechanical/temporal scanning processes.

OCIS codes: (110.4234) Multispectral and hyperspectral imaging; (300.6340) Spectroscopy, infrared

1. Introduction

Current NIR Hyper-Spectral Imaging (HSI) systems usually rely on some mechanical or temporal scanning processes to acquire the complete spatial/spectral information of the imaging scene [1]. The scanning process unavoidably carries a time penalty and undermines the performance of HSI systems in low light or high speed imaging applications.

In visible wavelengths, Coded Aperture Snapshot Spectral Imaging (CASSI) systems were developed to circumvent the scanning processes used in conventional HSI systems [2-4]. In this work, we report a CASSI system for NIR hyperspectral imaging applications. Specifically, we are interested in the wavelength range from 990-1450 nm. We use a photomask, which implements a Compressive Sensing (CS) measurement pattern, to impose intensity modulation on NIR optical images. The modulated image intensity is then collected into an NIR Relay lens/double-Amici Prism (R/P) structure. On the image plane of the R/P structure, an NIR FPA is used to capture the spectrally dispersed image of the modulated image intensity, which represents a set of CS measurement result for the original image cube. The original image cube can be reconstructed from the CS measurement result by solving an l_1 -regularized minimization problem [2-4]. We introduce the optical design and experimental realization of the NIR CASSI system and present an NIR image cube reconstructed from our experimental setup.

2. NIR CASSI System

Figure 1 shows the schematic drawing of the NIR CASSI system.

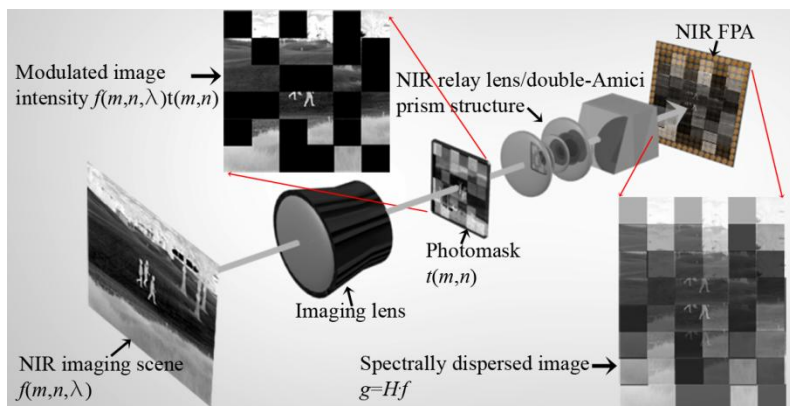


Fig. 1 Schematic drawing of the NIR CASSI system.

In Fig.1, a photomask is installed on the image plane of an NIR imaging lens. The photomask implements a CS measurement pattern, which is essentially a binary random pattern. The original image cube is represented as $f(m,n,\lambda)$ and the binary translucency of the photomask is represented as $t(m,n)$. In the transmission direction of the photomask and along the optical axis of the imaging lens, we install an NIR relay lens and an NIR double-Amici prism to generate spectrally dispersed image of the modulated image intensity on an NIR FPA (Xenics, model: XEVA 2508). The optical operations realized by the photomask, the relay lens, the double-Amici prism, and the NIR FPA were modeled as a system transfer matrix H in [2-4], and the spectrally dispersed image captured by the NIR FPA was represented as $g = H \cdot f$. The system transfer matrix H is not a square, and thus the image reconstruction problem $f = H^{-1} \cdot g$ is not directly solvable. In this work, we utilized the Two Step Iterative

Shrinkage/Thresholding (TwIST) algorithm to accomplish the image reconstruction task, which considers the following minimization problem [5]:

$$\min_f \|H \cdot f - g\|_2^2 + \delta \cdot TV(f), \tag{1}$$

where $TV(f)$ is a Total Variation (TV) regularization term, which is defined as: $TV(f) = \sum_{j,i,k} \sqrt{(f(j+1,i,k) - f(j,i,k))^2 + (f(j,i+1,k) - f(j,i,k))^2}$. δ is a regularization parameter for the TV term.

NIR imaging and relay lenses are commercially available. In our case, we used a pair of NIR achromatic lenses (Thorlabs, model: AC254-100-C-ML) to realize the functionality of optical relay. Another achromatic lens pair was used to form NIR optical images on the photomask. The NIR double-Amici prism is not commercially available. We designed it in our lab and customized it from Shanghai Optics. We defined an NIR Abbe number to quantitatively evaluate the dispersion performance of glass materials in the NIR spectrum: $v_{NIR} = \frac{n_2 - 1}{n_1 - n_3}$, where n_2, n_1, n_3 represent refractive indices of glass materials at wavelengths of 1250 nm, 950 nm, and 1450 nm, respectively [6]. Based on a comprehensive survey of glass materials from major glass vendors, we decided on using Schott glasses of N-PK52A and N-KZFS11 to build the NIR double-Amici prism. N-PK52A has a refractive index of 1.488 and an NIR Abbe number of 121.865 at 1250 nm. N-KZFS11 has a refractive index of 1.617 and an NIR Abbe number of 66.547 at 1250 nm. Both of the selected glasses have good transmissions at NIR wavelengths. Figure 2(a) shows the optical design of the NIR double-Amici prism and Fig. 2(b) shows the manufactured product. The photomask was customized from Advanced Reproduction. A binary random pattern was coated on the mask, with a pixel dimension of 128×128 and a pixel pitch of $19.8 \mu\text{m}$. Figure 2(c) shows the design of the photomask. Figure 2(d) shows the optical assembly of the photomask, the NIR R/P structure, and the NIR FPA.

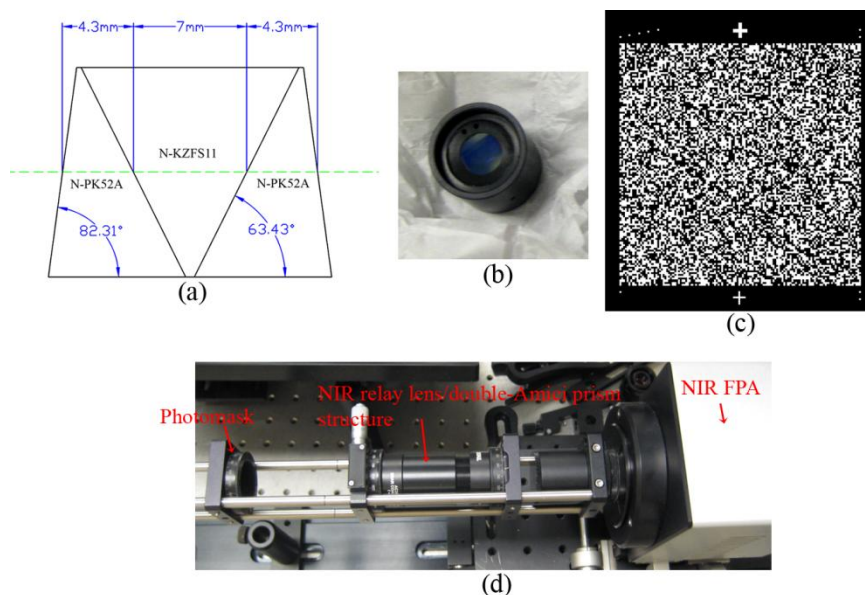


Fig. 2 (a) Optical design of the NIR double-Amici prism. (b) Manufactured product. (c) Photomask. (d) Experimental setup of the NIR CASSI system.

3. Experimental Result

The imaging target used in this experiment was a part of a translucent USAF resolution target. Figure 3(a) shows the imaging target and its illumination condition. This target was illuminated with two different NIR sources: in region 1, an NIR LED was used to offer illumination and in region 2, an NIR monochromator was used to offer illumination. Figure 3(b) shows a CS measurement result generated from our experimental setup when a 1050 nm LED was used to illuminate region 1 and a monochromator emission of 1400 nm was used to illuminate region 2. Figure 3(c) shows the NIR image cube reconstructed from the CS measurement result, which contains 24 spectral channels.

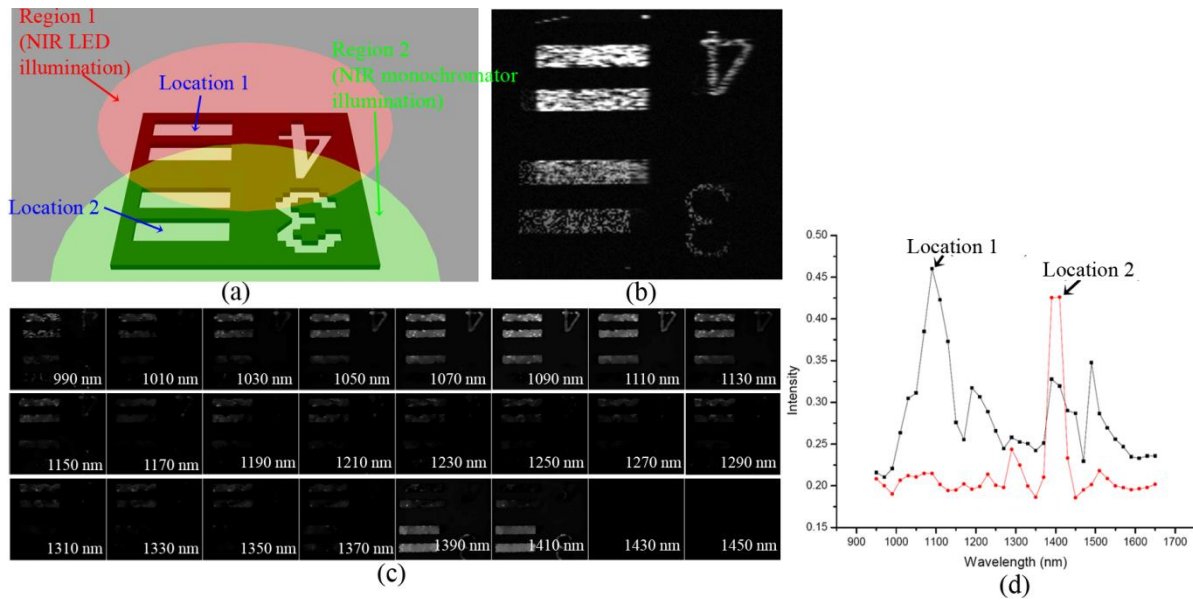


Fig. 3 (a) Imaging target. (b) CS measurement result generated when a 1050 nm LED was used to illuminate region 1 in the target and a monochromatic light of 1400 nm was used to illuminate region 2. (c) Reconstructed image cube. (d) Intensity variations of the reconstructed image cube at location 1 (black curve) and location 2 (red curve).

In the reconstructed image cube, we can see that the features of the imaging target in region 1 was reconstructed with strong intensity in spectral channels from 1030 nm to 1130 nm and features of the target in region 2 was reconstructed with strong intensity in spectral channels from 1390 nm to 1410 nm. We also evaluated the intensity variations of the reconstructed image cube at location 1 and location 2, which are located on region 1 and 2 respectively. Figure 3(d) shows those intensity variations. We can see that at location 1 of the imaging target, there is an intensity peak in the image cube at the spectral channel of 1090 nm, which is slightly different from the peak emission wavelength of the NIR LED specified in its user manual. At location 2, there is an intensity dual-peak in spectral channels of 1390 nm and 1410 nm. This is because the monochromator emission has a bandwidth of 20 nm at the wavelength of 1400 nm.

4. Conclusion

In this work, we report the development of an NIR CASSI system, which virtually does not introduce any time penalty in the process of acquiring NIR spatial/spectral image cubes. We present the optical design and the experimental realization of this system. We also verified/evaluated the system performance by presenting an image cube reconstructed for a real-world target, which contains 24 spectral channels for the wavelength range between 990-1450 nm.

5. References

- [1] J. R. Schott, *Remote Sensing: The Image Chain Approach (2nd edition)*, (Oxford University Press, 2007), Chap. 6.
- [2] A. A. Wagadarikar, N. P. Pitsianis, X. Sun, and D. J. Brady, "Spectral image estimation for coded aperture snapshot spectral imagers," *Proc. SPIE*, 7076, 707602, (2008).
- [3] A. A. Wagadarikar, R. John, R. Willett, and D. J. Brady, "Single disperser design for coded aperture snapshot spectral imaging," *Appl. Opt.*, 47(10), B44–B51, (2008).
- [4] A. A. Wagadarikar, N. P. Pitsianis, X. Sun, and D. J. Brady, "Video rate spectral imaging using a coded aperture snapshot spectral imager," *Opt. Express*, 17(8), 6368–6388, (2009).
- [5] J. M. Bioucas-Dias, and M. A. T. Figueiredo, "A new TwIST: two-step iterative shrinkage/thresholding for image restoration," *IEEE Transactions on Image Processing*, 16(12), 2992–3004, (2007).
- [6] Y. Wu, I. O. Mirza, G. R. Arce, and D. W. Prather, "Study of an NIR digital micromirror device-based snapshot spectral imaging system", *Proc. SPIE*, 8254, 82540O, (2012).

Addendum

OW4D.1 • Tutorial on Recent Advances in Ion Beam and Plasma Jet Processing,
Axel Schindler; Leibniz-Institut für Oberflächenmodifizierung, Germany

Tutorial on Recent Advances in Ion Beam and Plasma Jet Processing

A. Schindler

Leibniz-Institut für Oberflächenmodifizierung, Leipzig, Physical Dept., Leipzig, D-04318, Germany, axel.schindler@iom-leipzig.de

Abstract: The Tutorial will highlight recent advances achieved in R&D of Ion beam figuring (IBF), ion Beam Smoothing (IBS), Reactive Ion Beam Etching (RIBE) and atmospheric Plasma Jet Machining (PJM) (deep aspherization, nanometer shape correction, smoothing, film deposition) at IOM Leipzig.

OCIS codes (220.1250) Aspherics; (220.4610) Optical fabrication; (220.5450) Polishing; (350.3850) Materials processing

1. Ion beam figuring

Ion beam figuring (IBF) for ultra precision surface finishing is well established in high end optics fabrication for lithography, space and beam-line optics and advanced optical instrument, respectively [1, 2]. IBF standard technology uses a constant and stable ion beam that moves computer controlled across the entire optic via a meander like scanning with variable scan line velocity according to the local dwell time necessary for the specified removal of material at the certain place. The beam tool size has to be adjusted according to the spatial surface error size processing. One serious disadvantage of this method is connected with the continuous and constant beam and the limitations in maximum speed and acceleration/deceleration of the mechanical multi axes motion system. This causes wasting of material removal at least in that part of the surface where no material should be removed (absolute minimum of the surface figure). Further there can be some effects of direct additional surface error production in cases of steep gradients and small surface feature sizes of the surface topology where the beam can not follow the very small dwell times due to the limitations of the dynamics of the motion system.

The new solution uses a pulsed ion beam instead of a cw one combined with pulse width modulation (PWM) for variation of the mean beam power and the control of the PWM signal by the motion control of the multi axes system that moves the ion beam (source) across the surface to be figured. Using this trick we effectively extend the limited dwell time scale realized by the mechanical motion system by two orders of magnitude to lower values.

Figure 1 shows the scheme of the new technique. New IBF processing software (DtCalc) has been developed for a two dwell times algorithm velocity driven and PWM driven, respectively.

2. Ion beam smoothing / ion beam nano-structure generation by atomic self assembly

In contrast to the stringently deterministic process of ion beam figuring, ion beam induced smoothing of micron and nano meter features is strongly coupled to atomistic processes which are characteristic for the much shorter spatial length scales and are less deterministic. Nevertheless, within the last years low-energy ion beams have been developed as alternative tools that can be beneficially used to tailor the microscopic surface roughness of solid surfaces on a nanometer and micron scale. Recently developed different ion beam assisted processes for the preparation of ultra-smooth surfaces with RMS roughness values $r \leq 0.2$ nm. Especially, ion beam direct smoothing and smoothing with planarization or sacrificial layers are demonstrated. A review is given by Frost et al. [3].

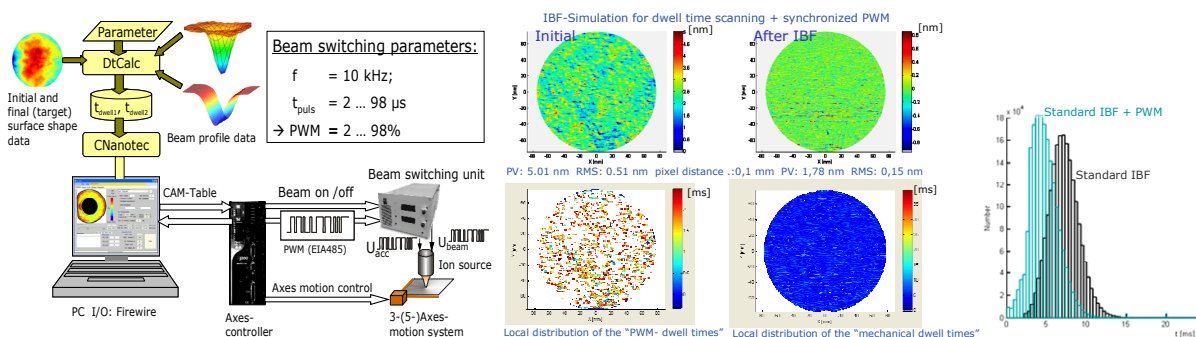


Fig. 1 left: Scheme of the motion synchronized PWM ion beam controlled ion beam figuring technique; middle: upper row: IBF simulation results of sub-nm figure mid spatial wavelength error features of a \varnothing 160 mm lens using new PWM technique, bottom row: local dwell time distributions of the PWM action only (left) and the axes velocity only (right); right: histograms of the dwell times for the standard cw beam dwell time IBF and of the new combined PWM ion beam mode.

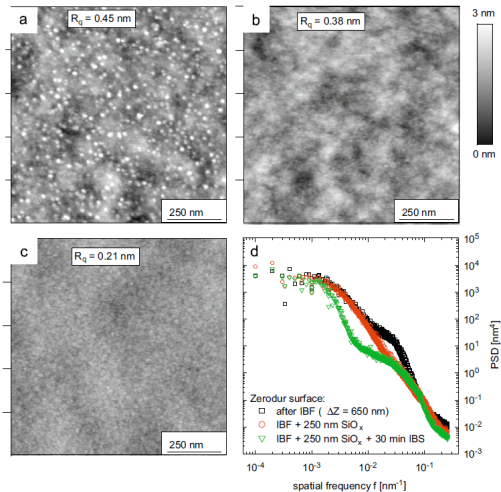


Fig. 2 Illustration of the processing sequence of Zerodur used as substrates for EUVL optical elements. In a first step a shape correction was made by ion beam figuring (IBF). Due to the special composition of Zerodur this results in an increased surface roughness 0.45 nm RMS (a). In the second step the substrate is coated with a thin SiO_2 layer ($\sim 50 \text{ nm}$) by ion beam sputtering, where the surface roughness is already reduced to values of $\leq 0.4 \text{ nm}$ RMS (b). Finally, an ion beam direct smoothing step was applied (c). The final HSFR is now $\leq 0.2 \text{ nm}$ RMS. From the PSD graph (d) it is seen that surface smoothing is achieved for all spatial frequencies that are $> f = 1 \times 10^{-3} \text{ nm}^{-1}$.

3. Plasma Jet Machining

There is a growing demand for aspheric and free-form optical elements with large deformations. High-Rate Plasma Jet Machining (HR-PJM) is a non-contact, local dry-etching method that can be used in the fabrication of such elements. It works best on fused silica and ULE® with material removal rates up to $50 \text{ mm}^3/\text{min}$. Thus, also large parts can be processed to achieve strong deviations from a suitable initial surface. As key advantages of the method there are nearly no limitations by local curvatures of the parts to be machined and no sub-surface damages are generated during the machining process. The latter fact enormously reduces the polishing effort afterwards and hence the formation of related mid-spatial structures is minimized. On the other hand the etching process is very sensitive on structural defects and chemical impurities, which can be used to specifically remove such kind of imperfections [4].

At IOM there is a more than 15 years experience in local reactive plasma etching processes primarily done under rough vacuum conditions and later realized at atmospheric pressure [5, 6, 7]. During this time a broad variety of plasma jet tools with different removal rates and tool widths has been developed covering a wide range of applications. In addition to the aspherization discussed here also ultra-precision surface machining in the sub-mm spatial range with nanometers depth accuracy can be performed [8, 9, 10, 11]. Figure 3 shows the high rate PJM of a fused silica cylindrical asphere

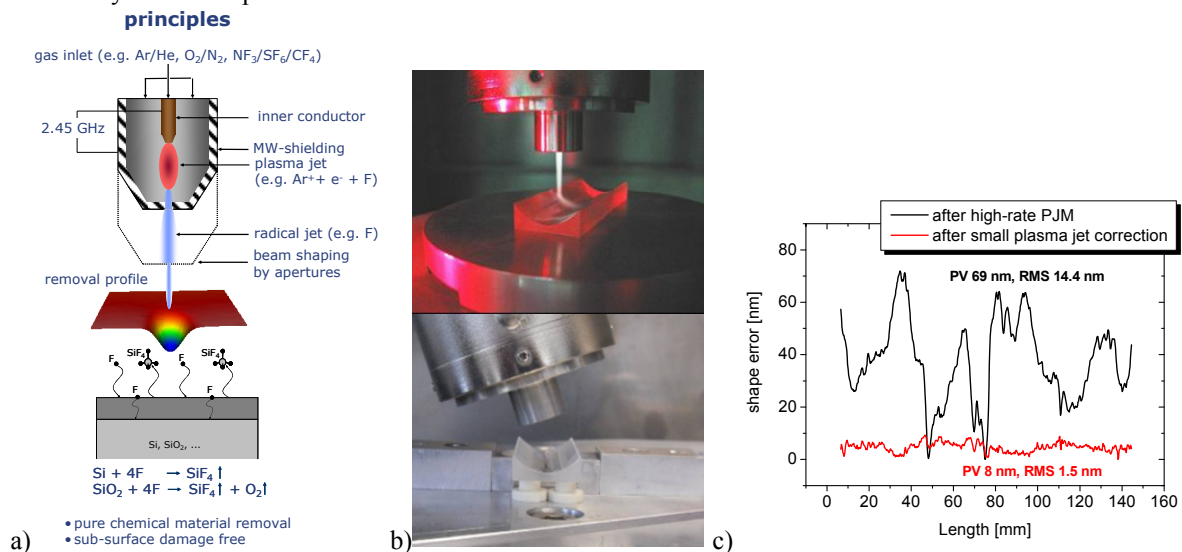


Fig. 3 High-rate plasma jet machining operating in microwave excited plasma jet cw-mode up to 600 W 2.45 GHz, a) scheme, b) fabrication of a strongly curved concave plane-parabola starting from a best fit plane-cylinder optic, c) centre line error of an off-axis plane-elliptical mirror blank manufactured by plasma-jet-machining techniques using two steps (i) high rate PJM aspheric figuring and (ii) low power small tool PJM figuring error correction.

4. Plasma jet polishing

As a third example for using an atmospheric plasma jet in optical surface fabrication the smoothing of e.g. ground surfaces with nearly no material removal and hence without changing the form will be presented. The big advantage of this technique is that not only the high-spatial-frequency-roughness (HSFR) is reduced to optical quality (< 0.5 nm RMS) but also the critical mid-spatial-frequency-roughness (MSFR) is significantly reduced in many cases. Furthermore, due to the dimension of the plasma-jet-tool the smoothing can be done in a very local way. This gives the opportunity either to polish small sub-areas or small-sized and strongly curved parts. Now, the idea for the future is to establish a cost efficient two-step process chain consisting of precision grinding and plasma-jet polishing for the manufacturing of aspheres and free-forms. If higher shape accuracy is necessary, the plasma-jet based surface error correction can be included just by switching the plasma jet process from smoothing to etching. Figure 4 shows examples of plasma-jet polishing of fine ground fused silica surfaces.

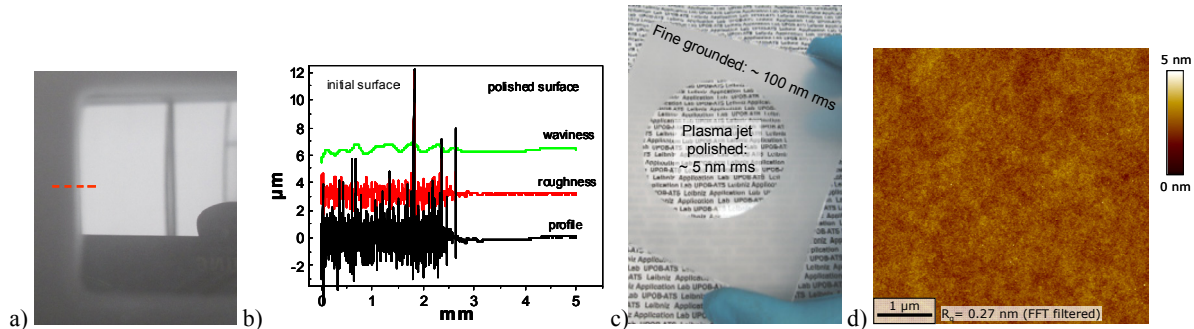


Fig. 4 Photographs of partially plasma-polished ground fused silica surfaces (a) and (c) with roughness's of ~ 100 nm rms in the ground part and b) the surface profile along red dotted line of a) measured by optical profilometry. Waviness and roughness curves have been extracted from the raw data (profile in b) by computer filter procedures, d) AFM-measurement of a plasma-jet polished fine ground fused silica surface.

5. Conclusions

New IBF, IBS and PJM techniques have been demonstrated with large technological potential. They will certainly have important impact on ultra precision surface processing and finishing for high end optics fabrication technology next future. Further new achievements on RIBE technique development for the transfer of 3D resist mask structures into hard optical material surfaces will be shown in the tutorial.

6. References

- [1] T. Hänsel, F. Frost, A. Nickel, A. Schindler, Ultra-precision Surface Finishing by Ion Beam Techniques, *Vakuum in Forschung und Praxis*, 19, 24-30 (2007)
- [2] M. Weiser, Ion beam figuring for lithography optics, *Nucl. Instr. Meth. B*, 267, 1390 -1393 (2009)
- [3] F. Frost, R. Fechner, B. Ziberi, J. Völlner, D. Flamm, A. Schindler, Large area smoothing of surfaces by ion bombardment: fundamentals and applications, *J. Phys.: Condens. Matter* 21 (2009) 224026
- [4] J. W. Carr, "Atmospheric pressure plasma processing for damage-free optics and surfaces" Engineering Research Development and Technology Lawrence Livermore National Laboratory FY-99, 3-1 (1999)
- [5] G. Boehm, W. Frank, A. Schindler, A. Nickel, H. -J. Thomas, F. Bigl, and M. Weiser, "Plasma Jet Chemical Etching - a Tool for the Figuring of Optical Precision Aspheres", in Proc of the 9th Int. Conf. on Production Engineering, Y. Furukawa, Y. Mori, T. Kataoka, eds., (Jap. Soc. of Prec. Eng. Publ. Series No. 3 Tokyo 1999), pp. 231 – 236
- [6] G. Boehm, W. Frank, and A. Schindler "Radical Jet Etching (RJE) - a New Tool for High Rate Figuring of Optical Surfaces", in Optical Fabrication and Testing, OSA Technical Digest, Optical Society of America, Washington DC, pp. 23 – 24, 2000
- [7] T. Arnold, G. Böhm, and A. Schindler, *J. Vac. Sci. Technol. A* 19 (2001), pp. 2586.
- [8] G. Böhm, I.-M. Eichentopf, and T. Arnold, Optical Fabrication and Testing, OSA Technical Digest (CD), (Optical Society of America, 2008), paper OThD4.
- [9] T. Arnold and G. Böhm, "Reactive plasma jet machining for free form surface correction", Proc. of the 9th euspen International Conference, San Sebastian, Spain 2009, paper P6.16
- [10] G.P.H. Gubbels, C. van Drunen, G. Böhm, Th. Arnold, F. Kamphues, and W.L.M. Gielezen, "Fabrication of strongly curved aspheric silicon carbide mirrors", Proc. of the 10th euspen International Conference, Delft, NL, June 2010
- [11] T. Arnold, G. Böhm, R. Fechner, J. Meister, A. Nickel, F. Frost, T. Hänsel, and A. Schindler, A. (2010), "Ultra-Precision Surface Finishing by Ion Beam and Plasma Jet Techniques - Status and Outlook", *Nuclear Instruments and Methods in Physics A*, Vol. 616, pp. 147-156.

Key to Authors

A

Agrawal, Amit - SW4C.1
Alverbro, Jorgen - SW4C.6
Andrews, Aaron M. - SW4C.3
Arce, Gonzalo R. - ATH1A.4
Armitage, N. Peter - SW4C.2

B

Barsic, Anthony J. - CW2C.1
Benz, Alexander - SW4C.3
Brandstetter, Martin - SW4C.3
Burdette, Don - SW4C.6

C

CastroCamus, Enrique - SW4C.5
Covarrubias, Alejandra A. - SW4C.5

D

Deibel, Jason A. - SW4C.4
Detz, Hermann - SW4C.3
Deutsch, Christoph - SW4C.3
Dietze, Daniel - SW4C.3

F

Fay, Patrick - SW4C.6

H

Haus, Joseph W. - SW4C.7

K

Kanaev, Andrey - CW2C.2
Krall, Michael - SW4C.3

L

Liu, Shuchang - SW4C.1

M

Miller, ChrisW. - CW2C.2
Morris, Christopher M. - SW4C.2
Mosbacker, Howard L. - SW4C.6

N

Nahata, Ajay - SW4C.1
Ni, Yang - SW4C.6

O

Owens, Lindsay - SW4C.4

P

Palomar, Miguel - SW4C.5
Petkie, Douglas T. - SW4C.4
Piestun, Rafael - CW2C.1
Powers, PeterE. - SW4C.7
Prather, DennisW. - ATH1A.4

R

Roedig, Chris - SW4C.6

S

Schrenk, Werner - SW4C.3
Schwarz, Stefan - SW4C.3
Sertel, Kubilay - SW4C.6
Shou, Xiang - SW4C.1
Stier, Andreas V. - SW4C.2
Strasser, Gottfried - SW4C.3

T

Topalli, Kagan - SW4C.6
Trichopoulos, Georgios - SW4C.6
Tufillaro, Nicholas - RTu2E.5

U

Unterrainer, Karl - SW4C.3

V

Valdes Aguilar, Rolando - SW4C.2

W

Wu, Yuehao - ATH1A.4

SAVE THE DATE

OSA OPTICS & PHOTONICS CONGRESS

Imaging and Applied Optics 2013

23-27 JUNE 2013 ■ ARLINGTON, VIRGINIA, USA

Imaging Systems and Applications (IS)

**Applied Industrial Optics:
Spectroscopy, Imaging & Metrology (AIO)**

**Hyperspectral Imaging and Sounding of
the Environment (HISE)**

**Adaptive Optics:
Methods, Analysis and Applications (AO)**

**Computational Optical Sensing and Imaging
(COSI)**

Signal Recovery & Synthesis (SRS)

Fourier Transform Spectroscopy (FTS)

OSA[®]

The Optical Society

2010 Massachusetts Ave., NW
Washington, DC 20036 USA

www.osa.org/meetings